RĪGAS TEHNISKĀ UNIVERSITĀTE
Materiālzinātnes un lietišķās ķīmijas fakultāte
Vispārīgās ķīmijas tehnoloģijas institūts

RIGA TECHNICAL UNIVERSITY
Faculty of Materials Science and Applied Chemistry
Institute of General Chemical Engineering

Jana Vecstaudža
Doktora studiju programmas "Materiālzinātne" doktorante
Doctoral Student of the Study Programme "Materials Science"

AMORFA KALCIJA FOSFĀTA BIOMATERIĀLI AR LIELU ĪPATNĒJO VIRSMAS LAUKUMU

Promocijas darbs

AMORPHOUS CALCIUM PHOSPHATE BIOMATERIALS WITH HIGH SPECIFIC SURFACE AREA

Doctoral Thesis

Zinātniskais vadītājs / Scientific supervisor
profesors *Dr. sc. ing.* / Professor Dr. sc. ing.
JĀNIS LOČS

RTU Izdevniecība / RTU Press
Rīga 2021 / Riga 2021

Vecstaudža, J. Amorfa kalcija fosfāta biomateriāli ar lielu īpatnējo virsmas laukumu. Promocijas darbs. Rīga: RTU Izdevniecība, 2021. 74 lpp.

Vecstaudža, J. Amorphous Calcium Phosphate Biomaterials with High Specific Surface Area. Doctoral Thesis. Riga: RTU Press, 2021. 74 p.

Iespiests saskaņā ar Vispārīgās ķīmijas institūta 2019. gada 3. jūnija lēmumu, protokols Nr. 3-18/19.

Published in accordance with the decision of the Institute of General Chemical Engineering of 3 June 2019, Protocol No 3-18/19.

Šis darbs izstrādāts ar Eiropas Sociālā fonda atbalstu projektā "Atbalsts RTU doktora studiju īstenošanai".

This work has been supported by the European Social Fund within the project "Support for the implementation of doctoral studies at Riga Technical University".

PROMOCIJAS DARBS IZVIRZĪTS ZINĀTNES DOKTORA GRĀDA IEGŪŠANAI RĪGAS TEHNISKAJĀ UNIVERSITĀTĒ

Promocijas darbs zinātnes doktora (*Ph. D.*) grāda iegūšanai tiek publiski aizstāvēts 2021. gada 21. jūnijā plkst. 15.00 Rīgas Tehniskās universitātes Materiālzinātnes un lietišķās ķīmijas fakultātē, Paula Valdena ielā 3/7, 272. auditorijā.

OFICIĀLIE RECENZENTI

Vadošais pētnieks *Dr. habil. sc. ing.* Jānis Grabis,
Rīgas Tehniskā universitāte, Latvija

Asociētā profesore *Dr. med.* Laura Neimane,
Rīgas Stradiņa universitāte, Latvija

Profesore *Ph. D. Christèle Combes*,
Institut National Polytechnique de Toulouse, CIRIMAT, Francija

APSTIPRINĀJUMS

Apstiprinu, ka esmu izstrādājusi šo promocijas darbu, kas iesniegts izskatīšanai Rīgas Tehniskajā universitātē zinātnes doktora (*Ph. D.*) grāda iegūšanai. Promocijas darbs zinātniskā grāda iegūšanai nav iesniegts nevienā citā universitātē.

Jana Vecstaudža ……. (paraksts)

Datums: ……

Promocijas darbs sagatavots kā tematiski vienota zinātnisko publikāciju kopa. Tajā ir kopsavilkums latviešu un angļu valodā un četras *SCI* publikācijas. Publikācijas uzrakstītas angļu valodā, to kopējais apjoms, ieskaitot elektroniski pieejamo informāciju, ir 34 lpp.

SATURS

PROMOCIJAS DARBA VISPĀRĒJS RAKSTUROJUMS

Ievads

Pasaulē nemitīgi pieaug tādu pacientu skaits, kas saskārušies ar kaulu slimībām, patoloģijām un muskuloskeletālās sistēmas traumām [1], tāpēc kaulu ārstēšanai un aizvietošanai ir nepieciešami efektīvi biomateriāli. Šādu biomateriālu sastāvam un struktūrai jāatdarina dabīgā kaula īpašības. Kaula unikālā ķīmiskā sastāva un struktūras dēļ to joprojām nav izdevies mākslīgi atdarināt tā, lai izgatavotā biomateriāla īpašības būtu salīdzināmas ar kaulu [2]. Kauls sastāv no neorganiskām (75 masas %, tai skaitā 10 masas % ūdens) un organiskām (25 masas %) sastāvdaļām [3]. Kaula neorganiskā daļa sastāv no nanoizmēra kalcija fosfāta daļiņām, kas izvietotas organiska sastāva matricā. Zināms, ka kalcija fosfātiem ir ļoti augsta biosaderība ar cilvēka audiem un ķermeņa vidi [4]. Tāpēc kalcija fosfāti ir perspektīvi kaula neorganiskās daļas aizvietotāji, ko ir iespējams sintezēt laboratorijas apstākļos un izmantot jaunu un efektīvu biomateriālu izstrādē.

Tomēr kaulu reģenerācijas jomā nemainīgs "zelta" standartmateriāls ir autografts jeb pacienta kaulaudi. Cita populāra izvēle ir ksenografts, piemēram, komerciāli pieejamie deproteinizēta liellopu kaula minerāla materiāli, kā izmantošana novērš ar autografta lietošanu izraisītos trūkumus (vairākas operāciju vietas, sāpes, paildzināta darba nespēja u. c.) [5]. Deproteinizēta liellopu kaula minerāla materiālu labā veiktspēja saistīta ar to mikro un nano struktūrām un to lielo īpatnējo virsmas laukumu (līdz 88 m^2/g [6]), kura vērtība ir tuva cilvēka kaulā esošo kalcija fosfāta daļiņu īpatnējā virsmas laukuma vērtībai (40–240 m^2/g [7]). Tikmēr komerciāli pieejamo kalcija fosfātu biomateriālu īpatnējais virsmas laukums ir ievērojami mazāks (līdz 3 m^2/g [8]). Liels īpatnējais virsmas laukums ir būtisks bioaktīvu molekulu (piemēram, proteīnu un citokīnu) adsorbcijai uz biomateriāla virsmas [9], kas veicina materiāla integrāciju ķermenī un audu reģenerāciju. Sintētiskie kalcija fosfāti ir ar augstu tīrību, pieejami lielos apjomos, ar atkārtojamu sastāvu, un tie nav dzīvnieku izcelsmes. Līdz ar to zinātniskā sabiedrība padziļināti pēta kalcija fosfātus – to sintēzi, fizikālķīmiskās īpašības, apstrādi, kā arī veic *in vitro, in vivo* un klīniskos pētījumus.

Amorfais kalcija fosfāts ir pirmā neorganiskā fāze, kas rodas, veidojoties jaunam kaulam [10]. Amorfo kalcija fosfātu uzskata arī par pirmo vai starpprodukta fāzi citu kalcija fosfātu, piemēram, hidroksilapatīta, veidošanās procesā. Līdz šim amorfais kalcija fosfāts ir salīdzinoši maz izmantots kā biomateriāls, kas skaidrojams ar tā metastabilitāti. Laika un dažādu faktoru ietekmē amorfais kalcija fosfāts kristalizējas citās kalcija fosfātu fāzēs [11]. Šajā promocijas darbā parādīts, ka iespējams iegūt stabilu amorfo kalcija fosfātu, tādējādi ievērojami paplašinot tā izmantošanas iespējas biomateriālu pētniecībā.

Promocijas darbā ir izstrādāta jauna sintēzes metode stabila amorfa kalcija fosfāta ar lielu īpatnējo virsmas laukumu ($\geq$100 m^2/g) iegūšanai, kā arī raksturotas iegūto materiālu fizikālķīmiskās īpašības. Pētīta amorfā kalcija fosfāta kristalizācija atkarībā no sintēzes tehnoloģiskajiem parametriem un risinājumiem (sintēzes pH un žāvēšanas metode). Amorfais kalcija fosfāts veiksmīgi saķepināts blīvā biokeramikā, izmantojot aukstās saķepināšanas procesa principus, tādējādi saglabājot tā amorfo struktūru.

Mērķis un darba uzdevumi

Promocijas darba mērķis ir izstrādāt sintēzes tehnoloģiju stabila amorfā kalcija fosfāta ar lielu īpatnējo virsmas laukumu iegūšanai un pētīt tā veidošanos, kristalizāciju un saķepināšanu.

Mērķa sasniegšanai definēti vairāki darba uzdevumi.

1. Pētīt sintēzes temperatūras un reaģentu Ca/P molārās attiecības ietekmi uz ar dubultās sāļu sadalīšanas metodi iegūta amorfa kalcija fosfāta īpatnējo virsmas laukumu.
2. Izstrādāt sintēzes metodi amorfa kalcija fosfāta ar paaugstinātu īpatnējo virsmas laukumu ($\geq$100 m^2/g) iegūšanai.
3. Pētīt žāvēšanas paņēmiena (liofilizēšana vai žāvēšana 80 °C temperatūrā) ietekmi uz amorfa kalcija fosfāta struktūru un kristalizāciju.
4. Pētīt amorfa kalcija fosfāta ilgtermiņa stabilitāti istabas temperatūrā.
5. Pētīt amorfa kalcija fosfāta saķepināšanu, izmantojot aukstās saķepināšanas procesa principus.

Aizstāvamās tēzes

1. Strauji paaugstinot gan kalcija, gan fosfātu jonus saturoša šķīduma pH līdz 10–11, tiek nodrošināta amorfa kalcija fosfāta ar lielu īpatnējo virsmas laukumu ($\geq$100 m^2/g) nogulsnēšanās.
2. Pie pH = 10–11 nogulsnēta amorfa kalcija fosfāta Ca/P molārā attiecība, kas lielāka par 1,5, nodrošina tā ilgtermiņa stabilitāti istabas temperatūrā.

Zinātniskā novitāte

Demonstrēta jauna, vienkārša un rentabla sintēzes metode ilgtermiņā stabila amorfa kalcija fosfāta ar lielu īpatnējo virsmas laukumu iegūšanai un aprakstītas iegūstamo produktu fizikālķīmiskās īpašības.

Praktiskā nozīme

Iegūts un pētīts ilgtermiņā stabils amorfais kalcija fosfāts, kura praktiskais lietojums rasts nanostrukturētu granulu izstrādē[1]:

1) ar stroncija joniem osteohondrālo implantu veiktspējas uzlabošanai[2];
2) ar biomimētisku ķīmisko sastāvu, kas nodrošinās biomimētiska kalcija fosfāta biosintēzi pēc implantācijas *in vivo*[3].

---

[1] RTU un RSU sadarbības projekts "Nanostrukturētu kaulu aizvietojošu materiālu izveide un imunoloģisko aspektu izpēte kaulaudu reģenerācijā", 2016.–2019. g.

[2] EuroNanoMed III projekts "Nanostrukturēta osteohondrāla pamatne: jauni biomimētiski aktivatori uzlabotai kaulu reģenerācijai, NANO-SCORES", 2018.–2021. g.

[3] Latvijas Zinātņu padomes fundamentālo un lietišķo pētījumu projekts Nr. lzp-2018/1-0238 "Biomimētiska hidroksilapatīta biosintēze *in vivo* – sintētisko kaulus aizvietojošo materiālu nākotne", 2018.–2021. g.

Darba struktūra un apjoms

Promocijas darbs ir tematiski vienota četru SCI publikāciju kopa ar kopsavilkumu latviešu un angļu valodā. Publikācijas ir uzrakstītas angļu valodā, to kopējais apjoms, ieskaitot elektroniski pieejamo informāciju, ir 34 lappuses.

Publikācijas un darba aprobācija

Promocijas darba rezultāti ir publicēti četrās SCI zinātniskajās publikācijās

1. **Vecstaudza, J.**, Locs, J. Effect of synthesis temperature and Ca/P ratios on specific surface area of amorphous calcium phosphate, *Key Engineering Materials*, 721, 2016, 172.–176. lpp. doi: 10.4028/www.scientific.net/KEM.721.172 (*Scopus*).
2. **Vecstaudza, J.**, Locs, J. Novel preparation route of stable amorphous calcium phosphate nanoparticles with high specific surface area, *Journal of Alloys and Compounds*, 700, 2017, 215.–222. lpp. doi: 10.1016/j.jallcom.2017.01.038 (*Scopus*).
3. **Vecstaudza, J.**, Gasik, M., Locs, J. Amorphous calcium phosphate materials: formation, structure and thermal behaviour, *Journal of the European Ceramic Society*, 39, 2019, 1642.–1649. lpp. doi: 10.1016/j.jeurceramsoc.2018.11.003 (*Scopus*, brīvpieejas publikācija).
4. Rubenis, K., Zemjane, S., **Vecstaudza, J.**, Bitenieks, J., Locs, J. Densification of amorphous calcium phosphate using principles of the cold sintering process, *Journal of the European Ceramic Society*, 41, 2021, 912.–919. lpp. doi: 10.1016/j.jeurceramsoc.2020.08.074 (*Scopus*, brīvpieejas publikācija).

Promocijas darba rezultāti ir prezentēti 18 zinātniskajās konferencēs

1. **Vecstaudza, J.**, Locs, J. Synthesis and characterization of amorphous calcium phosphate with biomimetic bone-like composition. *11th World Biomaterials Congress*, tiešsaiste, 11.–15. decembris, 2020 (stenda referāts).
2. **Vecstaudza, J.**, Locs, J. Amorphous calcium phosphate biomaterials for bone regeneration. *60th International Scientific Conference of RTU: Materials Science and Applied Chemistry*, Latvija, Rīga, 24. oktobris, 2019 (mutiskā prezentācija).
3. **Vecstaudza, J.**, Locs, J. Synthesis of amorphous calcium phosphate with biomimetic chemical composition. *30th Annual Conference of the European Society for Biomaterials*, Vācija, Drēzdene, 9.–13. septembris, 2019 (stenda referāts).
4. **Vecstaudza, J.**, Locs, J. Thermally treated carbonated amorphous calcium phosphate. *30th Annual Conference of the European Society for Biomaterials*, Vācija, Drēzdene, 9.–13. septembris, 2019 (stenda referāts).
5. **Vecstaudza, J.**, Locs, J. Biomimetic amorphous calcium phosphate. *XVI Conference of the European Ceramic Society*, Itālija, Turīna, 16.–20. jūnijs, 2019 (stenda referāts).
6. **Vecstaudza, J.**, Locs, J. Development of synthesis of amorphous calcium phosphate with biomimetic chemical composition. *Scandinavian Society for Biomaterials 2019 conference*, Somija, Kirkkonummi, 12.–14. jūnijs, 2019 (stenda referāts).

7. Makarova, E., **Vecstaudza, J.**, Vilskersts, R., Kupats, R., Kuka, J., Loca, D., Locs, J., Dambrova, M. Assessment of Biocompatibility and Osteoinductive Potential of Amorphous Calcium Phosphate in Mice: Experimental Model. *Rīga Stradiņš University International Conference on Medical and Health Care Sciences: Knowledge for Use in Practice*, Latvija, Rīga, 1.–3. aprīlis, 2019 (stenda referāts).
8. **Vecstaudza, J.**, Locs, J. Reduction of specific surface area of amorphous calcium phosphate during gradual heat treatments. *29th European Conference on Biomaterials ESB 2018*, Nīderlande, Māstrihta, 9.–13. septembris, 2018 (stenda referāts).
9. **Vecstaudza, J.**, Locs, J. Decrease of specific surface area of amorphous calcium phosphate during gradual heat treatments. *29th Symposium and Annual Meeting of the International Society for Ceramics in Medicine Bioceramics 29*. Francija, Tulūza, 25.–27. oktobris, 2017, 138. lpp. (stenda referāts).
10. **Vecstaudza, J.**, Locs, J. Impact of heat treatment on specific surface area of amorphous calcium phosphate. *58th International Scientific Conference of Riga Technical University*, Rīga, Latvija, 20. oktobris, 2017 (**labākais stenda referāts**).
11. **Vecstaudza, J.**, Locs, J. Calcium phosphate scaffolds with high specific surface area towards improved cell response in vitro. eCM Meeting Abstracts 2017, Collection 2; *TERMIS EU*, Šveice, Davosa, 26.–30. jūnijs, 2017, P809 (stenda referāts).
12. **Vecstaudza, J.**, Locs, J. Calcium phosphates with high specific surface area towards improved cell response *in vitro*, *10th annual meeting for Scandinavian Society for Biomaterials*, Norvēģija, Hafjella, 15.–17. marts, 2017 (stenda referāts).
13. **Vecstaudza, J.**, Locs, J. Novel preparation route of stable amorphous calcium phosphate nanoparticles with high specific surface area, *33rd Scientific Conference of the Institute of Solid State Physics*, Latvija, Rīga, 22.–24. februāris, 2017 (stenda referāts).
14. **Vecstaudza, J.**, Locs, J. Effect of synthesis temperature and Ca/P ratios on specific surface area of amorphous calcium phosphate. *25th International Baltic Conference Baltmattrib 2016*, Latvija, Rīga, 3.–4. novembris, 2016 (stenda referāts).
15. **Vecstaudza, J.**, Locs, J. Amorphous and low crystalline calcium phosphates for bone tissue regeneration, *57th International Scientific Conference of Riga Technical University*, Latvija, Rīga, 21. oktobris, 2016 (mutiskā prezentācija).
16. **Vecstaudza, J.**, Gasik, M., Locs, J. New biomimetic amorphous calcium phosphate biomaterials: structure and thermal properties. *The 2016 E-MRS Fall Meeting and Exhibition*, Polija, Varšava, 19.–22. septembris, 2016 (mutiskā prezentācija).
17. **Vecstaudza, J.**, Locs, J., Gasik, M. Biomimetic calcium phosphate nanoparticles with variable degree of crystallinity. *6th International congress on ceramics*, Vācija, Drēzdene, 21.–25. augusts, 2016 (stenda referāts).
18. **Vecstaudza, J.**, Locs, J. Rapid reprecipitation of nanosized calcium phosphates. *24th International Conference Baltmattrib 2015*. Igaunija, Tallina, 5.–6. novembris, 2015 (stenda referāts).

Dalība citās zinātniskajās konferencēs promocijas darba izstrādes laikā

1. Putnins, A., **Vecstaudza, J.**, Locs. J. Obtaining and characterization of C-shaped calcium phosphate granules for biomedical application. *9th International Granulation Workshop*, Šveice, Lozanna, 26.–28. jūnijs, 2019, 194. lpp. (stenda referāts).
2. Putnins, A., **Vecstaudza, J.**, Locs. J. Development of designed shape calcium phosphate granules. *9th International Granulation Workshop*, Šveice, Lozanna, 26.–28. jūnijs, 2019, 193. lpp. (stenda referāts).
3. Stīpniece, L., **Vecstaudža, J.**, Zālīte, V., Šalma-Ancāne, K., Loča, D., Bērziņa-Cimdiņa, L. Optimization of the Synthesis and Design of Calcium Phosphates for Biomedical Applications. *32nd Scientific Conference of the Institute of Solid State Physics*, Latvija, Rīga, 17.–19. februāris, 2016, 136. lpp. (stenda referāts).

Citas zinātniskās publikācijas, kas publicētas promocijas darba izstrādes laikā

1. Choudhary, R., Venkatraman, S. K., Chatterjee, A., **Vecstaudza, J.**, Yáñez-Gascón, M. J., Pérez-Sánchez, H., Locs, J., Abraham, J., Swamiappan, S. Biomineralization, antibacterial activity and mechanical properties of biowaste derived diopside nanopowders (2019) *Advanced Powder Technology*, 30 (9), 1950.–1964. lpp. doi: 10.1016/j.apt.2019.06.014 (*Scopus*).
2. Loca, D., Smirnova, A., Locs, J., Dubnika, A., **Vecstaudza, J.**, Stipniece, L., Makarova, E., Dambrova, M. Development of local strontium ranelate delivery systems and long term *in vitro* drug release studies in osteogenic medium (2018) *Scientific Reports*, 8 (1), Nr. 16754. doi: 10.1038/s41598-018-35197-7 (*Scopus*, brīvpieejas publikācija).
3. Choudhary, R., Manohar, P., **Vecstaudza, J.**, Yáñez-Gascón, M. J., Sánchez, H. P., Nachimuthu, R., Locs, J., Swamiappan, S. Preparation of nanocrystalline forsterite by combustion of different fuels and their comparative in-vitro bioactivity, dissolution behaviour and antibacterial studies (2017) *Materials Science and Engineering C*, 77, 811.–822. lpp. doi: 10.1016/j.msec.2017.03.308 (*Scopus*).
4. Stunda-Zujeva, A., **Vecstaudža, J.**, Krieķe, G., Bērziņa-Cimdiņa, L. Glass Formation and Crystallization in P_2O_5-Nb_2O_5-CaO-Na_2O System. *Materials Sciences and Applied Chemistry*, 2017, 34, 21.–28. lpp. doi: 10.1515/msac-2017-0003.
5. Choudhary, R., **Vecstaudza, J.**, Krishnamurithy, G., Raghavendran, H. R. B., Murali, M. R., Kamarul, T., Sasikumar, S., Locs, J. *In-vitro* bioactivity, biocompatibility and dissolution studies of diopside prepared from biowaste by using sol-gel combustion method (2016) *Materials Science and Engineering C*, 68, 89.–100. lpp. doi: 10.1016/j.msec.2016.04.110 (*Scopus*).

PROMOCIJAS DARBA GALVENIE REZULTĀTI

Reaģentu Ca/P molārās attiecības un sintēzes temperatūras ietekme uz *ACP* īpašībām

Analizējot zinātnisko literatūru konstatēts, ka amorfā kalcija fosfāta (*ACP*) sintēzes tehnoloģijas varētu modificēt tā, lai iegūtu produktu ar lielu īpatnējo virsmas laukumu ($\geq$100 m^2/g). Pēc turpmākas kalcija fosfātu (CaP) sintēžu protokolu analīzes identificēti divi sintēzes tehnoloģiskie parametri – reaģentu Ca/P molārā attiecība un sintēzes temperatūra, kas varētu ietekmēt *ACP* sintēzes produkta *SSA*. Visbiežāk *ACP* iegūst, izmantojot nogulsnēšanas metodi, piemēram, dubultās sāļu sadalīšanas metodi. Iepriekšminētajā metodē izmanto kalcija jonu un fosfātjonu saturošus ūdenī šķīstošu sāļu šķīdumus; abus šķīdumus sajauc vienā pie bāziska pH, tādā veidā nodrošinot *ACP* nogulsnēšanos. Šādā sintēzē var izmantot dažādus kalcija jonus un fosfātjonus saturošus sāļus, piemēram, $Ca(NO_3)_2 \cdot 4H_2O$ un $(NH_4)_2HPO_4$, $Ca(NO_3)_2 \cdot 4H_2O$ un $NH_4H_2PO_4$, $CaCl_2 \cdot 2H_2O$ un K_2HPO_4, $CaCl_2 \cdot 2H_2O$ un Na_2HPO_4 u. c.

Promocijas darbā *ACP* paraugi sintezēti ar dubultās sāļu sadalīšanas metodi, izmantojot $Ca(NO_3)_2 \cdot 4H_2O$ un $(NH_4)_2HPO_4$ (sāļi iegūti no *Sigma Aldrich*). Abu sāļu šķīdumi strauji salieti kopā un maisīti ar magnētisko maisītāju (1. att.). $Ca(NO_3)_2$ šķīduma koncentrācija visos eksperimentos bija 0,45 M. Lai noskaidrotu, vai, izmantojot dubultās sāļu sadalīšanas metodi, iespējams iegūt *ACP* ar paaugstinātu *SSA*, pārbaudīta šādu sintēzes tehnoloģisko parametru ietekme: 1) reaģentu Ca/P molārā attiecība (1,5; 1,67; 2,2); 2) sintēzes temperatūra (0 °C un 20 °C).

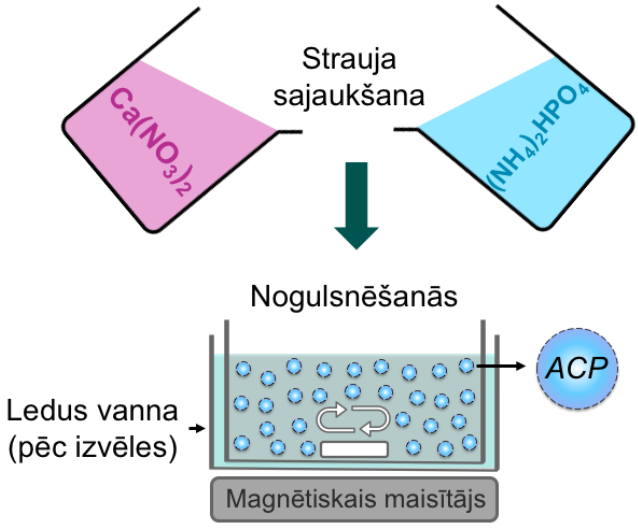

1. att. Vispārīga *ACP* sintēzes shēma, izmantojot dubultās sāļu sadalīšanas metodi.

Sintezēto un termiski apstrādāto (1100 °C, 1 h) *ACP* paraugu fāžu sastāvs pētīts, izmantojot rentgenstaru difraktometru *X'Pert Pro* (*PAnalytical*, Nīderlande). Kristālisko fāžu identifikācija veikta, izmantojot Starptautiskā Difrakcijas datu centra (*ICDD*) *PDF-2* datubāzi. Sintezēto paraugu īpatnējais virsmas laukums *SSA* (saīsinājums no angļu val.) noteikts ar Brunauera–Emmeta–Tellera (BET) metodi un *Quadrasorb SI* (*Quantachrome*, ASV) iekārtu.

Neatkarīgi no izvēlētās reaģentu Ca/P molārās attiecības (1,5; 1,67; 2,2) un sintēzes temperatūras (0 °C vai 20 °C) visu sintēžu produkti bija rentgenamorfi (2. a. att.). Termiski apstrādājot iegūtos *ACP* paraugus, to rentgenstaru difrakcijas (*XRD*) ainās identificēta β-trikalcija fosfāta (β-*TCP*, β-$Ca_3(PO_4)_2$) fāze vai β-*TCP* un α-trikalcija fosfāta (α-*TCP*, α-$Ca_3(PO_4)_2$) fāžu maisījums. Paraugos, kuros pēc termiskās apstrādes izveidojies α-*TCP* un β-*TCP* maisījums, dominējošā fāze bija β-*TCP*. Secināts, ka visu *ACP* paraugu Ca/P molārā attiecība bija 1,5 neatkarīgi no reaģentu Ca/P molārās attiecības un sintēzes temperatūras.

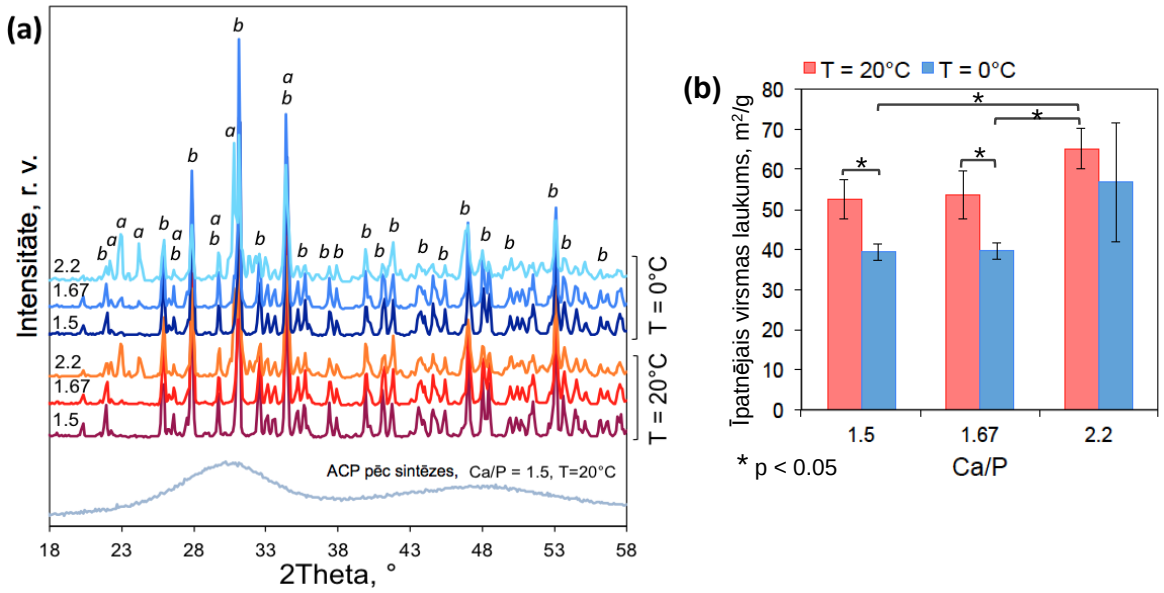

2. att. *XRD* ainas (a) sintezētam un termiski apstrādātam (1100 °C, 1 h) ACP, kur *a* – α-*TCP*, *b* – β-*TCP*; (b) īpatnējais virsmas laukums *ACP* paraugiem kā funkcija no sintēzes temperatūras un reaģentu Ca/P molārās attiecības [12].

Reaģentu Ca/P molārās attiecības un sintēzes temperatūras ietekme uz *ACP* paraugu *SSA* atainota 2. b att. Gan reaģentu Ca/P molārā attiecība, gan sintēzes temperatūra ietekmē *ACP*, kas iegūts ar dubultās sāļu sadalīšanas metodi, *SSA*. Lielāka Ca/P molārā attiecība sintēzes vidē nodrošināja *ACP* veidošanos ar lielāku vidējo *SSA* vērtību gan 0 °C, gan 20 °C temperatūrā. *ACP SSA* palielinājās no (53 ± 5) m^2/g līdz (65 ± 5) m^2/g 20 °C temperatūrā un no (39 ± 2) m^2/g līdz (57 ± 15) m^2/g 0 °C temperatūrā, ja reaģentu Ca/P molāro attiecību variēja robežās no 1,5 līdz 2,2. Visu iegūto paraugu Ca/P molārā attiecība bija 1,5, un tas norādīja uz to, ka kalcija jonu pārākums sintēzes vidē ir veicinājis CaP daļiņu ar lielāku *SSA* veidošanos. Augstākā iegūtā *SSA* vērtība *ACP* paraugam, kas sintezēts ar reaģentu Ca/P molāro attiecību 2,2 20 °C temperatūrā, sasniedza 65 m^2/g, kas arī nesasniedza paredzēto 100 m^2/g vērtību. Tādēļ nolemts pētīt un modificēt citas *ACP* sintēzes metodes, lai iegūtu produktu ar paredzēto *SSA* vērtību.

Iegūto rezultātu **novitāte** ir šāda: 1) *ACP* sintēze, izmantojot dubultās sāļu sadalīšanas metodi bez stabilizējošiem aģentiem zemākā temperatūrā (0 °C) nekā iepriekš ziņots literatūrā; 2) reaģentu Ca/P molārās attiecības ietekmes novērtējums uz *ACP SSA*. Turklāt zinātniskajā literatūrā tika identificēts sistemātisku pētījumu trūkums par CaP, it īpaši *ACP*, *SSA*, līdz ar to šis promocijas darbs papildina kopējo zināšanu bāzi.

Sintēzes metodes izstrāde *ACP* ar lielu īpatnējo virsmas laukumu iegūšanai

Sintezējot *ACP* ar dubultās sāļu sadalīšanas metodi, **divi šķīdumi** tiek sajaukti **vienā**, tāpēc tika izvirzīta hipotēze, ka **viena** kalcija jonus un fosfātjonu saturoša šķīduma izmantošana ir efektīva pieeja CaP ar paaugstinātu *SSA* iegūšanai. Pateicoties sākotnējai kalcija jonu un fosfātjonu homogenitātei, notiktu viendabīgu daļiņu nogulsnēšanās un augšana, līdz ar to tiktu iegūts CaP ar paaugstināts *SSA*. Līdzīgu hipotēzi par homogenizētu izejvielu šķīdumu piedāvāja *E. D. Eanes* un *E. L. Meyer* [13], kur bāzisks KOH šķīdums tika strauji pievienots paskābinātam kalcija jonu un fosfātjonu sāļu šķīdumam, izraisot CaP nogulsnēšanos.

Šajā promocijas darbā izstrādātajai sintēzes metodei, lai iegūtu *ACP* ar lielu *SSA*, ir divi etapi: 1) homogēna šķīduma, kas satur gan kalcija, gan fosfāta jonus, iegūšanas, izšķīdinot hidroksilapatītu sālsskābē; 2) straujas stipras bāzes pievienošanas kalcija un fosfāta jonu saturošajam šķīdumam un pH paaugstināšanas (3. att.). Otrā etapa laikā norisinās *ACP* nogulsnēšanās.

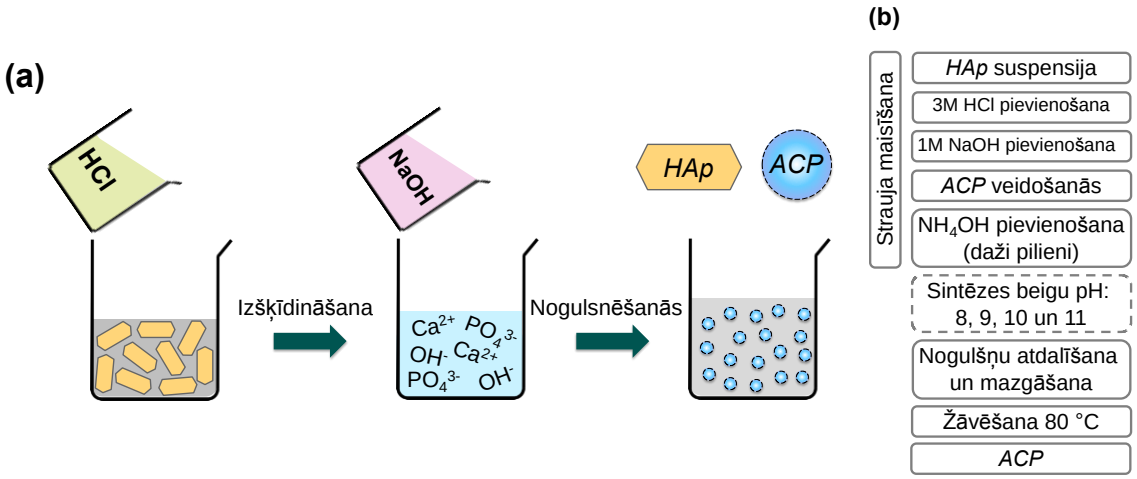

3. att. *ACP* sintēzes galvenie etapi (a) un detalizēta sintēzes gaita (b). Autores attēli. Sintēzes shēma balstīta uz *J. Vecstaudza* un *J. Locs* [14] attēlu.

Zināms, ka sintēzes vides pH piemīt nozīmīga ietekme uz ar nogulsnēšanas metodēm iegūtu CaP fāžu sastāvu. Tāpēc pētīta sintēzes beigu pH vērtības (8, 9, 10 un 11) ietekme uz ar izstrādāto metodi nogulsnēto produktu fāžu sastāvu, ķīmisko struktūru un *SSA*. Sintēzēs iegūtie materiāli raksturoti, izmantojot *XRD* (*X'Pert Pro, PAnalytical*, Nīderlande), Furjē transformāciju infrasarkanās spektrometrijas (*FT-IR, Scimitar 800, Varian Inc.*, ASV) un BET (*Quadrasorb SI, Quantachrome*, ASV) metodes. Sintezēto materiālu ilgtermiņa stabilitāte tika pētīta, izmantojot *XRD*. Kristāliskās fāzes tika identificētas, izmantojot *ICDD PDF-2* datubāzi; fāžu kvantitatīvo sastāvs tika noteikts ar Rietvelda metodi. Paraugu Ca/P molārā attiecība tika aprēķināta, balstoties uz kvantitatīvās fāžu analīzes datiem. Vidējo daļiņu diametrs d_{BET} tika aprēķināts saskaņā ar 1. vienādojumu, pieņemot, ka daļiņas ir sfēriskas un bez porām:

$$d_{BET} = 6/(\rho \cdot SSA), \quad (1.)$$

kur ρ – R-*HAp* blīvums (2,81 g/cm^3);

SSA – īpatnējais virsmas laukums (noteikts ar BET).

Nanoizmēra karbonāta jonus saturoši kalcija fosfāti (CaPi) ar amorfu vai mazkristālisku struktūru iegūti, izmantojot metodi, kas balstīta uz strauju pH palielināšanu kalcija un fosfāta jonus saturošā šķīdumā un nogulšņu žāvēšanu 80 °C temperatūrā. *ACP* fāze iegūta pie sintēzes beigu pH vērtībām 10 un 11; savukārt mazkristāliski CaPi iegūti pie sintēzes beigu vērtībām 8 un 9 (4. a att.). Attiecīgo materiālu ķīmisko grupu sastāvam arī novērota atkarība no sintēzes beigu pH (4. b att.) un *XRD* ainās novērotās atšķirības papildināja informācija, kas iegūta, analizējot *FT-IR* spektrus. Visos pētīto paraugu *FT-IR* spektros konstatēta karbonāta jonu grupu klātbūtne. Gan fāžu, gan ķīmisko grupu sastāva analīzes parādīja, ka *ACP*, kas iegūts ar izstrādāto metodi, ir derīgs žāvēšanai 80 °C temperatūrā, jo, nogulsnēts pie noteikta pH, tas saglabā amorfo fāzi. Iepriekšminētais ieguvums var noderēt *ACP* sintēzes mērogošanai un vēlākai komercializēšanai, pateicoties ievērojami īsākam apstrādes laikam, jo tradicionāli metastabilo *ACP* žāvē ar liofilizēšanas paņēmienu 48–72 h.

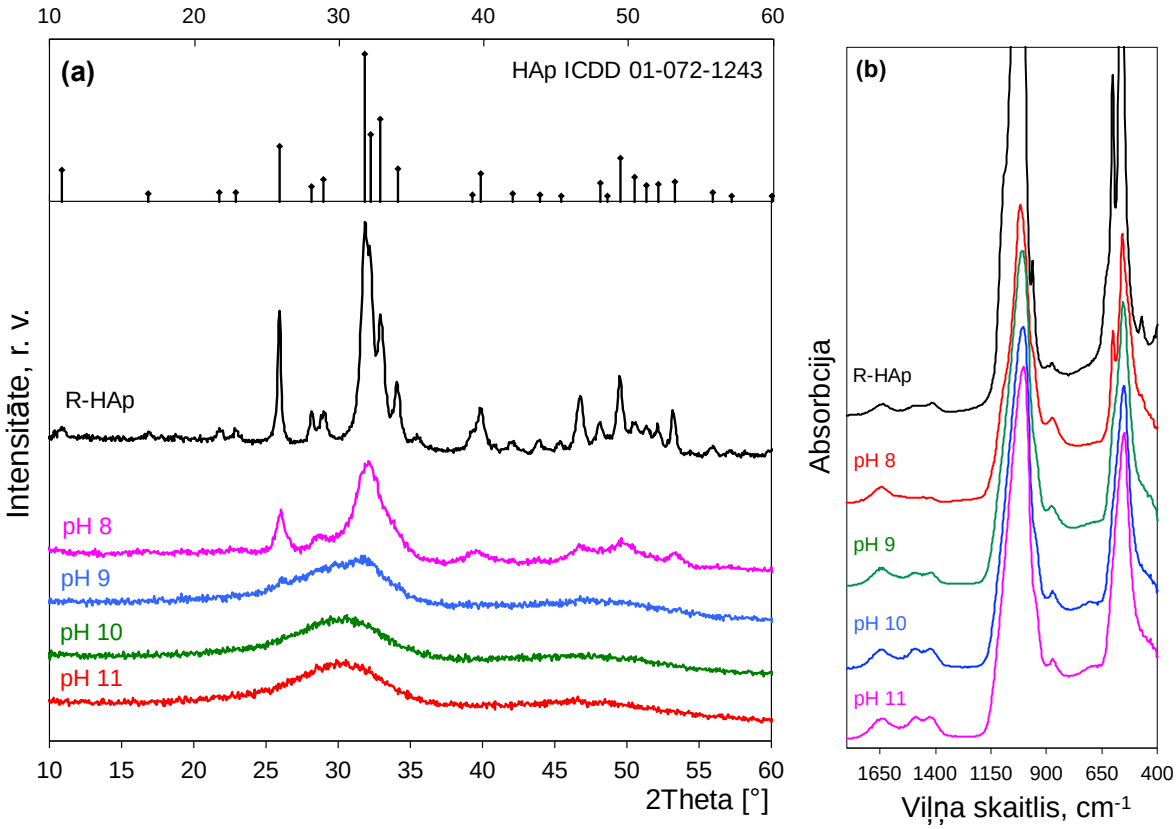

4. att. Rentgenstaru difrakcijas ainas (a) un *FT-IR* spektri, kas attēloti 1700–400 cm^{-1} diapazonā (b) kalcija fosfātiem, kas iegūti dažādos pH un žāvēti 80 °C temperatūrā, un R-*HAp* references paraugam [14].

Noteikts, ka iegūto kalcija fosfātu *SSA* ir robežās no 133 m^2/g līdz 154 m^2/g (1. tab.), kas izpilda definēto mērķi – iegūt *ACP* ar *SSA* ≥ 100 m^2/g. Savukārt aprēķinātais daļiņu izmērs d_{BET} ir robežās no 14 nm līdz 16 nm. Korelācija starp *SSA* un *ACP* sintēzes beigu pH netika konstatēta (rezultāti statistiski neatšķirās).

1. tabula

Iegūto kalcija fosfātu raksturlielumi, kur d_{BET} – daļiņu izmērs, *SSA* – īpatnējais virsmas laukums [14]

Paraugs	Sintēzes beigu pH	d_{BET}, nm	*SSA*, m^2/g
ACP-8	8	14 ± 1	154 ± 9
ACP-9	9	15 ± 1	141 ± 8
ACP-10	10	16 ± 3	133 ± 25
ACP-11	11	15 ± 3	150 ± 28
R-*HAp*	8,8	22 ± 1	95 ± 3

Neatkarīgi no sākotnējās Ca/P molārās attiecības sintēzes šķīdumā (visos gadījumos Ca/P = 1,67) termiski apstrādātu (1100 °C, 1 h) *ACP* sastāvā konstatēta dažādu fāžu veidošanās: β-*TCP* (pH = 8 un pH = 9) vai β-*TCP*/*HAp* (pH = 10 un pH = 11). Termiski apstrādātu paraugu Ca/P molārās attiecības vērtības redzamas 2. tabulā. Secināts, ka parauga Ca/P molāro attiecību ietekmē sintēzes beigu pH vērtība. Parauga Ca/P molārā attiecība pieaug līdz ar sintēzes beigu pH vērtību. Ca/P molārās attiecības pieaugums skaidrojams ar to, ka termiskās apstrādes laikā karbonāta joni atstāja CaP struktūru. Zināms, ka CaP sintēzēs pH ir viens no noteicošajiem faktoriem konkrēta sastāva produkta iegūšanai, kas apstiprinās arī šajā pētījumā.

2. tabula

Termiski apstrādātu paraugu kristālisko fāžu sastāvs un to Ca/P molārā attiecība [14]

Paraugs	Sintēzes beigu pH	β-*TCP*, masas %	*Hap*, masas %	Ca/P molārā attiecība
ACP-8	8	100	–	1,50
ACP-9	9	100	–	1,50
ACP-10	10	95,2 ± 1,5	4,8 ± 1,5	1,51
ACP-11	11	90,3 ± 1,6	9,7 ± 1,6	1,61

Iegūtie CaP paraugi sausā stāvoklī ir stabili vismaz septiņus mēnešus (5. att.), ja to sintēzes beigu pH ir pH = 8, pH = 10 un pH = 11. Ja sintēzes beigu pH ir 9, pēc pieciem mēnešiem sākas kristalizācija pēc iekšējās hidrolīzes mehānisma. Paraugu, kuru sintēzēs beigu pH bija pH = 10 un pH = 11, stabilitāti var izskaidrot ar karbonāta jonu iekļaušanos to struktūrā, tādējādi palielinot to Ca/P molāro attiecību. Līdz ar to karbonātu jonus saturoši *ACP* materiāli ar paaugstinātu Ca/P molāro attiecību (>1,50) uzrādīja stabilu amorfo fāzi ilgtermiņā.

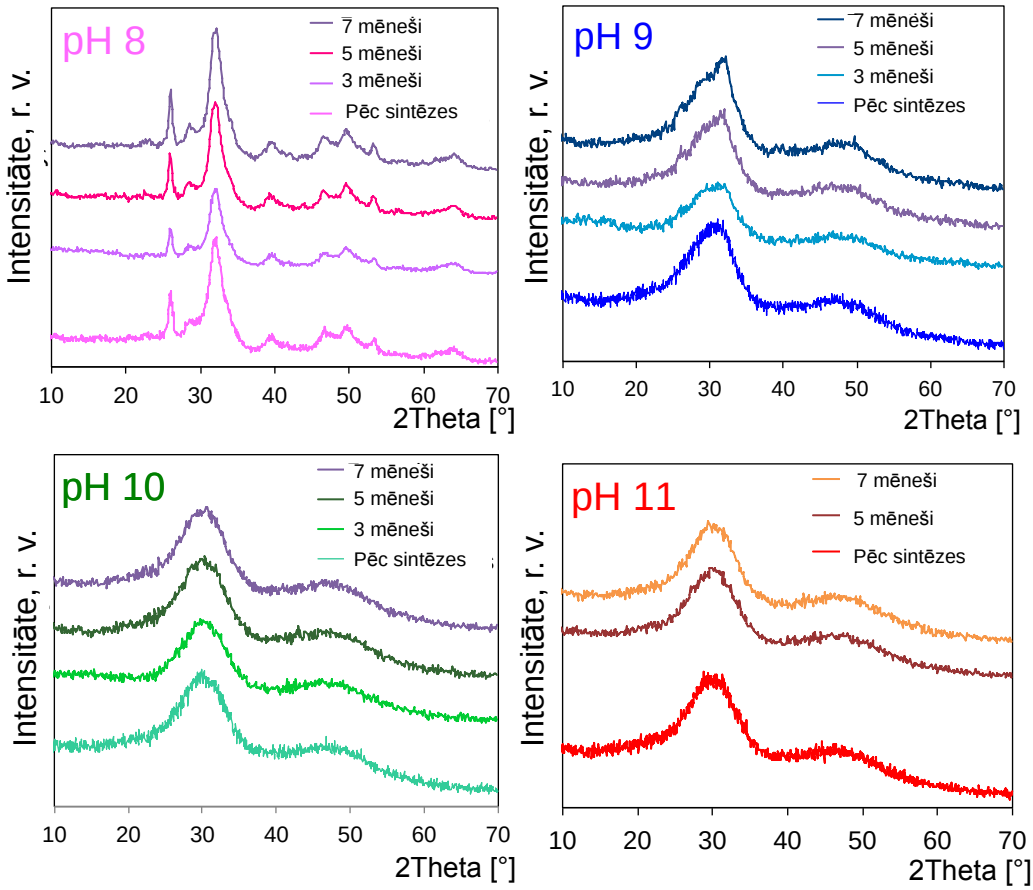

5. att. *XRD* ainas mazkristāliskiem un amorfiem CaP, kas iegūti dažādos pH un žāvēti 80 °C temperatūrā: uzreiz pēc sintēzes un pēc trim, pieciem un septiņiem mēnešiem [14].

Ar dažādām metodēm žāvētu *ACP* materiālu termiskās īpašības

Izmantojot izstrādāto sintēzes metodi, *ACP* iespējams izžāvēt 80 °C temperatūrā (1 h), un šajā gadījumā laikietilpīgā (72 h) liofilizēšanas žāvēšana nav nepieciešama, lai saglabātu amorfo struktūru. Tomēr ar izstrādāto metodi iegūtie CaPi tika izžāvēti arī ar liofilizēšanas paņēmienu, un veikts fizikālķīmisko īpašību salīdzinājums ar 80 °C temperatūrā žāvētiem CaP.

Visi liofilizētie paraugi bija rentgenamorfi neatkarīgi no sintēzes beigu pH vērtības. Tomēr liofilizētie pulveri vizuāli atšķīrās no 80 °C temperatūrā žāvētiem CaP (6. att.), kur brīvi plūstoši un apjomīgi pulveri tika iegūti liofilizēšanas gadījumā un aglomerēti pulveri – žāvējot 80 °C. 80 °C temperatūrā žāvētie paraugi (apzīmējums "*Ov*") veidoti no lielāka izmēra daļiņām un aizņēma mazāku tilpumu nekā liofilizētie (apzīmējums "*FrD*") paraugi. Apkopojot iepriekšminēto, tika formulēta hipotēze, ka ar dažādām metodēm žāvēts *ACP* kristalizējas atšķirīgās fāzēs, ko izraisa ar rutīnas analīzes metodēm (piemēram, *XRD* un *FT-IR*) neizšķiramas struktūras atšķirības. Iespējamās atšķirības ar dažādām metodēm žāvētiem CaP analizētas to kristalizācijas procesā, izmantojot termogravimetrijas (*TGA*) un diferenciāli skenējošās kalorimetrijas (*DSC*) metodes.

DSC-TGA mērījumiem izmantota *STA449C Jupiter*® (*Netzsch*, Vācija) iekārta. Salīdzināšanai izmantoti divi paraugi: n-*HAp* (nanokristālisks *HAp*, *Sigma Aldrich*) un R-*HAp* (iegūts RTU RBIAC), abi satur tikai *HAp*.

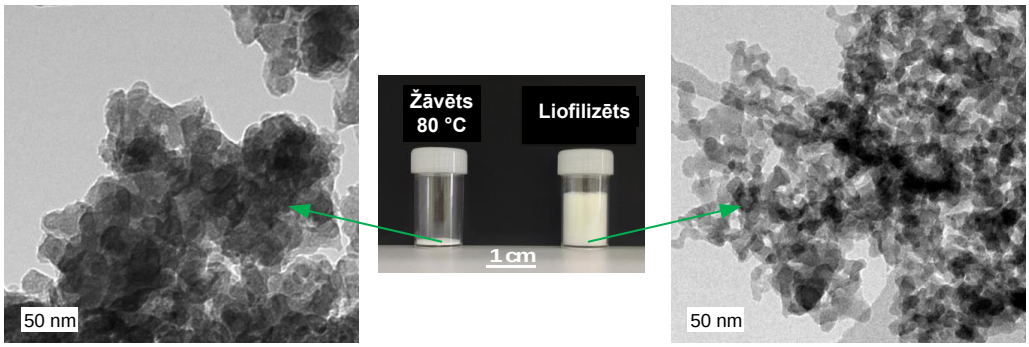

6. att. Fotogrāfijas un TEM attēli žāvēšanas skapī žāvētiem 80 °C (pa kreisi) un liofilizētiem (pa labi) *ACP* paraugiem ar vienādu svaru [15], sintēzes beigu pH = 10.

Ov un *FrD ACP* paraugu *TGA* līknes redzamas 7. attēlā. Novērotie masas zudumi ir pakāpeniski un bez straujām izmaiņām visiem *Ov* un *FrD* paraugiem. Savukārt kopējā masas zuduma vērtība paraugiem, kas iegūti sintēzēs ar dažādu sintēzes beigu pH vērtību, atšķiras, piemēram, skat. masas zudumus 800 °C temperatūrā.

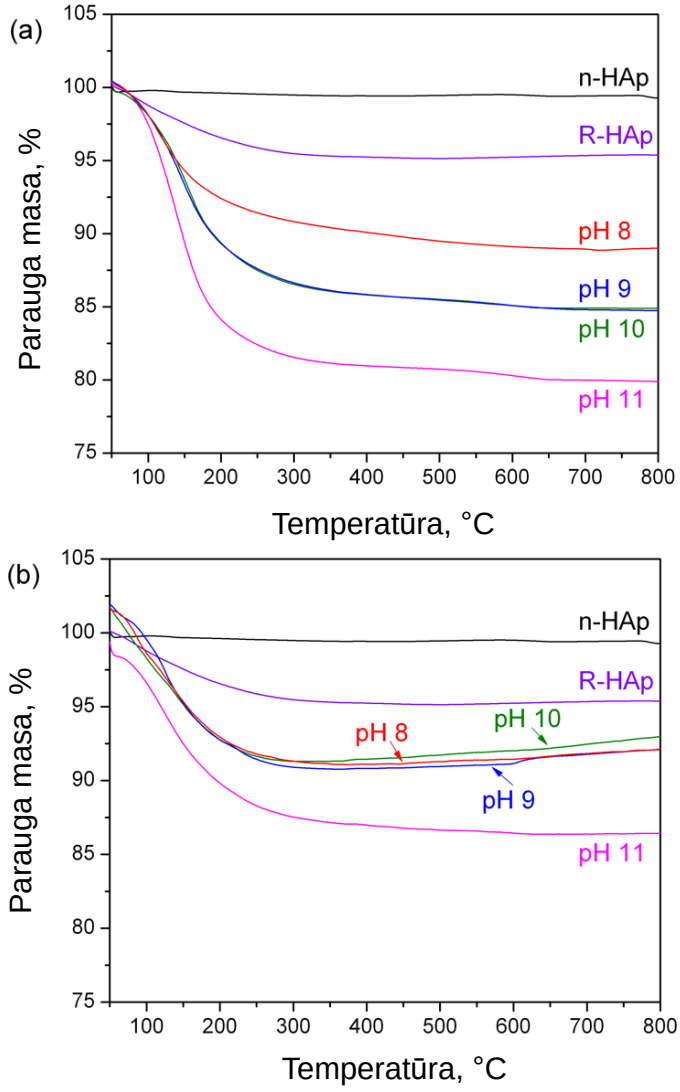

7. att. *TGA* līknes (a) 80 °C temperatūrā žāvētiem un (b) liofilizētiem *ACP* paraugiem temperatūru diapazonā no 50 °C līdz 800 °C; n-*HAp* un R-*HAp* ir references paraugi [15].

Abu žāvēšanas metožu salīdzinājumā konstatēts, ka *Ov* paraugi satur lielāku daudzumu fizikāli adsorbētā ūdens, kas izzūd līdz 200 °C temperatūrai (7. att.). Tas pats novērojums attiecās arī uz kopējo masas zudumu, kas noteikts pie 1200 °C. Kopējais masas zudums *Ov* paraugiem bija diapazonā no 11 masas % līdz 20 masas %, kur lielāki masas zudumi bija *Ov* paraugiem, kas iegūti pie augstāka sintēzes beigu pH. Savukārt *FrD* paraugu kopējo masas zudumu lielākā noteiktā vērtība bija 14 masas % paraugam, kas iegūts pie pH = 11. *FrD* paraugiem, kas iegūti pie pH = 8–10, kopējo masas zudumu vērtības bija līdzīgas un sintēzes beigu pH ietekme netika novērota.

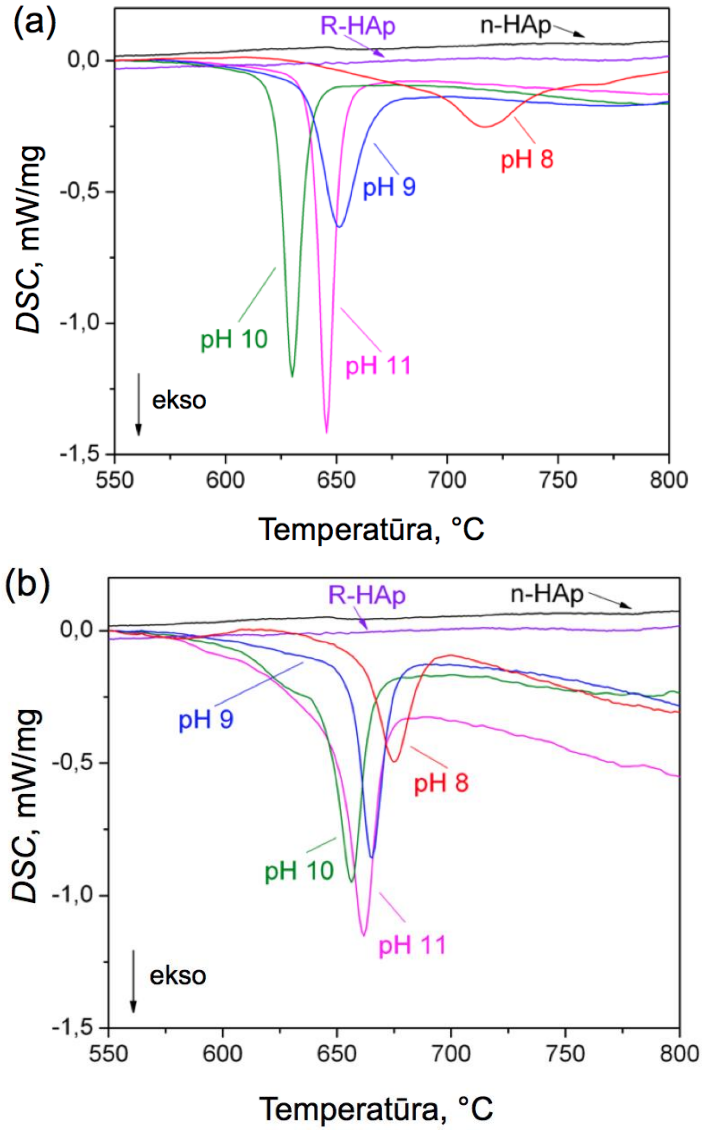

8. att. *DSC* līknes (a) 80 °C temperatūrā žāvētiem un (b) liofilizētiem *ACP* paraugiem temperatūru diapazonā no 550 °C līdz 800 °C; n-*HAp* un R-*HAp* ir references paraugi [15].

Visu *Ov* un *FrD* paraugu *DSC* līknēs novēroti eksotermiski kristalizēšanās efekti (8. att.). Šo efektu temperatūru diapazonā no 630 °C līdz 720 °C *ACP* pārveidojās kristāliskos CaP, ar dominējošo fāzi β-*TCP*. Pētīto *ACP* materiālu $T_{krist.sāk.}$ bija diapazonā no 600 °C līdz 650 °C; korelāciju starp kristalizācijas temperatūrām ($T_{krist.sāk.}$ un $T_{krist.beigu}$) un žāvēšanas metodēm vai sintēzes pH nenovēroja. *TGA* un *DSC* līkņu analīze norādīja, ka termiski ierosināta *ACP*

kristalizācija nav saistīta ar vienlaicīgu masas zudumu. *ACP* kristalizācija sākās par 150–200 °C augstākā temperatūrā nekā *TGA* līknē novērotais straujākais masas zudums (līdz 400 °C).

ACP sablīvēšana, izmantojot aukstās saķepināšanas procesa principus

Kaulam piemīt ne tikai unikāls fāžu un ķīmiskais sastāvs, bet arī unikāla fizikālā struktūra, kas veidota gan no blīviem, gan porainiem kaula apgabaliem. Līdz šim joprojām nav izdevies saķepināt *ACP* biokeramiku ar augstu relatīvo blīvumu, neietekmējot tā amorfo un hidratēto struktūru un īpašības. *ACP* sablīvēšanai ir izmantotas alternatīvas saķepināšanas metodes, piemēram, hidrotermiskā karstā presēšana un zemas temperatūras dzirksteles plazmas saķepināšana. Tomēr, pat izmantojot šīs tehnoloģijas, *ACP* sablīvēšana ir apgrūtinoša. Nesen dažādu pulveru saķepināšanai zemā temperatūrā (≤300 °C) sākts izmantot aukstās saķepināšanas process *CSP* (angļu val. – *cold sintering process*). Lai sablīvētu pulveri, izmantojot *CSP*, izmanto pārejas šķīdumu, uniaksiālu spiedienu un karstumu. Līdz ar to šī promocijas darba ietvaros pētīts *CSP* metodes lietojums *ACP* sablīvēšanai.

Lai noskaidrotu optimālos *CSP* tehnoloģiskos parametrus blīvas *ACP* biokeramikas iegūšanai, variēti šādi tehnoloģiskie parametri: 1) pārejas šķīduma (ūdens, 20 masas %) esamība vai neesamība; 2) saķepināšanas temperatūra (istabas temperatūra, 100 °C, 120 °C un 150 °C). Katrā *CSP* eksperimentā 0,5 g iepriekš sagatavota *ACP* pulvera (žāvēts 80 °C, 24 h) ievietoti viegli izjaucamā presēšanas formā (*ID* = 13 mm, *Across International*, ASV). Izmantots *ACP* ar augstu *SSA*, kas sintezēts saskaņā ar iepriekš izstrādāto sintēzes protokolu [14] un žāvēts, izmantojot liofilizēšanas paņēmienu. *ACP* pulvera samitrināšana veikta manuāli, izmantojot ahāta piestu un piestalu. *CSP* process veikts ar divu kolonnu laboratorijas presi *PW 40* (*P/O/WEBER*, Vācija), presējot uniaksiāli ar 500 MPa spiedienu. Katrs paraugs izgatavots vismaz trīs paralēlos atkārtojumos. *CSP* eksperimentālo apstākļu kopsavilkums redzams 9. attēlā.

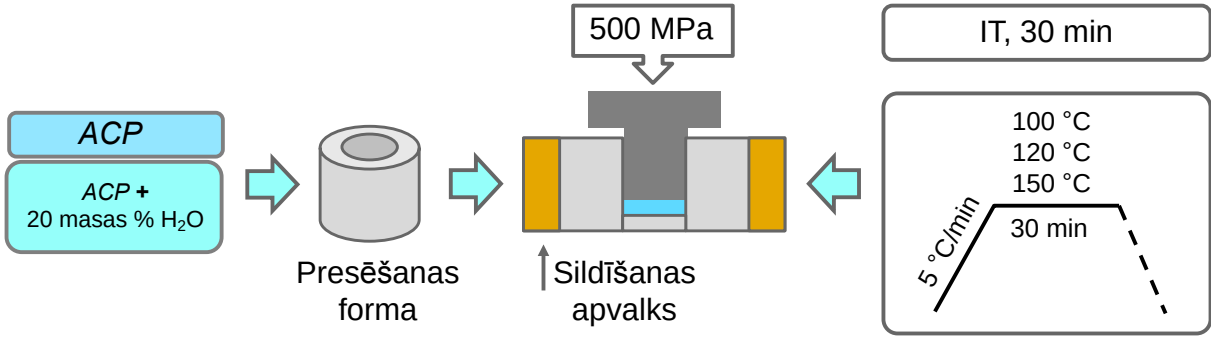

9. att. *ACP* sablīvēšana, izmantojot *CSP* principus, kur IT – istabas temperatūra.

Sintezētais *ACP* pulveris un ar *CSP* saķepinātie paraugi analizēti ar *XRD* (*X'Pert Pro, PAnalytical*, Nīderlande) un BET (*Quadrasorb SI, Quantachrome*, ASV) metodēm, lai noteiktu to fāžu sastāvu un *SSA*. Lai novērtētu *CSP* ietekmi uz paraugu sablīvēšanos, noteiktas paraugu šķietamā un relatīvā blīvuma vērtības, izmantojot hēlija piknometru *Micro UltraPyc 1200e* (*Quantachrome Instruments*, ASV). Pirms mērījumiem *CSP* saķepinātie

paraugi tika žāvēti (80 °C, 24 h) un samalti smalkā pulverī, izmantojot *Mini-Mill Pulverisette 23* (*FRITCH*, Vācija) vienas bumbas dzirnavas (3 min).

CSP ietekme uz *ACP* fāzes stabilitāti novērtēta, izmantojot *XRD* (10. att.). Pārejas šķīduma klātbūtne (ūdens, 20 masas %) veicināja *ACP* kristalizāciju nanokristāliska *HAp* fāzē. Kristalizācija notika zemākās temperatūrās (kristalizējās 100 °C), salīdzinot ar sausu *ACP* pulveri (kristalizējās 150 °C). Gan temperatūra, gan spiediens varēja aktivēt virsmas difūzijas procesus, kas veicināja fāžu pāreju no *ACP* uz nanokristālisku *HAp*.

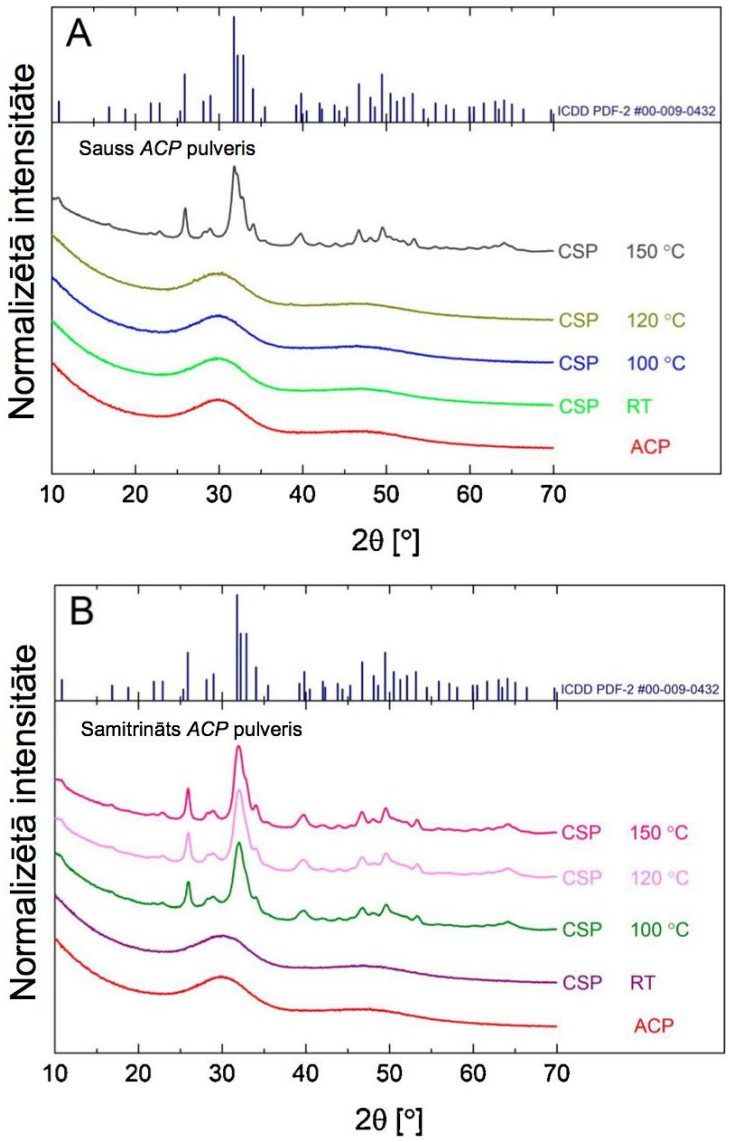

10. att. *XRD* ainas *ACP* pulverim un ar *CSP* saķepinātiem paraugiem, kas izgatavoti no sausa (A) un no samitrināta (B) *ACP* pulvera [16].

Ar *CSP* saķepinātu paraugu *SSA* samazinājās aptuveni piecas reizes (11. att.), salīdzinot ar sintezētā *ACP* pulvera *SSA* (109 $m^2/g \pm 11$ m^2/g). Konstatētais *SSA* samazinājums liecina par daļiņu saplūšanu *CSP* laikā. Turklāt nepilnīga sablīvēšanās izveido starpdaļiņu (slēgto) porainību ar virsmu, kas ir nepieejama BET mērījumos izmantotajai slāpekļa gāzei.

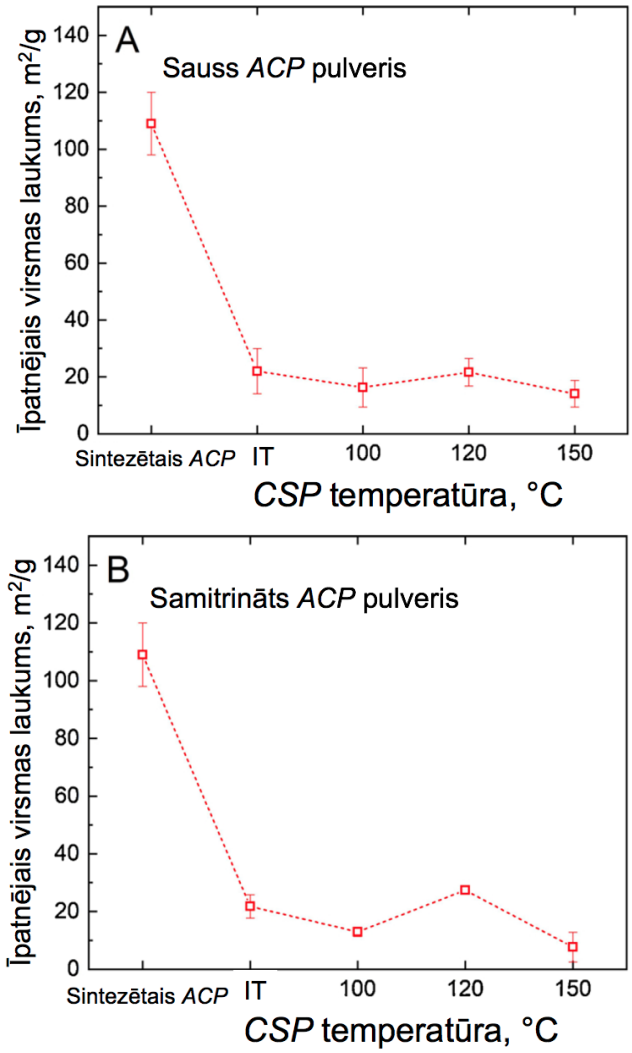

11. att. Īpatnējais virsmas laukums *ACP* pulverim un ar *CSP* saķepinātiem paraugiem, kas izgatavoti no sausa (A) un no samitrināta (B) *ACP* pulvera [16].

Izmantojot *CSP* principus, mērens, uniaksiāli lietots 500 MPa spiediens istabas temperatūrā nodrošināja *ACP* saķepināšanu līdz relatīvi augstam blīvumam (12. att.). Saķepināšanas temperatūras palielināšanai bija neliela ietekme uz paraugu, kas bija saglabājis amorfu struktūru pēc *CSP*, blīvuma vērtībām (10. att.). Secināms, ka zemās *CSP* saķepināšanas temperatūras nebija pietiekamas, lai uzlabotu sablīvēšanos caur difūzijas procesiem. Literatūrā atrodamā augstākā relatīvā blīvuma vērtība *ACP* keramikai ir ~45 % [17]. Šajā pētījumā ar *CSP* saķepinātas *ACP* keramikas relatīvais blīvums sasniedza vairāk nekā 75 %.

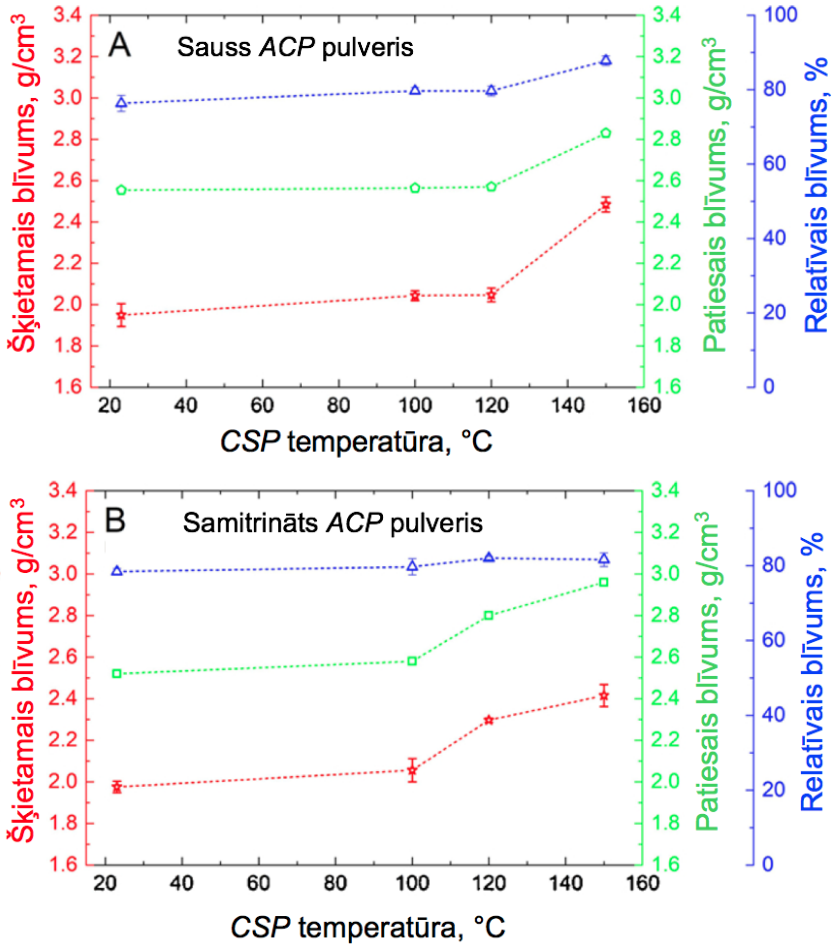

12. att. Šķietamais, patiesais un relatīvais blīvums ar *CSP* saķepinātiem paraugiem, kas izgatavoti no sausa (A) un no samitināta (B) *ACP* pulvera [16].

SECINĀJUMI

1. Sintezējot amorfo kalcija fosfātu ar dubultās sāļu sadalīšanas metodi no $Ca(NO_3)_2$ un $(NH_4)_2HPO_4$ un variējot izejvielu Ca/P molāro attiecību (1,5, 1,67 vai 2,2) un sintēzes temperatūru (0 °C vai 20 °C), būtisks īpatnējā virsmas laukuma palielinājums nav konstatēts, kā arī izejvielu Ca/P molārā attiecība neietekmē iegūtā amorfā kalcija fosfāta Ca/P molāro attiecību.
2. Ir izstrādāta vienkārša, ātra un rentabla sintēzes metode amorfu vai daļēji kristālisku kalcija fosfātu iegūšanai ar lielu īpatnējo virsmas laukumu ($\geq$100 m^2/g), kas balstīta uz strauju pH vērtības paaugstināšanu sintēzes vidē, kas satur gan kalcija, gan fosfāta jonus.
3. Amorfa kalcija fosfāta izgulsnēšanas pH (8–11) un žāvēšanas metode (liofilizēšana vai žāvēšana 80 °C temperatūrā) termiskās apstrādes laikā neietekmē amorfā kalcija fosfāta kristalizācijas temperatūru, kas novērojama no 600 °C līdz 650 °C, bet ietekmē ar ūdens zaudēšanu saistītos masas zudumus.
4. Amorfa kalcija fosfāta materiāliem ar paaugstinātu Ca/P molāro attiecību (>1,50), tos uzglabājot istabas temperatūrā, piemīt ilgtermiņa stabilitāte.
5. Izmantojot aukstās saķepināšanas procesa principus, ir iespējams iegūt blīvu amorfa kalcija fosfāta keramiku ļoti zemās temperatūrās (istabas, 100 °C un 120 °C), presējot uniaksiāli 500 MPa spiedienā.

ATSAUCES

[1] K. Pawelec, J. A. Planell, *Bone Repair Biomaterials: Regeneration and Clinical Applications*, 2.izd. Woodhead Publishing, 2018.

[2] A. Tsetsekou, D. Brasinika, V. Vaou, E. Chatzitheodoridis, "On the synthesis of tailored biomimetic hydroxyapatite nanoplates through a bioinspired approach in the presence of collagen or chitosan and L-arginine.," *Mater. Sci. Eng. C. Mater. Biol. Appl.*, vol. 43, pp. 555–65, Oct. 2014.

[3] M. J. Olszta *et al.*, "Bone structure and formation: A new perspective," *Mater. Sci. Eng. R Reports*, vol. 58, no. 3–5, pp. 77–116, 2007.

[4] S. Bose, S. Tarafder, "Calcium phosphate ceramic systems in growth factor and drug delivery for bone tissue engineering: a review," *Acta Biomater.*, vol. 8, no. 4, pp. 1401–21, 2012.

[5] H.-S. Sohn, J.-K. Oh, "Review of bone graft and bone substitutes with an emphasis on fracture surgeries," *Biomater. Res.*, vol. 23, no. 1, p. 9, Dec. 2019.

[6] D. S. H. Lee, Y. Pai, S. Chang, "Physicochemical characterization of InterOss® and Bio-Oss® anorganic bovine bone grafting material for oral surgery – A comparative study," *Mater. Chem. Phys.*, vol. 146, no. 1–2, pp. 99–104, Jul. 2014.

[7] J. Kolmas, A. Ślósarczyk, A. Wojtowicz, W. Kolodziejski, "Estimation of the specific surface area of apatites in human mineralized tissues using 31P MAS NMR," *Solid State Nucl. Magn. Reson.*, vol. 32, no. 2, pp. 53–58, 2007.

[8] R. Duan *et al.*, "Variation of the bone forming ability with the physicochemical properties of calcium phosphate bone substitutes," *Biomater. Sci.*, vol. 6, no. 1, pp. 136–145, 2018.

[9] D. Xiao *et al.*, "The role of calcium phosphate surface structure in osteogenesis and the mechanisms involved," *Acta Biomater.*, vol. 106, pp. 22–33, Apr. 2020.

[10] J. Mahamid, A. Sharir, L. Addadi, S. Weiner, "Amorphous calcium phosphate is a major component of the forming fin bones of zebrafish: Indications for an amorphous precursor phase," *Proc. Nat. Acad. Sci. USA*, vol. 105, no. 35, pp. 12748–12753, 2008.

[11] R. Gelli, F. Ridi, P. Baglioni, "The importance of being amorphous: calcium and magnesium phosphates in the human body," *Adv. Colloid Interface Sci.*, vol. 269, pp. 219–235, 2019.

[12] J. Vecstaudza, J. Locs, "Effect of Synthesis Temperature and Ca/P Ratios on Specific Surface Area of Amorphous Calcium Phosphate," *Key Eng. Mater.*, vol. 721, pp. 172–176, 2016.

[13] E. D. Eanes, "Amorphous Calcium Phosphate: Thermodynamic and Kinetic Considerations," in *Calcium Phosphates in Biological and Industrial Systems*, Boston, MA: Springer US, 1998, pp. 21–39.

[14] J. Vecstaudza, J. Locs, "Novel preparation route of stable amorphous calcium phosphate nanoparticles with high specific surface area," *J. Alloys Compd.*, vol. 700, pp. 215–222, 2017.

[15] J. Vecstaudza, M. Gasik, J. Locs, "Amorphous calcium phosphate materials: Formation, structure and thermal behaviour," *J. Eur. Ceram. Soc.*, Nov. 2018.

[16] K. Rubenis, S. Zemjane, J. Vecstaudza, J. Bitenieks, J. Locs, "Densification of amorphous calcium phosphate using principles of the cold sintering process," *J. Eur. Ceram. Soc.*, vol. 41, no. 1, pp. 912–919, 2021.

[17] M. Luginina *et al.*, "First successful stabilization of consolidated amorphous calcium phosphate (ACP) by cold sintering: toward highly-resorbable reactive bioceramics," *J. Mater. Chem. B*, vol. 8, no. 4, pp. 629–635, 2020.

DOCTORAL THESIS PROPOSED TO RIGA TECHNICAL UNIVERSITY FOR THE PROMOTION TO THE SCIENTIFIC DEGREE OF DOCTOR OF SCIENCE

To be granted the scientific degree of Doctor of Science (Ph. D.), the present Doctoral Thesis has been submitted for the defence at the open meeting of RTU Promotion Council at 15:00 on June 21, 2021 at the Faculty of Materials Science and Applied Chemistry of Riga Technical University, 3/7 Paula Valdena Street, Room 272.

OFFICIAL REVIEWERS

Lead Researcher Dr. habil. sc. ing. Jānis Grabis,
Riga Technical University, Latvia

Associate Professor Dr. med. Laura Neimane,
Rīga Stradiņš University, Latvia

Professor Ph. D. Christèle Combes,
Institut National Polytechnique de Toulouse, CIRIMAT, France

DECLARATION OF ACADEMIC INTEGRITY

I hereby declare that the Doctoral Thesis submitted for the review to Riga Technical University for the promotion to the scientific degree of Doctor of Science (Ph. D.) is my own. I confirm that this Doctoral Thesis had not been submitted to any other university for the promotion to a scientific degree.

Jana Vecstaudža ……. (signature)

Date: ……

The Doctoral Thesis has been written as collection of articles. It consists of summary in Latvian and English and four SCI publications. Publications are written in English with total volume of 34 pages including electronically available supplementary information.

CONTENTS

GENERAL OVERVIEW OF THE THESIS

Introduction

Due to increasing number of patients that encounter musculoskeletal system traumas, bone related diseases and pathologies worldwide [1], there is ongoing need for more effective biomaterials for bone treatment and replacement. These biomaterials should resemble the composition and structure of natural bone. Due to the unique chemical composition and structure of bone, it has not been artificially imitated so that the properties of produced biomaterial would be comparable to the bone [2]. The bone is composed of inorganic (75 wt. %, including 10 wt. % water) and organic (25 wt. %) components [3]. The inorganic part of the bone is composed of nanosized calcium phosphate particles that are embedded within the organic matrix. It is known that calcium phosphates have very high biocompatibility with human tissue and body environment [4]. Therefore, calcium phosphates are promising substituents of the inorganic part of the bone; and they can be synthesized in laboratory and used for the development of new and effective biomaterials.

However, the *gold* standard in bone regeneration is autograft, i.e., bone tissue from the same patient. Another popular option is to use xenograft, e.g., commercially available deproteinized bovine bone mineral (DBBM) materials, to avoid shortcomings of the autograft (several operation sites, pain, prolonged inability to work, etc.) [5]. DBBM materials are successful because of their micro and nano structures having high specific surface area (up to 88 m^2/g [6]), which is close to the value of specific surface area of the calcium phosphate particles found in bone (40–240 m^2/g [7]). Meanwhile, commercial calcium phosphate biomaterials are still far behind (up to 3 m^2/g [8]). High specific surface area is critical for bioactive molecule (e.g., protein and cytokine) adsorption on surface of biomaterials [9] that further promotes material integration and tissue regeneration. Synthetic calcium phosphates offer high purity, availability and repeatability and are not of animal origin. Therefore, scientific community carries out in-depth studies of calcium phosphates – synthesis, physicochemical properties and processing thereof, as well as performs *in vitro, in vivo* and clinical studies.

Amorphous calcium phosphate is the first inorganic phase that forms during a new bone formation [10]. Furthermore, amorphous calcium phosphate is designated as the first or an intermediate phase in formation of other calcium phosphates, e.g., hydroxyapatite. So far, the amorphous calcium phosphate is rarely used as stand-alone biomaterial due to its metastability; over time and under influence of other factors it crystallizes into other calcium phosphate phases [11]. In this PhD Thesis it is shown that it is possible to obtain stable amorphous calcium phosphate, thus significantly widening its potential applications in biomaterials research.

In the current PhD Thesis, novel synthesis method of stable amorphous calcium phosphate with high specific surface area (≥100 m^2/g) was developed and physicochemical properties were characterized. Crystallization of the amorphous calcium phosphate has been studied in conjunction with technological parameters of the synthesis (synthesis pH and drying method). Further, the amorphous calcium phosphate was successfully sintered into dense bioceramics using the principles of cold sintering, thus preserving the amorphous structure thereof.

Aim and Objectives

The aim of the Thesis was to develop a synthesis technology for obtaining stable amorphous calcium phosphate with high specific surface area and study formation, crystallization and sintering thereof. In order to fulfill the aim, the following objectives were set.

1. To study the impact of synthesis temperature and Ca/P molar ratio of reagents on the specific surface area of amorphous calcium phosphate obtained by the double salt decomposition method.
2. To develop a synthesis method for obtaining amorphous calcium phosphate with high specific surface area ($\geq$100 m^2/g).
3. To study the impact of drying method (freeze-drying or drying at 80 °C temperature) on the structure and crystallization of amorphous calcium phosphate.
4. To study long term stability of amorphous calcium phosphate at room temperature.
5. To study sintering of amorphous calcium phosphate using principles of cold sintering process.

Thesis to Defend

1. Rapid increase of pH up to pH = 10–11 of calcium and phosphate ions containing solution ensures precipitation of amorphous calcium phosphate with high specific surface area ($\geq$100 m^2/g).
2. Ca/P molar ratio larger than 1.5 of amorphous calcium phosphate precipitated at pH = 10–11 ensures its long-term stability at room temperature.

Scientific Novelty

New, simple, fast and cost-effective synthesis method of long-term stable amorphous calcium phosphate with high specific surface area has been demonstrated and physicochemical properties of the obtained products have been characterized.

Practical Significance

Long-term stable amorphous calcium phosphate was obtained and studied, and applicability thereof was found in the development of nanostructured granules[1]:

1) with strontium ions for improvement of performance of osteochondral implants[2],
2) with biomimetic chemical composition that will ensure biosynthesis of biological calcium phosphate after implantation *in vivo*[3].

---

[1] Collaborative project between RTU and RSU "Development of nanostructured bone substituting materials and studies of immunologic aspects in bone regeneration", 2016–2019.

[2] EuroNanoMed III project "NANOstructured oSteoChOndral scaffold: novel biomimetic tRiggErS for enhanced bone regeneration", 2018–2021.

[3] Latvian Council of Science project No lzp-2018/1-0238 "Future of synthetic bone graft materials – *in vivo* guided biosynthesis of biomimetic hydroxyapatite", 2018–2021.

Structure of the Thesis

The Thesis is a collection of four SCI publications with a summary in Latvian and English. Publications are written in English; total volume of which is 34 pages, including electronically available supplementary information.

Publications and Approbation of the Thesis

Results of the Thesis are published in four SCI scientific publications

1. **Vecstaudza, J.**, Locs, J. Effect of synthesis temperature and Ca/P ratios on specific surface area of amorphous calcium phosphate, *Key Engineering Materials*, 721, 2016, pp. 172–176. doi: 10.4028/www.scientific.net/KEM.721.172 (Scopus).
2. **Vecstaudza, J.**, Locs, J. Novel preparation route of stable amorphous calcium phosphate nanoparticles with high specific surface area, *Journal of Alloys and Compounds*, 700, 2017, pp. 215–222. doi: 10.1016/j.jallcom.2017.01.038 (Scopus).
3. **Vecstaudza, J.**, Gasik, M., Locs, J. Amorphous calcium phosphate materials: formation, structure and thermal behaviour, *Journal of the European Ceramic Society*, 39, 2019, pp. 1642–1649. doi: 10.1016/j.jeurceramsoc.2018.11.003 (Scopus, Open Access).
4. Rubenis, K., Zemjane, S., **Vecstaudza, J.**, Bitenieks, J., Locs, J. Densification of amorphous calcium phosphate using principles of the cold sintering process, *Journal of the European Ceramic Society*, 41, 2021, pp. 912–919. doi: 10.1016/j.jeurceramsoc.2020.08.074 (Scopus, Open Access).

Results of the Thesis were presented at 18 scientific conferences

1. **Vecstaudza, J.**, Locs, J. Synthesis and characterization of amorphous calcium phosphate with biomimetic bone-like composition. *11th World Biomaterials Congress*, Virtual event, 11–15 December 2020 (poster).
2. **Vecstaudza, J.**, Locs, J. Amorphous calcium phosphate biomaterials for bone regeneration. *60th International Scientific Conference of RTU: Materials Science and Applied Chemistry*, Latvia, Riga, October 24, 2019 (oral presentation).
3. **Vecstaudza, J.**, Locs, J. Synthesis of amorphous calcium phosphate with biomimetic chemical composition. *30th Annual Conference of the European Society for Biomaterials*, Germany, Dresden, 9–13 September 2019 (poster).
4. **Vecstaudza, J.**, Locs, J. Thermally treated carbonated amorphous calcium phosphate. *30th Annual Conference of the European Society for Biomaterials*, Germany, Dresden, 9–13 September 2019 (poster).
5. **Vecstaudza, J.**, Locs, J. Biomimetic amorphous calcium phosphate. *XVI Conference of the European Ceramic Society*, Italy, Turin, 16–20 June 2019 (poster).
6. **Vecstaudza, J.**, Locs, J. Development of synthesis of amorphous calcium phosphate with biomimetic chemical composition. *Scandinavian Society for Biomaterials 2019 conference*, Finland, Kirkkonummi, 12–14 June 2019 (poster).

7. Makarova, E., **Vecstaudza, J.**, Vilskersts, R., Kupats, R., Kuka, J., Loca, D., Locs, J., Dambrova, M. Assessment of Biocompatibility and Osteoinductive Potential of Amorphous Calcium Phosphate in Mice: Experimental Model. *Rīga Stradiņš University International Conference on Medical and Health Care Sciences: Knowledge for Use in Practice*, Latvia, Riga, 1–3 April 2019 (poster).
8. **Vecstaudza, J.**, Locs, J. Reduction of specific surface area of amorphous calcium phosphate during gradual heat treatments. *29th European Conference on Biomaterials ESB 2018*, the Netherlands, Maastricht, 9–13 September 2018 (poster).
9. **Vecstaudza, J.**, Locs, J. Decrease of specific surface area of amorphous calcium phosphate during gradual heat treatments. *29th Symposium and Annual Meeting of the International Society for Ceramics in Medicine Bioceramics 29*: Book of Abstracts, France, Toulouse, 25–27 October 2017, p. 138 (poster).
10. **Vecstaudza, J.**, Locs, J. Impact of heat treatment on specific surface area of amorphous calcium phosphate. *58th International Scientific Conference of Riga Technical University*, Riga, Latvia, October 20, 2017 (**best poster award**).
11. **Vecstaudza, J.**, Locs, J. Calcium phosphate scaffolds with high specific surface area towards improved cell response in vitro. eCM Meeting Abstracts 2017, Collection 2; *TERMIS EU*, Switzerland, Davos, 26–30 June 2017, P809 (poster).
12. **Vecstaudza, J.**, Locs, J. Calcium phosphates with high specific surface area towards improved cell response *in vitro*, *10th annual meeting for Scandinavian Society for Biomaterials*, Norway, Hafjell, 15–17 March 2017 (poster).
13. **Vecstaudza, J.**, Locs, J. Novel preparation route of stable amorphous calcium phosphate nanoparticles with high specific surface area, *33rd Scientific Conference of the Institute of Solid State Physics*, Latvia, Riga, 22–24 February 2017 (poster).
14. **Vecstaudza, J.**, Locs, J. Effect of synthesis temperature and Ca/P ratios on specific surface area of amorphous calcium phosphate. *25th International Baltic Conference Baltmattrib 2016*, Latvia, Riga, 3–4 November 2016 (poster).
15. **Vecstaudza, J.**, Locs, J. Amorphous and low crystalline calcium phosphates for bone tissue regeneration, *57th International Scientific Conference of Riga Technical University*, Latvia, Riga, October 21, 2016 (oral presentation).
16. **Vecstaudza, J.**, Gasik, M., Locs, J. New biomimetic amorphous calcium phosphate biomaterials: structure and thermal properties. *The 2016 E-MRS Fall Meeting and Exhibition*, Poland, Warsaw, 19–22 September 2016 (oral presentation).
17. **Vecstaudza, J.**, Locs, J., Gasik, M. Biomimetic calcium phosphate nanoparticles with variable degree of crystallinity. *6th International congress on ceramics*, Germany, Dresden, 21–25 August 2016 (poster).
18. **Vecstaudza, J.**, Locs, J. Rapid reprecipitation of nanosized calcium phosphates. *24th International Conference Baltmattrib 2015*. Estonia, Tallinn, 5–6 November 2015 (poster).

Participation at other scientific conferences during development of the Ph. D. Thesis

1. Putnins, A., **Vecstaudza, J.**, Locs. J. Obtaining and characterization of C-shaped calcium phosphate granules for biomedical application. *9th International Granulation Workshop*, Switzerland, Lausanne, 26–28 June 2019, p. 194 (poster).
2. Putnins, A., **Vecstaudza, J.**, Locs. J. Development of designed shape calcium phosphate granules. *9th International Granulation Workshop*, Switzerland, Lausanne, 26–28 June 2019, p. 193 (poster).
3. Stīpniece, L., **Vecstaudža, J.**, Zālīte, V., Šalma-Ancāne, K., Loča, D., Bērziņa-Cimdiņa, L. Optimization of the Synthesis and Design of Calcium Phosphates for Biomedical Applications. *The 32nd Scientific Conference of the Institute of Solid State Physics*, Latvia, Riga, 17–19 February 2016, p. 136 (poster).

Other scientific publications published during development of the Ph. D. Thesis

1. Choudhary, R., Venkatraman, S. K., Chatterjee, A., **Vecstaudza, J.**, Yáñez-Gascón, M. J., Pérez-Sánchez, H., Locs, J., Abraham, J., Swamiappan, S. Biomineralization, antibacterial activity and mechanical properties of biowaste derived diopside nanopowders (2019) *Advanced Powder Technology*, 30 (9), pp. 1950–1964. doi: 10.1016/j.apt.2019.06.014 (Scopus).
2. Loca, D., Smirnova, A., Locs, J., Dubnika, A., **Vecstaudza, J.**, Stipniece, L., Makarova, E., Dambrova, M. Development of local strontium ranelate delivery systems and long term *in vitro* drug release studies in osteogenic medium (2018) *Scientific Reports*, 8 (1), art. no. 16754. doi: 10.1038/s41598-018-35197-7 (Scopus, Open Access).
3. Choudhary, R., Manohar, P., **Vecstaudza, J.**, Yáñez-Gascón, M. J., Sánchez, H. P., Nachimuthu, R., Locs, J., Swamiappan, S. Preparation of nanocrystalline forsterite by combustion of different fuels and their comparative in-vitro bioactivity, dissolution behaviour and antibacterial studies (2017) *Materials Science and Engineering C*, 77, pp. 811–822. doi: 10.1016/j.msec.2017.03.308 (Scopus).
4. Stunda-Zujeva, A., **Vecstaudža, J.**, Krieķe, G., Bērziņa-Cimdiņa, L. Glass Formation and Crystallization in P_2O_5-Nb_2O_5-CaO-Na_2O System. *Materials Sciences and Applied Chemistry*, 2017, 34, pp. 21–28. doi: 10.1515/msac-2017-0003.
5. Choudhary, R., **Vecstaudza, J.**, Krishnamurithy, G., Raghavendran, H. R. B., Murali, M. R., Kamarul, T., Sasikumar, S., Locs, J. *In-vitro* bioactivity, biocompatibility and dissolution studies of diopside prepared from biowaste by using sol-gel combustion method (2016) *Materials Science and Engineering C*, 68, pp. 89–100. doi: 10.1016/j.msec.2016.04.110 (Scopus).

MAIN RESULTS OF THE THESIS

Effect of Ca/P Molar Ratio of Reagents and Synthesis Temperature on the Properties of ACP

Literature analysis showed that synthesis technologies of amorphous calcium phosphate (ACP) could be modified in order to obtain product with high specific surface area (SSA) (≥100 m^2/g). Further analysis on calcium phosphate (CaP) synthesis protocols highlighted two technological parameters of synthesis – Ca/P molar ratio of reagents and synthesis temperature, that could have impact on the SSA of the product of ACP synthesis. Usually, ACP is obtained by precipitation method, e.g., double salt decomposition method. For this method calcium and phosphate ion containing water soluble salt solutions are used; both solutions are combined into one at a basic pH, thus ensuring precipitation of ACP. In such synthesis variety of calcium and phosphate ion containing salts may be used, e. g., $Ca(NO_3)_2 \cdot 4H_2O$ and $(NH_4)_2HPO_4$, $Ca(NO_3)_2 \cdot 4H_2O$ and $NH_4H_2PO_4$, $CaCl_2 \cdot 2H_2O$ and K_2HPO_4, $CaCl_2 \cdot 2H_2O$ and Na_2HPO_4, etc.

In the PhD Thesis ACP samples were synthesized by the double salt decomposition method where solutions of $Ca(NO_3)_2 \cdot 4H_2O$ and $(NH_4)_2HPO_4$ (both salts purchased from Sigma Aldrich) were rapidly poured together under rapid mixing with magnetic stirrer (Fig. 1). Molarity of the $Ca(NO_3)_2$ was kept 0.45 M in all experiments. In order to evaluate whether it is possible to obtain ACP with high SSA using double salt decomposition method, effect of the following technological parameters was studied: 1) **Ca/P molar ratio of reagents** (1.5, 1.67 and 2.2) and 2) **synthesis temperature** (0 °C and 20 °C).

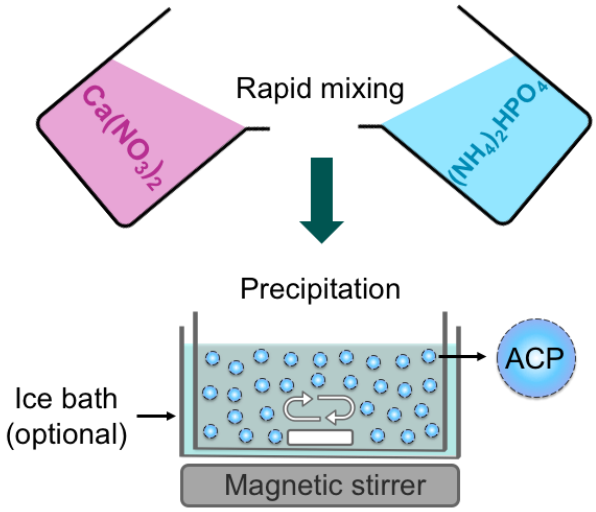

Fig. 1. General scheme of ACP synthesis by double salt decomposition method.

As-synthesized and heat treated (1100 °C, 1 h) samples were studied for their phase composition using x-ray diffractometer X'Pert Pro (PAnalytical, the Netherlands). Crystalline phase identification was done using PDF-2 database from International Centre for Diffraction Data (ICDD). SSA of the as-synthesized samples was determined using Brunauer–Emmett–Teller (BET) method and Quadrasorb SI (Quantachrome, USA) instrument.

Regardless of Ca/P molar ratio (1.5, 1.67 or 2.2) of reagents and synthesis temperature (0 °C or 20 °C), all synthesis products were x-ray amorphous (Fig. 2 (a)). In x-ray diffraction (XRD) patterns of the heat-treated ACP samples (Fig. 2 (a)) only β-tricalcium phosphate (β-TCP, β-$Ca_3(PO_4)_2$) or mixture of β-TCP and α-tricalcium phosphate (α-TCP, α -$Ca_3(PO_4)_2$) phases were identified. In samples where mixture of α-TCP and β-TCP was identified the dominant phase was β-TCP. Hence, the Ca/P molar ratio of all ACP samples was 1.5 regardless of the Ca/P molar ratio of the reagents and synthesis temperature.

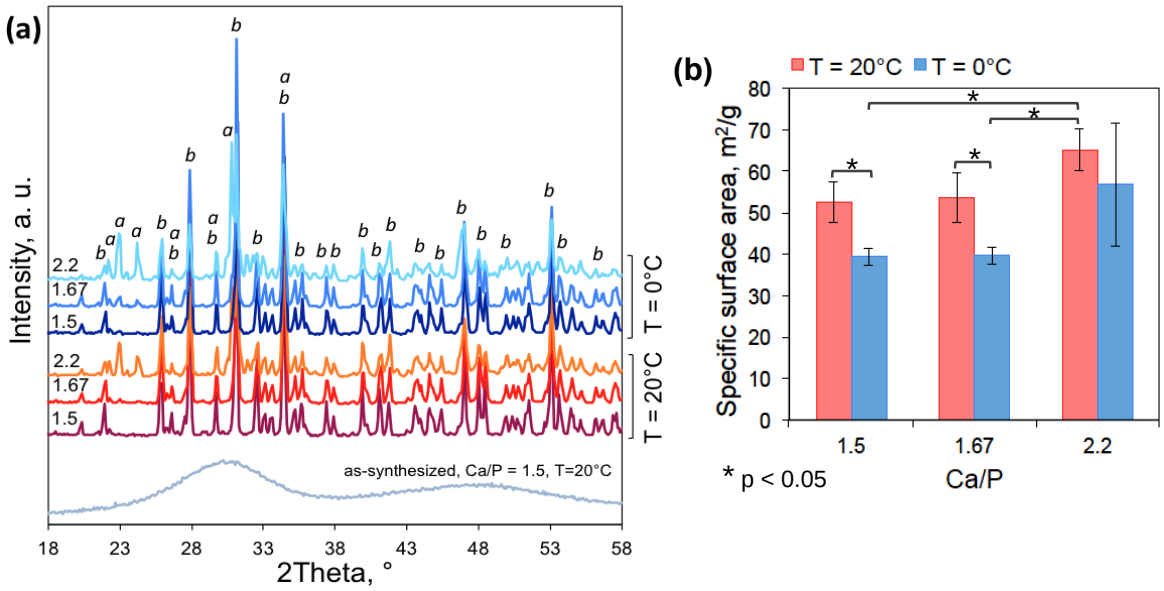

Fig. 2. XRD patterns (a) of as-synthesized and heat treated (1100 °C, 1 h) ACP, where *a* – α-TCP, *b* - β-TCP; (b) specific surface area of ACP samples as a function of synthesis temperature and Ca/P molar ratio of reagents [12].

Fig. 2 (b) presents the influence of Ca/P molar ratio of reagents and synthesis temperature on SSA of ACP. Both Ca/P molar ratio of reagents and synthesis temperature have influence on SSA of ACP obtained by double salt decomposition method. Higher initial Ca/P ratio produced ACP with higher average value of SSA both at 0 °C and 20 °C temperature. Overall, it was possible to increase SSA of ACP from (53 ± 5) m^2/g to (65 ± 5) m^2/g at 20 °C and from (39 ± 2) m^2/g to (57 ± 15) m^2/g at 0 °C by varying Ca/P molar ratio of reagents from 1.5 till 2.2. As all samples had Ca/P of 1.5, it suggested that excess of calcium ions in synthesis media has fostered formation of particles with higher SSA. The highest SSA value was for ACP synthesized from reagents with Ca/P molar ratio of 2.2 at 20 °C – 65 m^2/g which did not reach the expected value of 100 m^2/g. Therefore, other synthesis methods of ACP should be explored and modified in order to synthesize the product with intended value of SSA.

The novelty of the obtained results is twofold: 1) synthesis of ACP using double salt decomposition method without stabilizing agents at a lower temperature (0 °C) than reported in the literature before and 2) assessment of an impact of Ca/P molar ratio of the reagents on the SSA of ACP. Furthermore, as systematic studies on SSA of CaPs, especially ACP, were lacking in the literature, the current PhD Thesis partially filled the identified gap of knowledge.

Development of Synthesis Method for Obtaining ACP with High Specific Surface Area

In the double salt decomposition method of ACP synthesis **two solutions** are joined into *one*, thus it was hypothesized that use of a **single solution** containing both calcium and phosphate ions is efficient for obtaining CaPs with higher SSA. The initial homogeneity of calcium and phosphate ions would lead to uniform formation and growth of precipitated particles and thus to CaP with high SSA. Similar hypothesis of homogenized reactant solution was presented by E. D. Eanes and E. L. Meyer [13], where basic solution of KOH was rapidly added to an acidic mix of calcium and phosphate salts inducing precipitation of CaP.

In the current PhD Thesis, the developed synthesis method for obtaining ACP with high SSA consists of two steps: 1) obtaining of homogenous solution containing both calcium and phosphate ions by dissolving hydroxyapatite in hydrochloric acid and 2) rapid addition of strong base to the solution of calcium and phosphate ions and rise of pH (Fig. 3). The second step is immediately proceeded with precipitation of ACP.

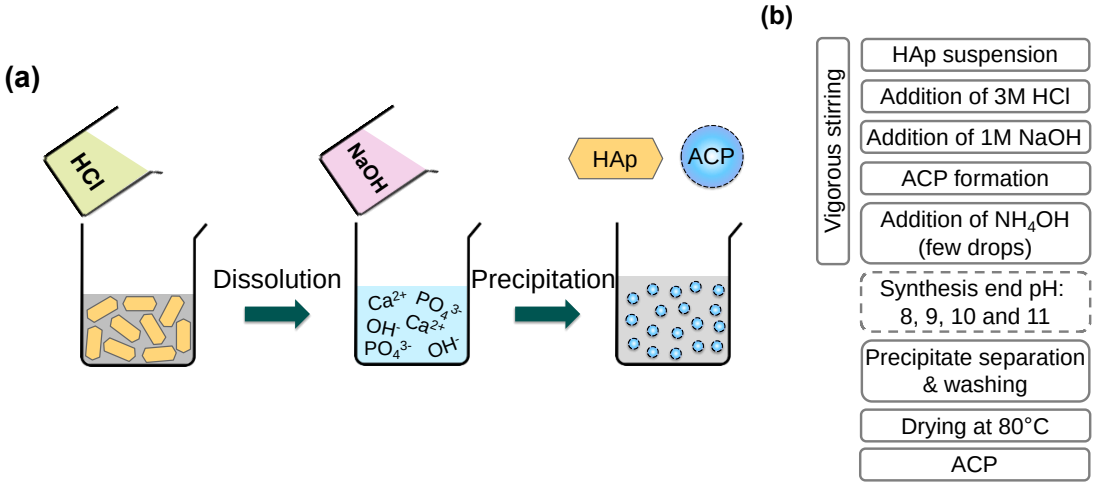

Fig. 3. Main steps (a) and detailed overview (b) of ACP synthesis (developed by author). Synthesis scheme is based on the image by J. Vecstaudza and J. Locs [14].

It is known that pH of the synthesis medium has a significant effect on CaP phase composition obtained by precipitation methods, therefore effects of synthesis end pH (8, 9, 10 and 11) on phase composition, chemical structure and SSA of the products obtained by the developed precipitation method were studied. The synthesized materials were characterized using XRD (X'Pert Pro, PAnalytical, the Netherlands), Fourier transform infrared spectrometry (FT-IR, Scimitar 800, Varian Inc., USA) and BET (Quadrasorb SI, Quantachrome, USA) methods. In addition, long-term phase stability of synthesized materials was studied using XRD. Crystalline phases were identified using ICDD PDF-2 database; phases were quantified using Rietveld refinement. Ca/P molar ratio of the samples was calculated based on quantitative phase analysis. Calculation of average particle diameter d_{BET} was done according to Equation (1) assuming particles to be spherical and nonporous:

$$d_{BET} = 6/(\rho \cdot SSA), \quad (1)$$

where ρ is the density of R-HAp (2.81 g/cm^3), SSA is a specific surface area (determined by BET).

Nanosized carbonated calcium phosphates (CaPs) with amorphous or low crystalline structure were obtained by a novel method based on fast pH increase of calcium and phosphate ions containing solution and drying of precipitates at 80 °C temperature. Phase of ACP was obtained at synthesis end pH values of 10 and 11; in turn, low crystalline CaPs were obtained at synthesis end pH values of 8 and 9 (Fig. 4 (a)). Chemical composition of respective materials was dependent on synthesis end pH as well (Fig. 4 (b)); differences observed in XRD patterns were complemented by information gained from FT-IR spectra. Furthermore, FT-IR spectra revealed presence of carbonate groups within all studied samples. Both the phase and chemical group composition analysis showed that ACP synthesized by the developed method is valid for drying at 80 °C temperature, as it remains amorphous when precipitated at certain pH. Later advancement holds promise for upscaling of ACP synthesis and later commercialization due to substantially shorter processing time, as usually, the metastable ACP is dried using lyophilization technique for 48–72 h.

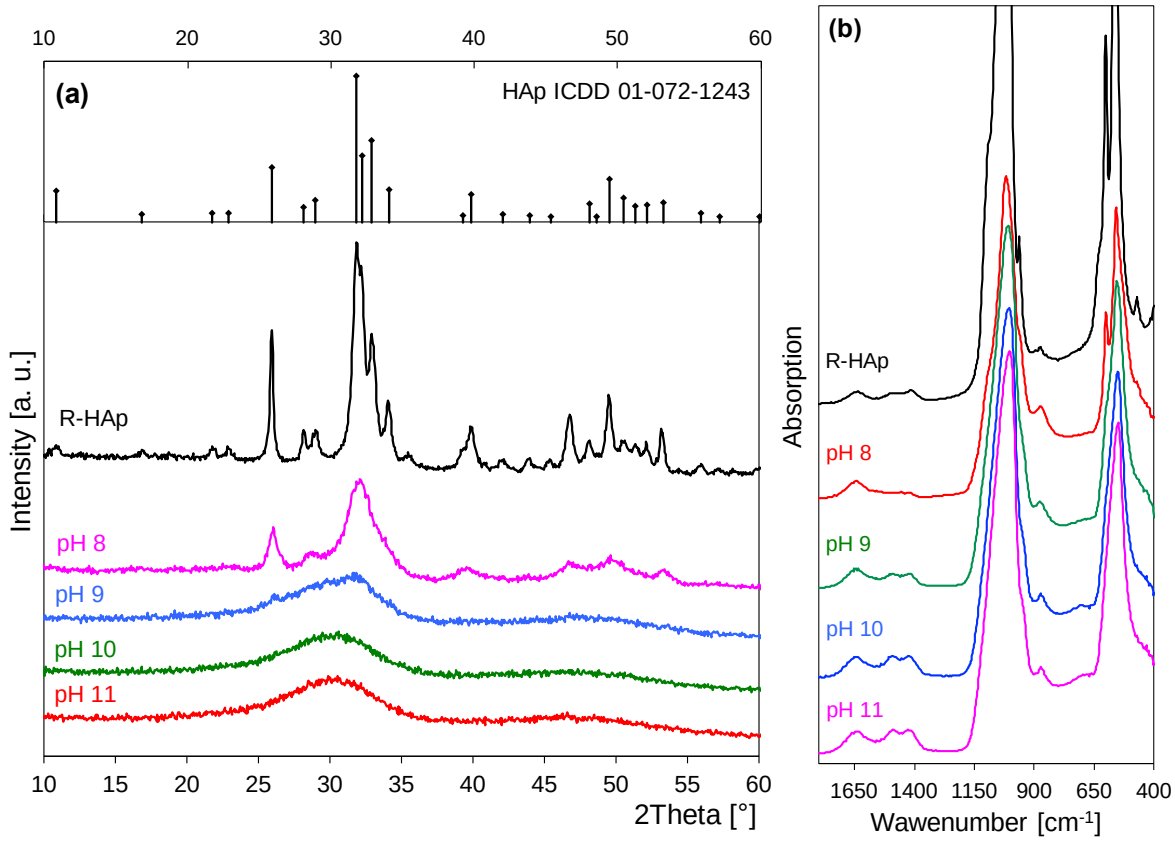

Fig. 4. X-ray diffraction patterns (a) and FT-IR spectra presented in 1700–400 cm^{-1} range (b) of calcium phosphates obtained at different pH values and R-HAp, samples dried at 80 °C temperature [14].

The obtained CaPs have SSA within a range from 133 m^2/g to 154 m^2/g (Table 1), thus fulfilling the set goal of obtaining ACP with SSA ≥ 100 m^2/g. Next, the calculated particle size d_{BET} was in the range from 14 nm to 16 nm. However, correlation between SSA and the synthesis end pH of ACP was not found (results were not statistically significant).

Table 1

Characteristics of the Obtained Calcium Phosphates, where d_{BET} – Particle Size, SSA – Specific Surface Area [14]

Sample	Synthesis end pH	d_{BET}, nm	SSA, m^2/g
ACP-8	8	14 ± 1	154 ± 9
ACP-9	9	15 ± 1	141 ± 8
ACP-10	10	16 ± 3	133 ± 25
ACP-11	11	15 ± 3	150 ± 28
R-HAp	8.8	22 ± 1	95 ± 3

Regardless the initial Ca/P molar ratio in synthesis solution (in all cases Ca/P = 1.67), different crystalline phases formed upon heat treatment (1100 °C, 1 h) of ACP: β-TCP (pH = 8 and pH = 9) or β-TCP/HAp (pH = 10 and pH = 11) was identified. Ca/P molar ratio of the heat-treated samples can be seen in Table 2. Ca/P molar ratio of the samples was affected by synthesis end pH value – it increased with increasing synthesis end pH. The increase of Ca/P molar ratio of the sample may be due to carbonate ions that left the structure of CaP during the heat treatment. It is known that in CaP synthesis pH is one of the main factors that contributes to obtaining of the product with specific composition; it is confirmed in the current study as well.

Table 2

Crystalline Phase Composition of Heat-Treated Samples and Ca/P Molar Ratios Thereof [14]

Sample	Synthesis end pH	β-TCP, wt. %	Hap, wt. %	Ca/P molar ratio
ACP-8	8	100	–	1.50
ACP-9	9	100	–	1.50
ACP-10	10	95.2 ± 1.5	4.8 ± 1.5	1.51
ACP-11	11	90.3 ± 1.6	9.7 ± 1.6	1.61

The obtained CaPs are stable in dried state at least up to 7 months (Fig. 5) when synthesis end pH values thereof are pH = 8, pH = 10 and pH = 11. After 5 months, the sample obtained at pH = 9 started to crystallize because of internal hydrolysis mechanism. The stability of samples obtained at pH = 10 and pH = 11 could be explained by incorporation of carbonate ions within the structure of the samples, thus increasing the Ca/P molar ratio. Therefore, ACP samples with increased Ca/P molar ratio (>1.50) demonstrated a long-term stability of amorphous phase.

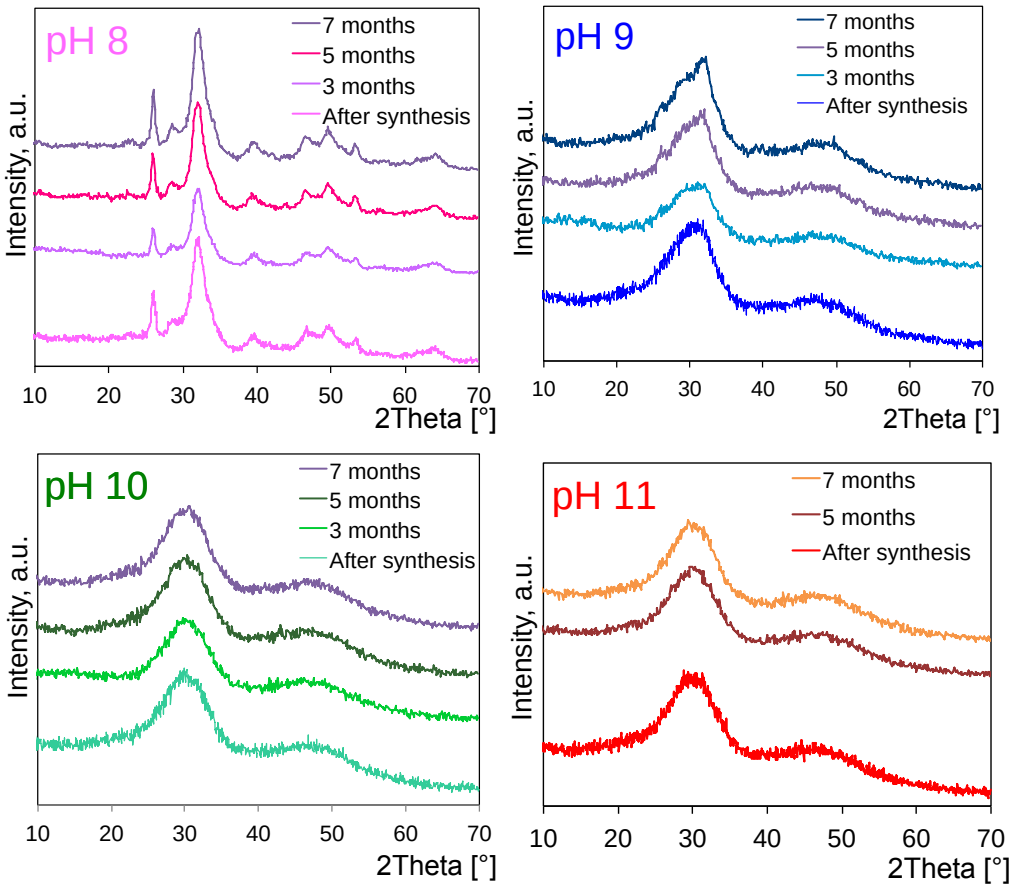

Fig. 5. XRD patterns of low crystalline and amorphous CaPs obtained at different pH and dried at 80 °C temperature: as-synthesized, 3, 5 and 7 months after synthesis [14].

Thermal Behaviour of Differently Dried ACP Materials

The developed synthesis method allowed drying of ACP even at 80 °C temperature (1 h) without the need for the time-consuming freeze-drying (72 h) to preserve the amorphous structure. However, CaPs synthesized using the developed method were freeze-dried as well, and their physicochemical characteristics were compared to CaPs dried at 80 °C temperature.

All freeze-dried samples were x-ray amorphous, regardless of synthesis end pH value. However, the freeze-dried powders visually differed from CaPs dried at 80 °C temperature (Fig. 6), where free flowing voluminous powders for freeze-dried and agglomerated powders for oven dried materials were obtained. The samples dried at 80 °C temperature (abbreviated as "Ov") had a larger particle size and occupied less volume than the freeze-dried (abbreviated as "FrD") samples. A hypothesis was formulated: differently dried ACP will crystallize into different phases because of structural differences that were not detectable by means of routine analysis tools (e.g., XRD and FT-IR). Possible differences of differently dried CaPs were analyzed within crystallization process thereof using thermogravimetry (TGA) and differential scanning calorimetry (DSC) methods.

DSC-TGA measurements were performed with STA449C Jupiter® (Netzsch, Germany) instrument. Two samples were used for comparison: n-HAp (nanocrystalline HAp, Sigma Aldrich) and R-HAp (produced at RTU RBIDC), both contain only HAp..

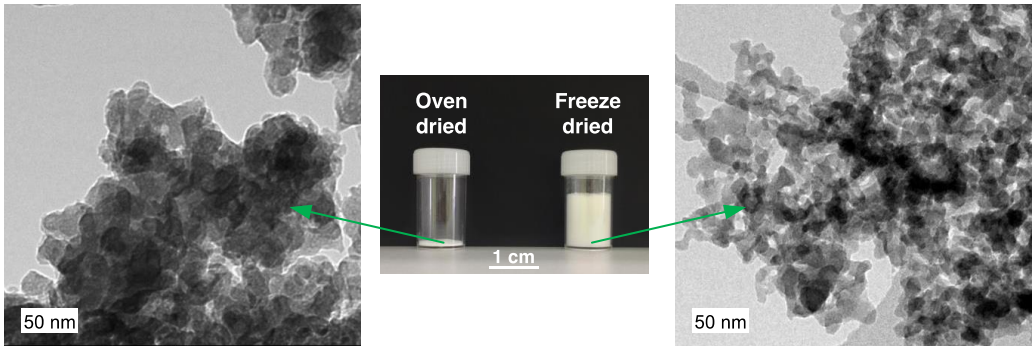

Fig. 6. Photographs and TEM images of oven dried at 80 °C (left) and freeze-dried (right) ACP samples of the same weight [15], synthesis end pH = 10.

TGA curves of Ov and FrD ACP samples are shown in Fig. 7. The observed mass losses are gradual and without abrupt changes for all Ov and FrD samples. However, the total mass loss value differs for samples that were obtained at synthesis with different synthesis end pH value, e.g., see mass loss at 800 °C temperature.

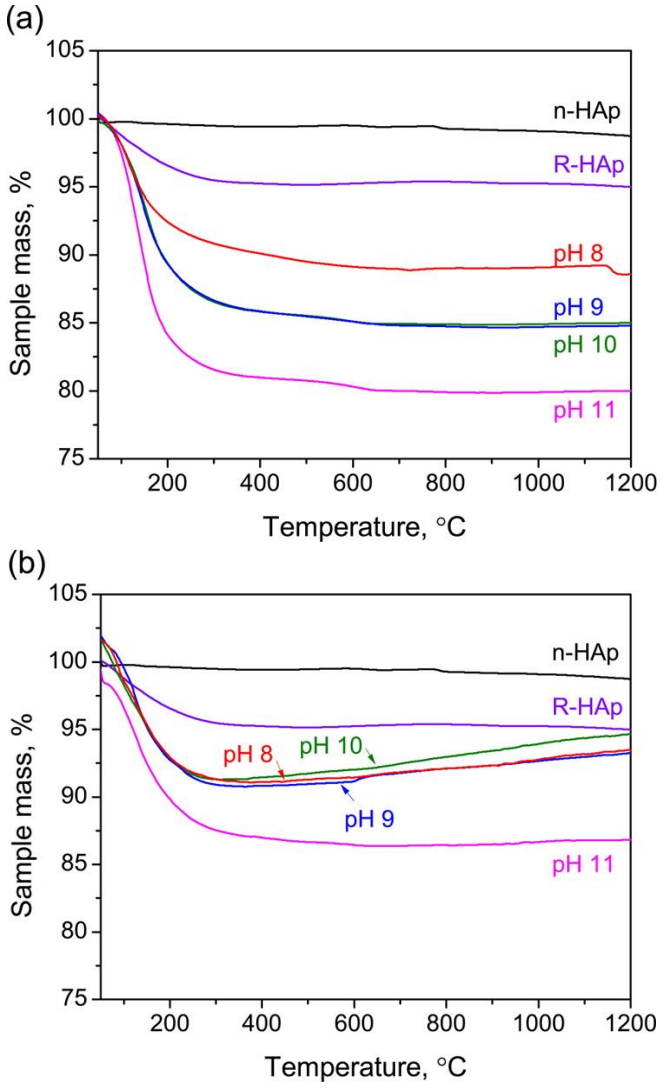

Fig. 7. TGA curves of (a) 80 °C temperature dried and (b) freeze-dried ACP shown in the temperature range of 50 °C to 800 °C; n-HAp and R-HAp are for reference purpose [15].

The comparison of both drying methods revealed that Ov samples had larger amount of physically adsorbed water that was lost up to 200 °C temperature (Fig. 7). The same observation applies for the total mass loss determined at 1200 °C. The total mass loss of Ov samples ranged from 11 wt. % to 20 wt. %, where higher values of mass loss were for Ov samples that were obtained at higher synthesis end pH. In turn, the total mass loss of FrD samples reached maximum of 14 wt. % for the sample that was obtained at pH = 11. The total mass loss values were approximately the same for FrD samples obtained at pH = 8–10; the effect of synthesis end pH here was not observed.

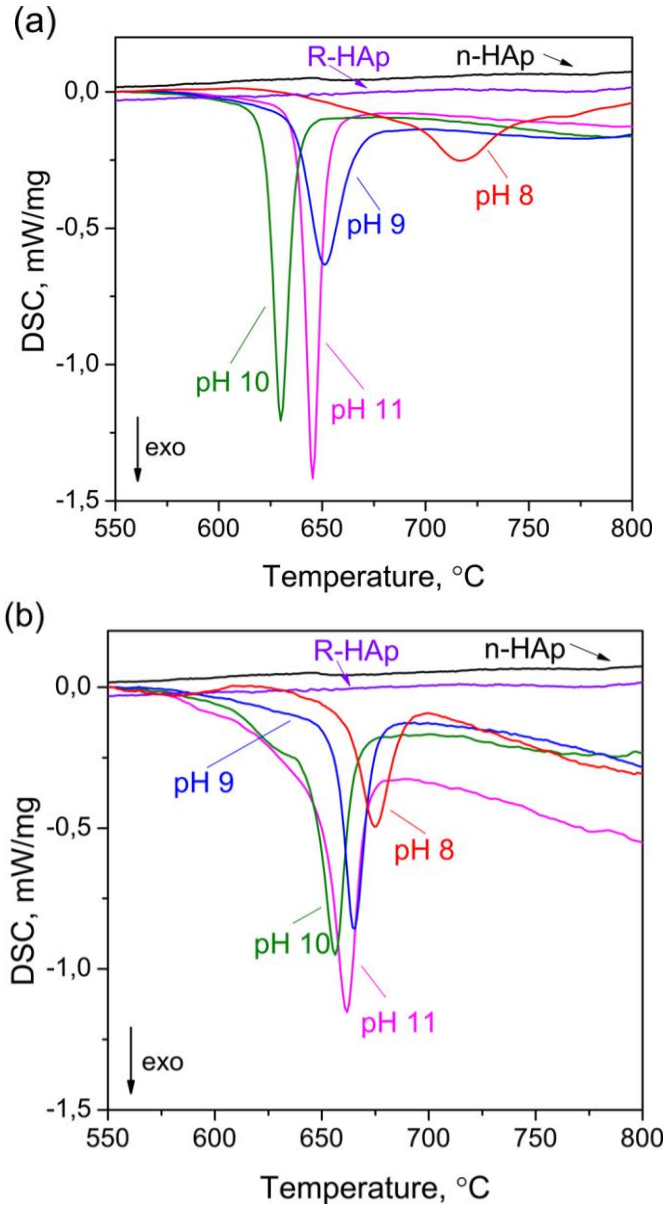

Fig. 8. DSC curves of (a) 80 °C temperature dried and (b) freeze-dried ACP in temperature range from 550 °C to 800 °C; n-HAp and R-HAp are for reference purpose [15].

In all DSC curves of Ov and FrD samples exothermic crystallization effects were observed (Fig. 8). Within the temperature range of these effects at 630–720 °C ACP transformed into crystalline CaPs with dominant crystalline phase being β-TCP. $T_{cryst.onset}$ of

the studied ACP was in the range from 600 °C to 650 °C; correlation between crystallization temperatures ($T_{cryst.onset}$ and $T_{cryst.end}$) and drying method or synthesis pH was not observed. The analysis of both TGA and DSC curves indicated that thermally induced crystallization of ACP was not associated with simultaneous mass loss. Crystallization of ACP started at 150–200 °C higher temperature from the point where in TGA curve the greatest mass loss (up to 400 °C) was observed.

Densification of ACP Using the Principles of Cold Sintering Process

Besides the unique phase and chemical composition, the bone has a unique physical structure as well, which is comprised of both dense and porous bone regions. So far it has remained a challenge to sinter ACP bioceramics to high relative density without affecting its amorphous, hydrated structure and properties. Therefore, alternative sintering techniques such as hydrothermal hot-pressing and low-temperature spark plasma sintering have been used for densification of ACP. However, densification of ACP is challenging even with these technologies. Recently, cold sintering process (CSP) has been used for low-temperature (≤300 °C) densification of various powders. In CSP transient liquid, applied uniaxial pressure and heat is used to densify a powder compact. Thus, use of the CSP technique for densification of ACP has been explored in the current Thesis.

In order to determine optimal technological parameters of CSP for obtaining dense ACP bioceramics, two technological parameters were tested: 1) presence or absence of a transient liquid (water, 20 wt. %) and 2) sintering temperature (room temperature, 100 °C, 120 °C and 150 °C). For each CSP experiment 0.5 g of previously prepared ACP powder (dried at 80 °C, 24 h) were transferred to an easy retrieve pressing die (*ID* = 13 mm, Across International, USA). Here ACP with high SSA was used, that was synthesized according to the developed synthesis protocol [14] and dried using freeze-drying. Moistening of the ACP powder was done manually using agate mortar and pestle. CSP process was done using a two-column lab press PW 40 (P/O/WEBER, Germany) by applying uniaxial pressure of 500 MPa. At least three samples were made for each sintering condition. See overview of CSP experimental conditions in Fig. 9.

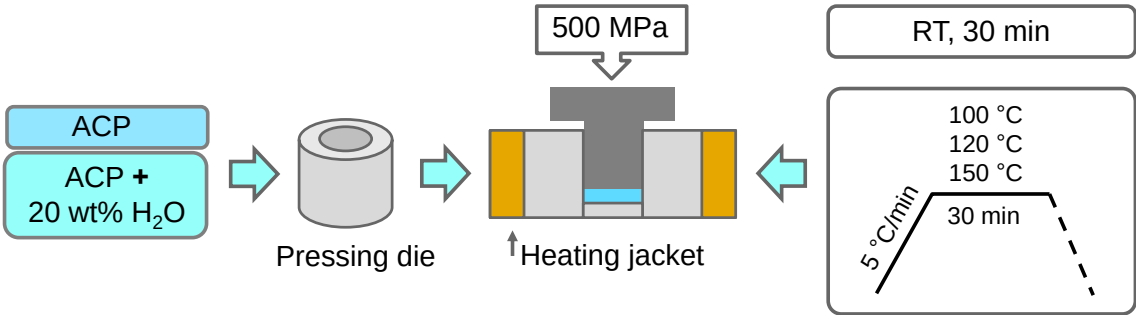

Fig. 9. Densification of ACP using principles of CSP, where RT – room temperature.

Starting ACP powder and CSP-sintered samples were analyzed using XRD (X'Pert Pro, PAnalytical, the Netherlands) and BET (Quadrasorb SI, Quantachrome, USA) methods to determine the phase composition and SSA. In order to evaluate the effect of CSP on densification of the samples, bulk and relative density values of CSP-sintered samples were determined using helium pycnometer Micro UltraPyc 1200e (Quantachrome Instruments, USA). Before each measurement the CSP-sintered samples were pre-dried (80 °C, 24 h) and milled to fine powder using Mini-Mill Pulverisette 23 (FRITCH, Germany) one ball mill for 3 min.

The impact of CSP on phase stability of ACP was evaluated using XRD (Fig. 10). Presence of transient liquid (water, 20 wt. %) led to crystallization of ACP into nanocrystalline HAp phase. The crystallization occurred at lower temperatures (crystallized at 100 °C) when compared to the dry ACP powder (crystallized at 150 °C). Both the temperature and pressure could have activated the surface diffusion processes leading to the phase transition from ACP to nanocrystalline HAp.

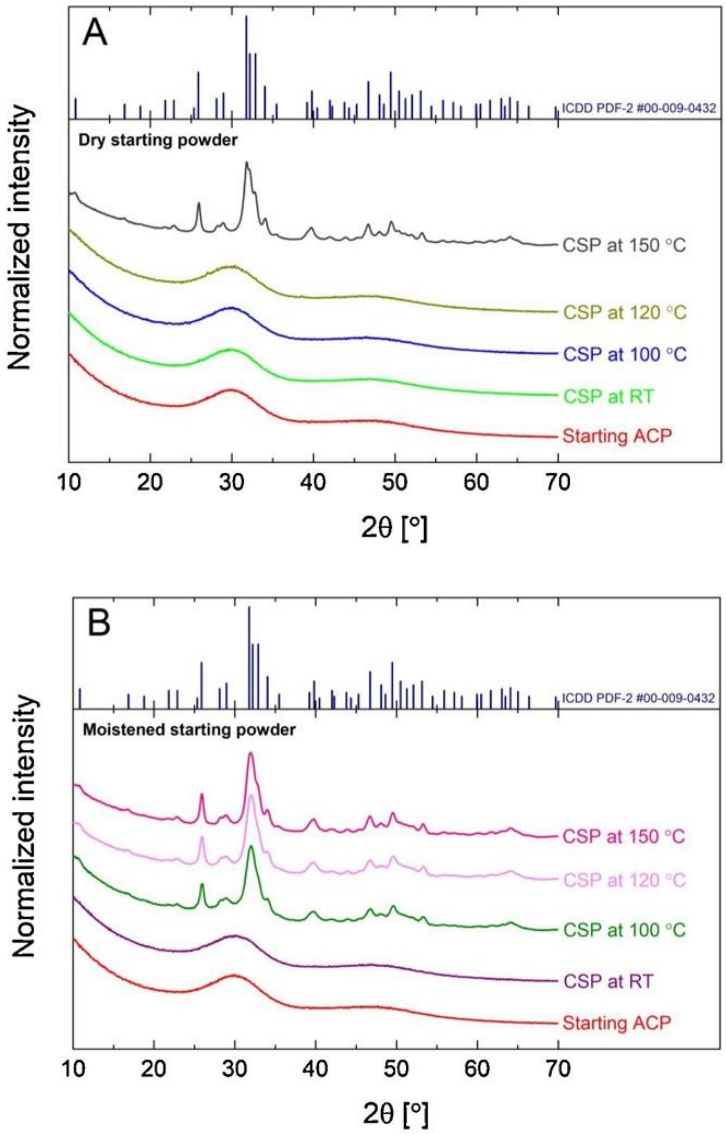

Fig. 10. XRD patterns of the starting ACP and the CSP-sintered samples produced from dry (A) and from moistened starting powder (B) [16].

SSA of the CSP-sintered samples was reduced approximately 5-fold (Fig. 11) comparing to one of the as-synthesized ACP powder (109 $m^2/g \pm 11$ m^2/g). The observed reduction of SSA indicates to particle coalescence during the CSP. Further, insufficient densification produces interparticle (closed) porosity with a surface that may be inaccessible to nitrogen gas that was used in BET measurements.

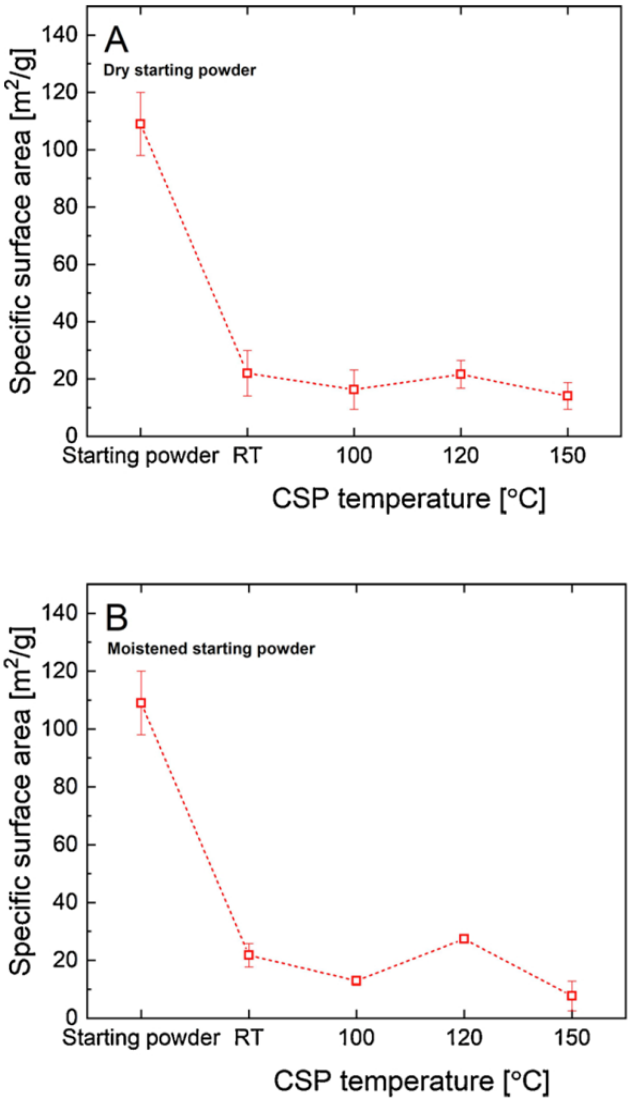

Fig. 11. Specific surface area of the starting ACP powder and the CSP-sintered samples produced from dry (A) and from moistened starting powder (B) [16].

Application of a moderate uniaxial pressure of 500 MPa at room temperature enabled sintering of ACP to relatively high density by using principles of the CSP (Fig. 12). Increase of sintering temperature had only a slight effect on the density values of the samples that remained amorphous after the CSP (refer to Fig. 10). Apparently, the low sintering temperatures were not sufficient in order to increase densification by diffusion processes. The highest relative density value reported for ACP ceramics so far was ~45 % [17]. In current study, relative density of ACP CSP-sintered ceramics was over 75 %.

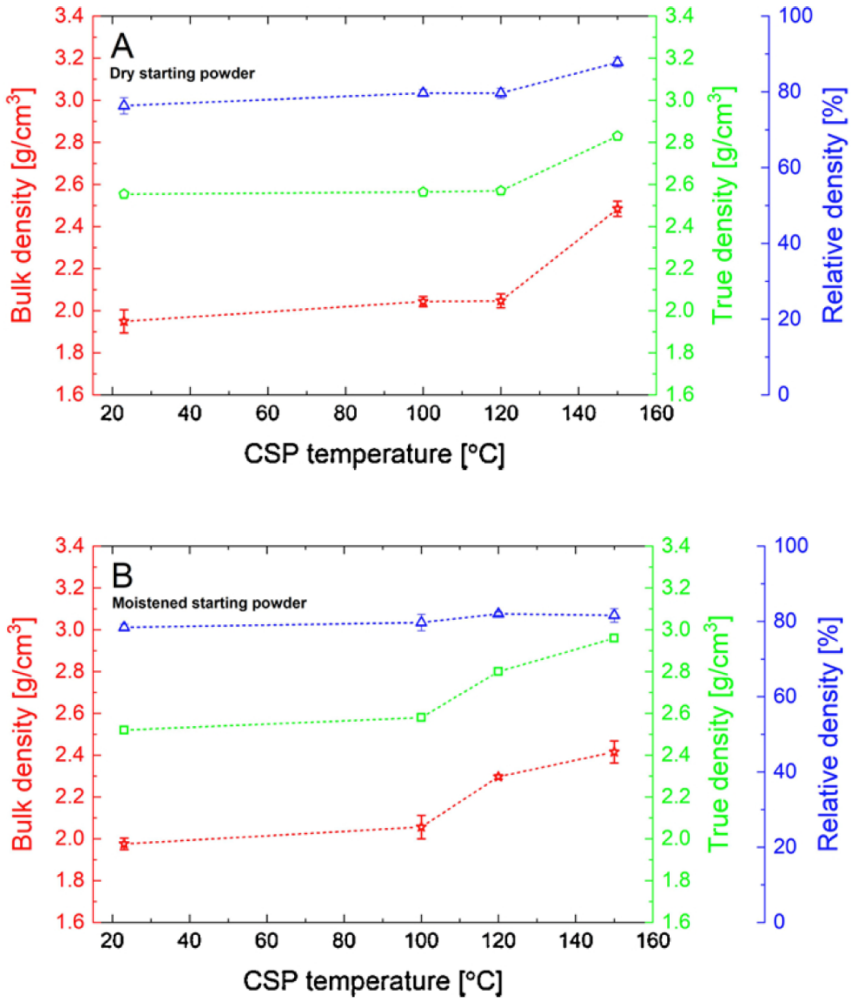

Fig. 12. Bulk, true and relative densities of the CSP-sintered samples produced from dry (A) and from moistened (B) ACP powder [16].

CONCLUSIONS

1. Synthesis of amorphous calcium phosphate by double salt decomposition method from $Ca(NO_3)_2$ and $(NH_4)_2HPO_4$ by varying Ca/P molar ratio of the reagents (1.5, 1.67 or 2.2) and synthesis temperature (0 °C or 20 °C) produces negligible increase of the specific surface area; furthermore, Ca/P molar ratio of the reagents does not affect Ca/P molar ratio of the produced ACP.
2. A simple, fast and cost-effective synthesis method for preparation of nanosized calcium phosphates, amorphous or low crystalline, with a high specific surface area ($\geq$100 m^2/g) has been developed based on a fast increase of pH value in synthesis media containing both calcium and phosphate ions.
3. Synthesis pH (8–11) and drying method (freeze-drying or drying at 80 °C temperature) of amorphous calcium phosphate does not affect crystallization temperature (600–650 °C) of amorphous calcium phosphate during heat treatment, however mass losses associated with the removal of water are affected.
4. Amorphous calcium phosphate materials with increased Ca/P molar ratio (>1.50) exhibit long term stability when stored in room temperature.
5. Use of cold sintering process principles enables obtaining dense amorphous calcium phosphate ceramics at very low temperatures (room, 100 °C and 120 °C) by uniaxial pressing at a pressure of 500 MPa.

REFERENCES

[1] K. Pawelec and J. A. Planell, *Bone Repair Biomaterials: Regeneration and Clinical Applications*, 2nd ed. Woodhead Publishing, 2018.

[2] A. Tsetsekou, D. Brasinika, V. Vaou, and E. Chatzitheodoridis, "On the synthesis of tailored biomimetic hydroxyapatite nanoplates through a bioinspired approach in the presence of collagen or chitosan and L-arginine.," *Mater. Sci. Eng. C. Mater. Biol. Appl.*, vol. 43, pp. 555–65, Oct. 2014.

[3] M. J. Olszta *et al.*, "Bone structure and formation: A new perspective," *Mater. Sci. Eng. R Reports*, vol. 58, no. 3–5, pp. 77–116, 2007.

[4] S. Bose and S. Tarafder, "Calcium phosphate ceramic systems in growth factor and drug delivery for bone tissue engineering: a review," *Acta Biomater.*, vol. 8, no. 4, pp. 1401–21, 2012.

[5] H.-S. Sohn and J.-K. Oh, "Review of bone graft and bone substitutes with an emphasis on fracture surgeries," *Biomater. Res.*, vol. 23, no. 1, p. 9, Dec. 2019.

[6] D. S. H. Lee, Y. Pai, and S. Chang, "Physicochemical characterization of InterOss® and Bio-Oss® anorganic bovine bone grafting material for oral surgery – A comparative study," *Mater. Chem. Phys.*, vol. 146, no. 1–2, pp. 99–104, Jul. 2014.

[7] J. Kolmas, A. Ślósarczyk, A. Wojtowicz, and W. Kolodziejski, "Estimation of the specific surface area of apatites in human mineralized tissues using 31P MAS NMR," *Solid State Nucl. Magn. Reson.*, vol. 32, no. 2, pp. 53–58, 2007.

[8] R. Duan *et al.*, "Variation of the bone forming ability with the physicochemical properties of calcium phosphate bone substitutes," *Biomater. Sci.*, vol. 6, no. 1, pp. 136–145, 2018.

[9] D. Xiao *et al.*, "The role of calcium phosphate surface structure in osteogenesis and the mechanisms involved," *Acta Biomater.*, vol. 106, pp. 22–33, Apr. 2020.

[10] J. Mahamid, A. Sharir, L. Addadi, and S. Weiner, "Amorphous calcium phosphate is a major component of the forming fin bones of zebrafish: Indications for an amorphous precursor phase," *Proc. Nat. Acad. Sci. USA*, vol. 105, no. 35, pp. 12748–12753, 2008.

[11] R. Gelli, F. Ridi, and P. Baglioni, "The importance of being amorphous: calcium and magnesium phosphates in the human body," *Adv. Colloid Interface Sci.*, vol. 269, pp. 219–235, 2019.

[12] J. Vecstaudza and J. Locs, "Effect of Synthesis Temperature and Ca/P Ratios on Specific Surface Area of Amorphous Calcium Phosphate," *Key Eng. Mater.*, vol. 721, pp. 172–176, 2016.

[13] E. D. Eanes, "Amorphous Calcium Phosphate: Thermodynamic and Kinetic Considerations," in *Calcium Phosphates in Biological and Industrial Systems*, Boston, MA: Springer US, 1998, pp. 21–39.

[14] J. Vecstaudza and J. Locs, "Novel preparation route of stable amorphous calcium phosphate nanoparticles with high specific surface area," *J. Alloys Compd.*, vol. 700, pp. 215–222, 2017.

[15] J. Vecstaudza, M. Gasik, and J. Locs, "Amorphous calcium phosphate materials: Formation, structure and thermal behaviour," *J. Eur. Ceram. Soc.*, Nov. 2018.

[16] K. Rubenis, S. Zemjane, J. Vecstaudza, J. Bitenieks, and J. Locs, "Densification of amorphous calcium phosphate using principles of the cold sintering process," *J. Eur. Ceram. Soc.*, vol. 41, no. 1, pp. 912–919, 2021.

[17] M. Luginina *et al.*, "First successful stabilization of consolidated amorphous calcium phosphate (ACP) by cold sintering: toward highly-resorbable reactive bioceramics," *J. Mater. Chem. B*, vol. 8, no. 4, pp. 629–635, 2020.

PIELIKUMI

Publikāciju pilnie teksti

APPENDICES

Full texts of publications

1. PIELIKUMS / APPENDIX 1

1. PUBLIKĀCIJA / PUBLICATION 1

Vecstaudža, J., Ločs, J. Effect of Synthesis Temperature and Ca/P Ratios on Specific Surface Area of Amorphous Calcium Phosphate. *Key Engineering Materials*, Vol. 721, **2016**, pp.172-176.

doi: 10.4028/www.scientific.net/KEM.721.172

Key Engineering Materials
ISSN: 1662-9795, Vol. 721, pp 172-176
doi:10.4028/www.scientific.net/KEM.721.172

Submitted: 2016-06-07
Revised: 2016-08-15
Accepted: 2016-08-15
Online: 2016-12-01

Effect of Synthesis Temperature and Ca/P Ratios on Specific Surface Area of Amorphous Calcium Phosphate

Jana Vecstaudza[a *] and Janis Locs[b]

Rudolfs Cimdins Riga Biomaterials Innovations and Development Centre of RTU, Institute of General Chemical Engineering, Faculty of Materials Science and Applied Chemistry, Riga Technical University, Pulka 3, Riga, LV-1007, Latvia

[a]jana.vecstaudza@rtu.lv, [b]janis.locs@rtu.lv

Keywords: Specific surface area, amorphous calcium phosphate, nanoparticles, low temperature synthesis.

Abstract. Amorphous and low crystalline calcium phosphates are prospective candidates for bone implant manufacturing. Amorphous calcium phosphate (ACP) preparation technologies could be improved in terms of specific surface area (SSA) of obtained products. Current study is dedicated to the effect of synthesis temperature and Ca and P molar ratios (Ca/P) on SSA of ACP. Higher SSA can improve bioactivity of biomaterials. ACP was characterized by XRD, FT-IR, SEM and BET N_2 adsorption techniques. Spherical nanoparticles (<45 nm in size) were obtained independently of initial Ca/P ratio and synthesis temperature. For the first time comparison of SSA was shown for ACP obtained at different temperatures (0 °C and 20 °C) and Ca/P molar ratios (1.5, 1.67 and 2.2).

Introduction

Nanomaterials are of practical concern in biomaterial engineering for hard tissue repairing and replacement materials [1]. High specific surface area (SSA) is an important parameter of nanomaterials that ensures reactivity and bioactivity of biomaterial [2]. Inorganic phase of natural bone is partially amorphous nano sized calcium phosphate (CaP) with ionic substitutions in crystalline lattice [3] and it has high SSA up to 240 m^2/g [4]. Amorphous calcium phosphate (ACP), due to variable Ca/P ratio from 1.2 to 2.2 and therefore tunable properties, is significant candidate for bone mineral phase substitution [5]. The aim of current study was to find the influence of synthesis temperature and initial Ca/P ratio of starting materials on SSA of ACP nanoparticles.

Several studies on CaP precipitated from solutions [6-8] demonstrate the dependence of synthesis temperature on SSA. The trend is following: lowering the synthesis temperature increases the SSA. While in most *"low temperature"* studies, the lowest temperature used is 20, 25 or 37 °C, in some studies synthesis of CaP have been done at temperatures lower than 20-25 °C. For example, Moghimian et al [9] have prepared low crystalline CaP at 5 °C, Layrolle et al [10] obtained CaP at 5 °C in anhydrous ethanol and Li et al [11] succeeded to obtain ACP at 5 °C applying stabilizing agents. SSA value for ACP synthesized at 5 °C was 123 m^2/g given by Li et al [11].

Impact of initial Ca/P ratio of the reagents on SSA of CaP precipitates is unclear and might depend on synthesis technology. For instance, low crystalline CaP with apatitic structure prepared from solutions had higher SSA if the Ca/P ratio was lower [12]. However in study on flame spray pyrolysed CaP (mixture of hydroxyapatite, α-tricalcium phosphate, β-calcium pyrophosphate), increasing Ca/P ratio lead to formation of CaP with higher SSA [13]. At the same time no impact of Ca/P molar ratio on SSA of ACP could be found in literature reviewed by the authors.

The novelty of current study is twofold: 1) synthesis of ACP without stabilizing agents at lower temperature (0 °C) than reported in literature before and 2) analysis of impact of Ca/P molar ratio of the solutions on SSA of ACP.

Materials and Methods

Materials. ACP was obtained by rapid mixing of $Ca(NO_3)_2 \times 4H_2O$ and $(NH_4)_2HPO_4$. Molarity of calcium ion rich solution was kept constant in all experiments – 0.45 M. pH of reactant solutions

2. PIELIKUMS / APPENDIX 2

2. PUBLIKĀCIJA / PUBLICATION 2

Vecstaudza, J., Locs, J. Novel preparation route of stable amorphous calcium phosphate nanoparticles with high specific surface area, *Journal of Alloys and Compounds*, Vol. 700, **2017**, pp.215-222.

doi: 10.1016/j.jallcom.2017.01.038

Journal of Alloys and Compounds 700 (2017) 215–222

Contents lists available at ScienceDirect

Journal of Alloys and Compounds

journal homepage: http://www.elsevier.com/locate/jalcom

Novel preparation route of stable amorphous calcium phosphate nanoparticles with high specific surface area

Jana Vecstaudza*, Janis Locs

Rudolfs Cimdins Riga Biomaterials Innovations and Development Centre of RTU, Institute of General Chemical Engineering, Faculty of Materials Science and Applied Chemistry, Riga Technical University, Pulka Street 3, Riga, LV-1007, Latvia

ARTICLE INFO

Article history:
Received 17 September 2016
Received in revised form
15 December 2016
Accepted 3 January 2017
Available online 4 January 2017

Keywords:
Calcium compounds
Phosphates
Nanomaterials
Biomaterials

ABSTRACT

Novel and effective method for preparation of nanosized and stable calcium phosphates (CaPs) is developed. Amorphous or partially crystalline CaP nanoparticles are rapidly reprecipitated from synthesis solution due to fast change of pH. Basic steps of the proposed approach are: to dissolve CaP salt (e.g. hydroxyapatite) with acid and add base thus inducing reprecipitation of new CaP nanoparticles. It is well known that pH of synthesis medium has a significant effect in CaP precipitation, therefore we varied synthesis pH from 8 to 11. Study reveals impact of synthesis pH on chemical structure (FT-IR), phase composition (XRD) for as-synthesized and heat-treated (300–1100 °C) CaPs and specific surface area (BET). Partially crystalline CaPs form at pH 8 and pH 9, while amorphous calcium phosphate precipitates at pH 10 and pH 11. CaPs prepared by the novel technology have high specific surface area (133–154 m^2/g). Their amorphous state corresponds to amorphous tricalcium phosphate with carbonate ion substitutions depending on pH of the synthesis. Effectiveness of technology is the use of conventional drying instead of lyophilisation.

1. Introduction

Amorphous and partially crystalline calcium phosphates (CaPs) are of special interest in the biomaterial field due to their attractive properties in comparison with traditional polycrystalline CaPs [1]. The size of amorphous calcium phosphate (ACP) is in nanometer scale and a high surface to volume ratio of ACP nanoparticles governs to high reactivity, solubility, biocompatibility and bioactivity [2]. Hence ACP has promising applications in biomedical engineering especially in repair and regeneration of hard tissue.

ACP forms as by-product during preparation of high temperature CaP coatings when using plasma spraying deposition, electrostatic spray deposition or pulsed laser deposition technologies [2]. Therefore studies of ACP formation and property investigation are of high practical importance in development of ceramic coatings. ACP is considered as initial phase in formation of crystalline CaPs from solutions as well [3]. Furthermore, amorphous phase forms during extensive milling of crystalline CaPs or mixtures of calcium and phosphorus containing salts [4]. ACP phase can always be present at some point in preparation or treatment processes of various CaPs.

According to previous studies [5,6] ACP has short stability times in solution or humid atmosphere and this leads to formation of crystalline phase, e.g. hydroxyapatite (HAp). Some researchers add stabilizing agents (e.g. polyethylene glycol, Mg^{2+}, CO_3^{2-}) to stop the conversion and to stop the growth of crystals or at least to obtain nanocrystalline CaP with nanosized particles [1]. In most of the papers classic calcium nitrate-ammonium phosphate route is used that is followed by immediate removal of precipitates and lyophilisation (usually for 48–72 h) [7–9]. It is time and cost consuming process. Therefore another approach that gives stable CaP nanoparticles with variable crystallinity and much shorter processing times are needed for upscaling and use in industry.

Aim of the study was to obtain amorphous or partially crystalline CaP nanoparticles by a different approach than a classical reaction [2] between calcium nitrate and ammonium phosphate solutions. In our case fast pH change of the synthesis solution was utilized to induce precipitation of ACP, similarly to *Eanes* [10,11], where KOH was rapidly added to acidic mix of calcium and phosphate salts.

The originality of our work is twofold: 1) use of a dissolved calcium phosphate salt as a source of calcium and phosphate ions for formation of nanosized calcium phosphates; 2) synthesis of ACP without stabilizing agents (Mg^{2+}, polyethylene glycol etc.) or extra

* Corresponding author.
E-mail address: jana.vecstaudza@rtu.lv (J. Vecstaudza).

http://dx.doi.org/10.1016/j.jallcom.2017.01.038
0925-8388/

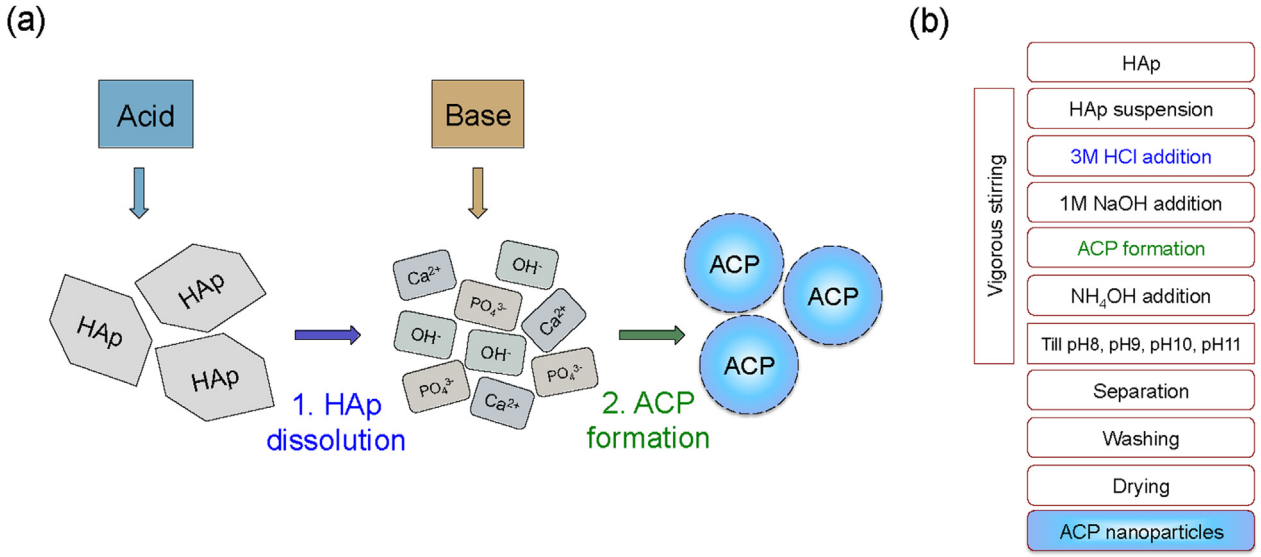

Fig. 1. Synthesis scheme of amorphous calcium phosphate nanoparticles: (a) general and (b) in detail.

techniques (lyophilisation, microwave, ultrasound etc.) only by pH change and conventional drying. Thus calcium and phosphate ions are already homogenously distributed in synthesis solution opposite to double salt decomposition approach where one salt solution is usually rapidly added to another. Therefore, in our case more uniform formation and growth of particles is expected. A new, simple, fast, cost-effective and scalable method for preparation of nanosized calcium phosphates - amorphous or low crystalline, with a high specific surface area has been developed. Use of conventional drying in hot air should be highlighted because it reduces time and costs of the overall technology. To the authors knowledge such technology has yet never been reported anywhere else.

2. Materials and methods

2.1. Synthesis of CaP nanoparticles

We used reagent grade reagents: HCl, NaOH and 26% NH_3 solution from Sigma Aldrich and pure nanosized hydroxyapatite (HAp) to synthesize CaP nanoparticles. HAp was prepared by precipitation reaction from calcium hydroxide and orthophosphoric acid [12]. Chosen method is cost effective approach for preparation of HAp by wet chemistry and thereby the novel synthesis using this HAp is cost-effective as well. The total price of calcium oxide and orthophosphoric acid is three to four times smaller when compared to price of calcium and phosphate salts used in other methods. Step by step description of the synthesis process with dissolution step of HAp followed by ACP formation after rapid addition of base is shown on Fig. 1b, while Fig. 1a depicts generalized version of the same.

At first vigorous stirring of HAp powder in deionized water at room temperature (22 ± 2 °C) gave homogenous suspension (1 g of HAp per 300 mL of H_2O). There was continuous control of pH and temperature during the synthesis. Then solution of 3M HCl was added to completely dissolve HAp with a rate of 1 mL/min. Dissolved Ca and P species were sparingly mixed and 1M NaOH was added in a fast manner to change the pH of the solution. At this point precipitation of ACP occurred. End pH (8, 9, 10 or 11) of the synthesis was adjusted with ammonia solution. Immediately formed precipitates were left to stir for 5 min and separated from solution by centrifugation afterwards. Gel-like precipitates were washed three times: firstly, with deionized water, secondly, with

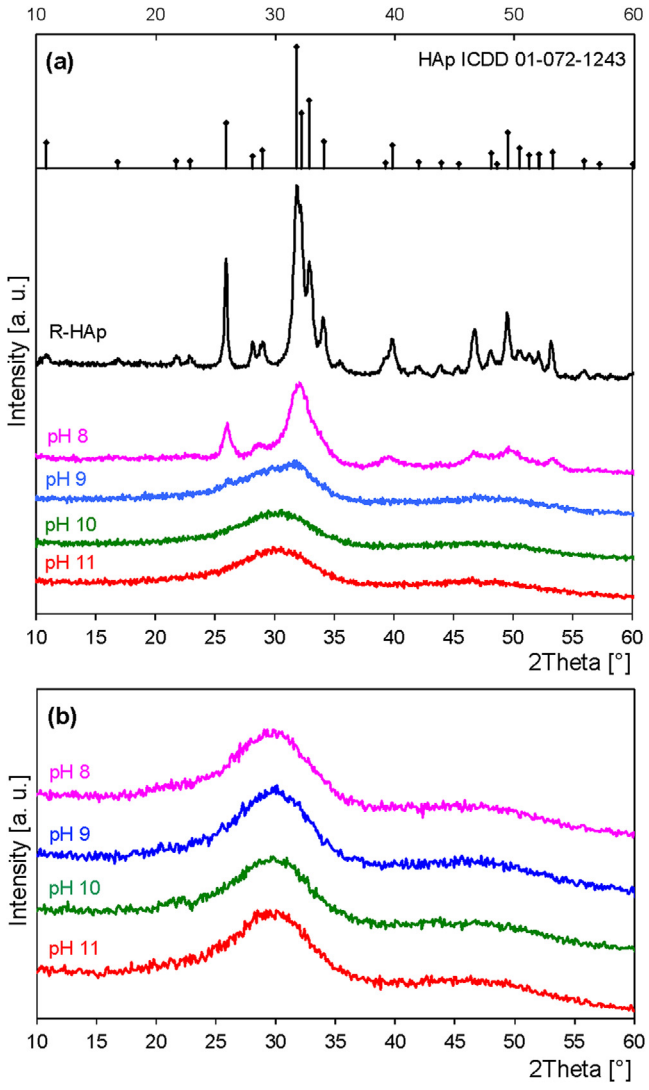

Fig. 2. X-Ray diffraction patterns of calcium phosphates obtained at different pH values and R-HAp, where on (a) samples dried at 80 °C and on (b) dried by lyophilisation for comparison.

water-ethanol solution (50–50 vol%) and finally with deionized water. Obtained precipitates were transferred to Petri dishes, evenly distributed and covered with 15 mL of ethanol. Ethanol provided fast drying of ACP precipitates. Drying was done in air at 80 °C for 1 h. Each of the synthesis was repeated three times and all measurements were performed for each of them. The same HAp used in synthesis was used as a reference in measurements (further designated as R-HAp).

2.2. Analytical methods

X-Ray diffractometer X'Pert Pro (PAnalytical, the Netherlands) operated at 40 kV and 30 mA was used to check presence of crystalline phases of as-synthesized and thermally treated ACP. Quantitative amount of β-$Ca_3(PO_4)_3$ (β-TCP) and HAp phases was determined with Rietveld refinement procedure with Profex software [13] for samples heat treated at 1100 °C for 1 h. These amounts were used to calculate Ca/P molar ratio as well. We calculated mean particle size d_{XRD} with Scherer formula after [002] peak, knowing it is only applicable when domain (crystallite) size of the sample does not exceed 100 nm [14]. For crystalline phase identification following ICDD entries were used – #01-072-1243 for HAp and #009-0169 for β-TCP.

Fourier transform infrared spectrometer Varian 800 Scimitar Series (USA) with attenuated total reflectance (ATR) unit was employed to characterize functional groups of as-synthesized CaPs. Spectra were collected with resolution of 4 cm^{-1} averaging 50 scans in the wavenumber range of 400–4000 cm^{-1}.

Morphological features of as-synthesized CaP nanoparticles were observed with transmission electron microscope (TEM) FEI Tecnai G2 F20 operated at 200 kV. Detailed sample preparation for TEM analysis is described elsewhere [15].

Specific surface area (SSA) was measured with N_2 adsorption system Quadrasorb *SI* (Quantachrome Instruments, USA). Degasser Autosorb AD-9 (Quantachrome Instruments, USA) was used to degass samples at room temperature for 24 h prior to analysis to remove any excess moisture and vapours. Particle size d_{BET} was calculated according to Eq. (1) stated in ISO standard No. 13779-3 "Implants for surgery – Hydroxyapatite – Part 3: Chemical analysis and characterization of crystallinity and phase purity", assuming particles to be spherical and nonporous:

$$d_{BET} = 6/(\rho \times SSA), \quad (1)$$

where ρ – density of R-HAp (2.81 g/cm^3), determined with Micromeritics AccuPyc 1330.

Structural stability of dried CaPs after three, five and seven months after the synthesis was evaluated with XRD to check whether ACP has transformed into crystalline CaP. During the experiment samples were kept in air atmosphere in sealed sample bags.

To gain insight into the crystallization process of ACP, samples were subjected to heat treatments at 1100, 900, 700, 500 and 300 °C (heating rate 5 °C/min, hold time 1 h).

3. Results

Amorphous and partially crystalline CaPs were successfully prepared by the novel rapid reprecipitation method at different synthesis pH values. X-Ray diffraction (XRD) patterns and FT-IR spectra of as-synthesized CaP nanoparticles are shown on Figs. 2 and 3. Identification of chemical groups in FT-IR spectra are

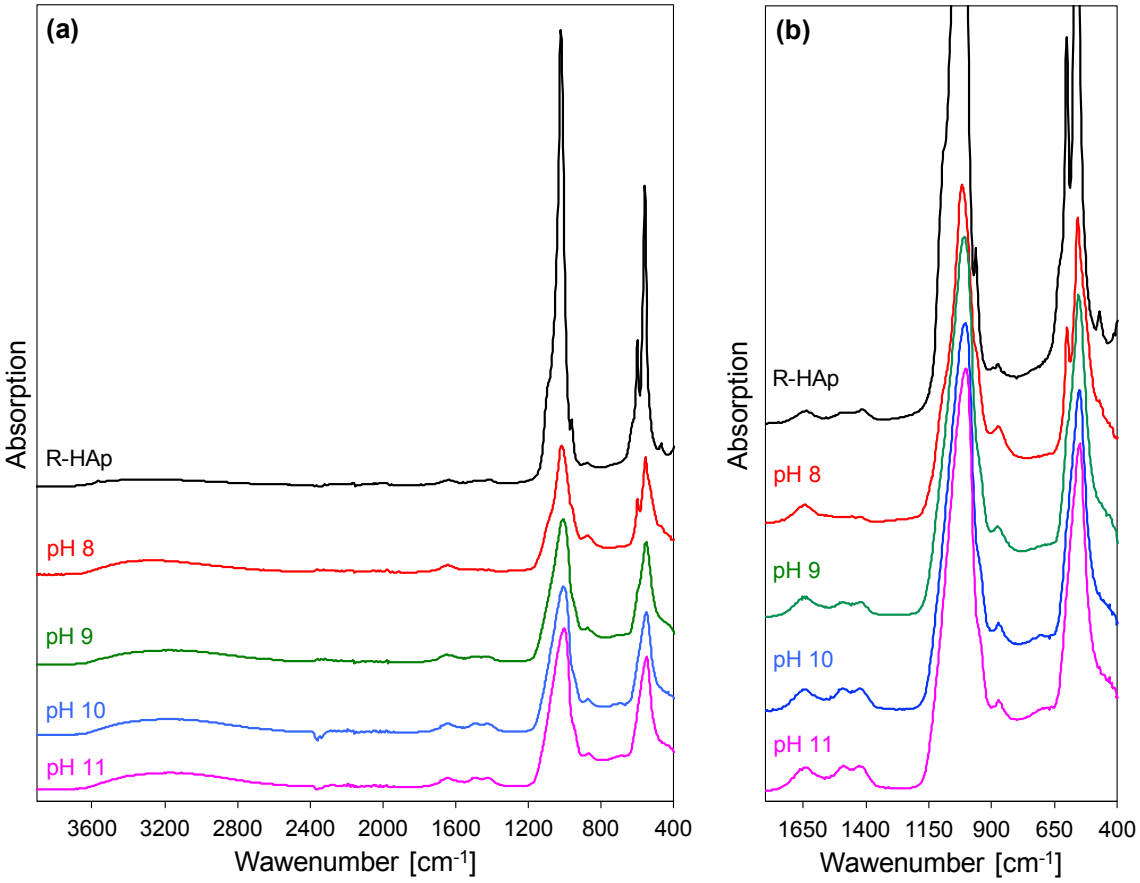

Fig. 3. Fourier transform infrared spectra of as-synthesized calcium phosphates obtained at different pH values and R-HAp in 4000–400 cm^{-1} (a) and 1700–400 cm^{-1} (b) ranges.

Table 1
Fourier transform infrared spectrometry data of chemical groups of as-synthesized calcium phosphates and R-HAp, where *sh.* – shoulder, *v.l.i.* – very low intensity.

Assignment	pH 11	pH 10	pH 9	pH 8	R-HAp
	Absorption band (cm^{-1})				
Bending mode, v_2 PO_4^{3-}	–	–	–	462 *sh.*	469
Bending mode, v_4 PO_4^{3-}	545	545	549	553	559
Bending mode, v_4 PO_4^{3-}	–	–	597 *sh.*	600	599
Symmetric stretching mode, v_5 HPO_4^{2-}; bending mode, v_2 CO_3^{2-}	866	866	869	866	869
Symmetric stretching mode, v_1 PO_4^{3-}	–	–	–	959 *sh.*	962
Asymmetric stretching mode, v_3 PO_4^{3-}	997	999	1003	1008	1022
Asymmetric stretching mode, v_3 PO_4^{3-}	–	–	–	1089 *sh.*	1089 *sh.*
Stretching mode, v_3 CO_3^{2-}	1412	1412	1412	1412	1415
Stretching mode, v_1 CO_3^{2-}	1479	1479	1479	1479 v.*l.i.*	1479
Bending mode, v_2 H_2O	1638	1637	1641	1641	1637
Stretching mode, v_s OH^-	–	–	–	–	3574
Adsorbed H_2O molecules	3680–2510	3680–2510	3655–2510	3650–2550	3650–2580

presented on Table 1. Differences between synthesis pH values are evident both on XRD patterns (Fig. 2a) and FT-IR spectra (Fig. 3a). Diffraction peaks characteristic to crystalline HAp were detected for samples obtained at pH 8 and pH 9 while CaPs precipitated at pH 10 and pH 11 gave XRD patterns of amorphous character (Fig. 2a). XRD pattern of thermally non-treated R-HAp in Fig. 2a shows typical appearance of nanocrystalline HAp. XRD patterns of lyophilised samples are presented on Fig. 2b for comparison to proposed drying method at 80 °C. FT-IR spectra of CaPs obtained at pH 9 till pH 11 resemble ones of ACP with broad absorption bands. Spectra of CaP obtained at pH 8 contain a pair of sharp absorption bands indicating presence of crystalline domains.

Morphology of obtained ACP particles is presented on TEM image on Fig. 4. Particles were moderately agglomerated and had distorted spherical shape with sizes in the range of 11 up to 30 nm (average value 20 ± 4 nm).

Specific surface area (SSA) and particle sizes calculated after Scherer equation (d_{XRD}) and after BET (d_{BET}) of as synthesized materials are summarized on Table 2.

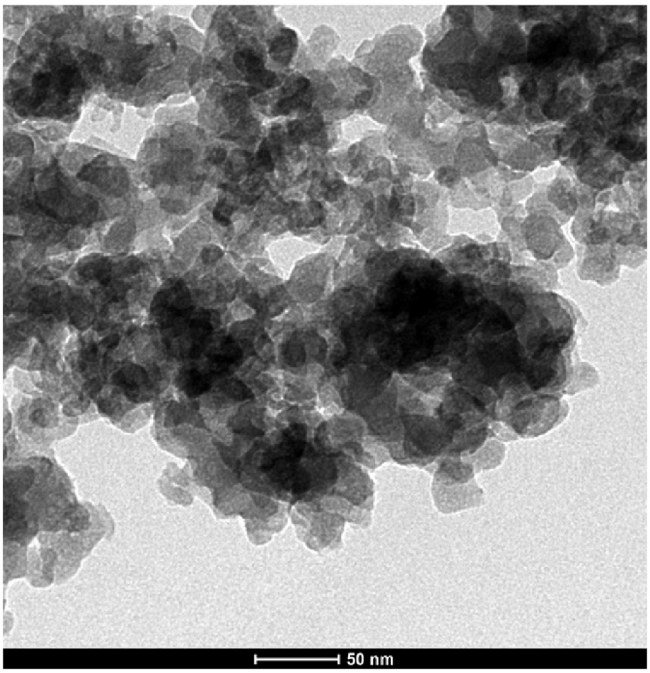

Fig. 4. Transmission electron microscopy image of particle morphology of as-synthesized amorphous calcium phosphate obtained at pH 10.

Heat treatments of CaP nanoparticles at 1100°C/1 h revealed what kind of crystalline phases evolved (see Fig. 5) from CaPs obtained at different pH. HAp and β-TCP phases were present. β-TCP was found in samples obtained at pH 8 and pH 9 and mix of both phases obtained at pH 10 and pH 11.

Further the calculated Ca/P molar ratio and quantitative phase composition at 1100 °C are shown on Table 3. Gradual heat treatments at 300, 500, 700, 900 and 1100 °C (see Fig. 6) revealed increase in crystallinity of CaP samples.

Structural stability of obtained CaPs after 3, 5 and 7 months storage in air is shown on Fig. 7. From presented XRD patterns no distinct changes are visible for samples obtained at pH 8, pH 10 and pH 11. Structural ordering has started for sample synthesized at pH 9.

4. Discussion

4.1. Structure and morphology of as-prepared CaP nanoparticles

As shown on Fig. 2a as-synthesized CaPs at pH 10 and pH 11 are X-Ray amorphous – they have no long-range order that is characteristic to crystalline materials. Pattern of sample obtained at pH 9 has very small peak “bumps” around 26° 2Theta and 32° 2Theta, while the rest of diffractogram shows the same pattern as pH 10 and pH 11. Sample obtained at pH 8 has more pronounced peaks that resembles weakly ordered partially crystalline hydroxyapatite [1]. Overall relationship between amorphous state and pH corresponds to literature, where ACP prepared by wet chemistry without stabilizing agents can be obtained at pH values of 9 till 11 [16].

There could be several scenarios for crystalline CaP formation at pH 8 and 9. For example, Eanes [10] have studied ACP stability in different pH and have concluded that stability of ACP increases with increasing pH from 7.4 till 10–10.5, at even higher pH stability starts to decline. At pH 7.4 ACP was stable only for 30 minutes, at pH 10–10.5 – for more than 9 hours. Furthermore, Meyer and Eanes [17] have investigated the ACP stability within pH range from 7.40 to 9.25 by monitoring uptake of OH^- ions in time. Here it was

Table 2
Characteristics of obtained calcium phosphates, where d_{XRD} and d_{BET} – particle sizes calculated after Scherer equation (XRD) and specific surface area SSA (BET).

Sample	Synthesis end pH	d_{XRD} [nm]	d_{BET} [nm]	SSA [m^2/g]
ACP-8	8	15 ± 1	14 ± 1	154 ± 9
ACP-9	9	–	15 ± 1	141 ± 8
ACP-10	10	–	16 ± 3	133 ± 25
ACP-11	11	–	15 ± 3	150 ± 28
R-HAp	8.8	30 ± 1	22 ± 1	95 ± 3

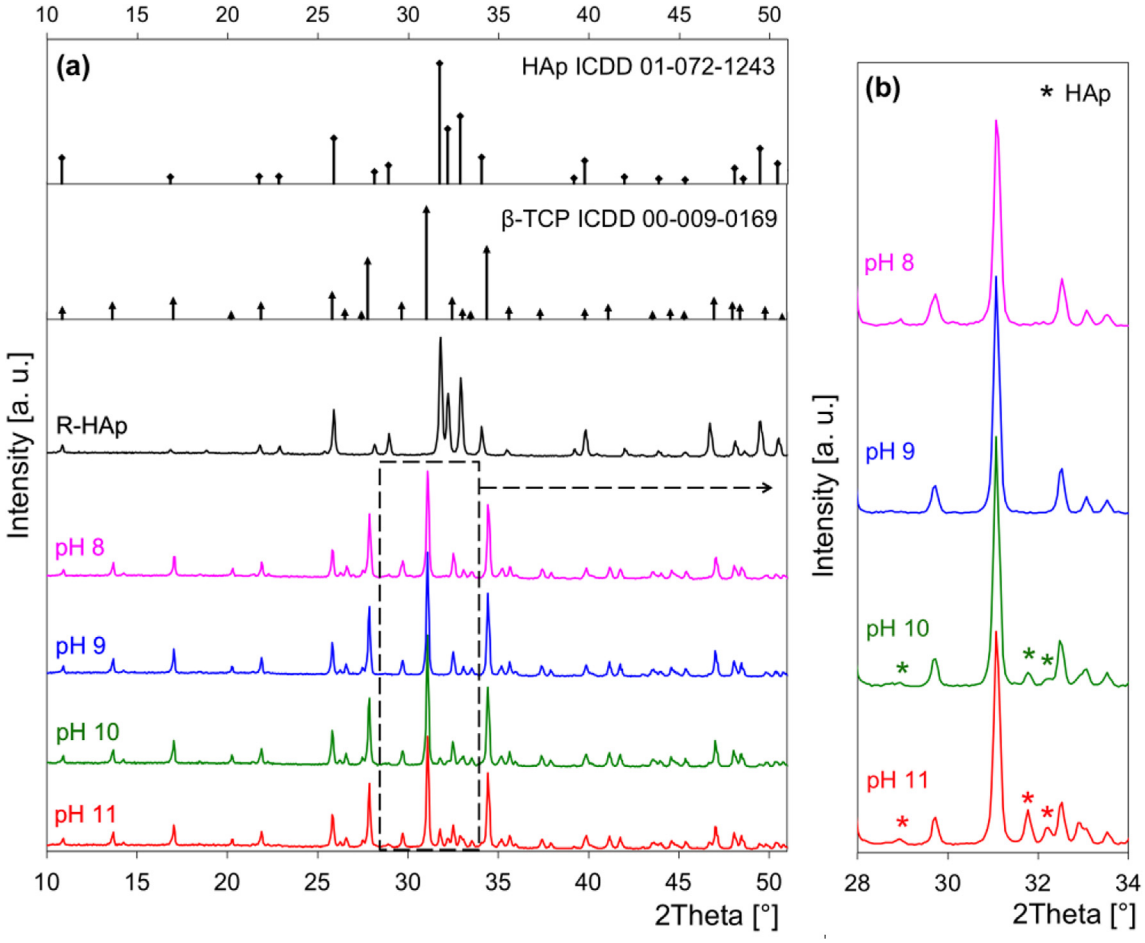

Fig. 5. (a) X-Ray diffraction patterns of calcium phosphates obtained at different pH and R-HAp heat-treated at 1100 °C temperature. ICDD cards of HAp and β-TCP are presented for identification; (b) close-up of XRD patterns in the range of 28–34° 2Theta with HAp peaks marked (*).

demonstrated that at lower pH uptake of OH^- ions was achieved faster to transform into crystalline CaP. This matches our case where in solutions with more hydroxyl ions (higher pH) transformation to poorly crystalline structure is hindered. Mechanism of internal hydrolysis of PO_4^{3-} ions could lead to formation of calcium deficient apatite from ACP [18] as well. In order to obtain ACP at pH 8 instead of crystalline CaP temperature and duration of drying could be varied based on study [19] where ACP (Ca/P 1.33) stayed stable in wet atmosphere for longer time at 40 °C than 80 °C. One must agree that effect of pH on amorphous-crystalline transformation is quite complex and not yet fully clear as mentioned in Ref. [1]. Variation of synthesis pH in the range of 8–9 might produce CaPs with different degree of crystallinity right after the synthesis without further treatment (e.g. thermally induced crystallization).

It is possible to obtain ACP with proposed drying regime at 80 °C in the pH range of 10 till 11 (Fig. 2a) and low crystalline CaP in the pH range of 8 till 9. However, if the same samples are dried using lyophilisation ACP is obtained in whole tested pH range from 8 up to 11 (Fig. 2b). Precipitates of ACP prior to lyophilisation are frozen in liquid nitrogen. This stops transformation of ACP to crystalline CaP. At this time point (approximately 30 min from precipitation event) product precipitated at any pH is still amorphous. If these samples are put in 80 °C for 1 h, samples obtained at pH 8 and 9 crystallizes. Prolonged contact of ACP with moisture at elevated temperature fosters the amorphous-crystalline transition and in our case it depends on pH of synthesis as well. Furthermore, none of possible by-products (e.g. NaCl, $CaCl_2$) have been detected with XRD that proves effectiveness of washing procedure.

Table 3
Amount of crystalline phases in heat treated low crystalline and amorphous calcium phosphates and respective Ca/P molar ratios.

Sample	β-TCP [wt%]	HAp [wt%]	Ca/P molar ratio
ACP-8	100	–	1.50
ACP-9	100	–	1.50
ACP-10	95.2 ± 1.5	4.8 ± 1.5	1.51
ACP-11	90.3 ± 1.6	9.7 ± 1.6	1.61

The size (11–30 nm) of prepared ACP nanoparticles observed in TEM image (Fig. 4) is in the range and even smaller than particles described in literature, where ACP particles of 30–100 nm [6,20] in size have been reported. Hence the new synthesis approach allows to obtain considerably smaller particles than one of classical synthesis routes, e.g. from $CaCl_2$ and $(NH_4)_2HPO_4$ [6]. This might be of already homogenous mix of calcium and phosphate ions that make up CaP particles after addition of base. Because in double salt decomposition methods there is nonequal distribution of reagent concentrations at the moment of mixing of solutions. Usually in these methods there is considerable amount of other ions from calcium and phosphorus salts, and pH regulation agents (e.g. NH_4^+) that might foster growth of CaP particles [21].

Similar trend is observed in FT-IR spectra (Fig. 3) as in XRD patterns – samples obtained at pH 9-11 are structurally similar.

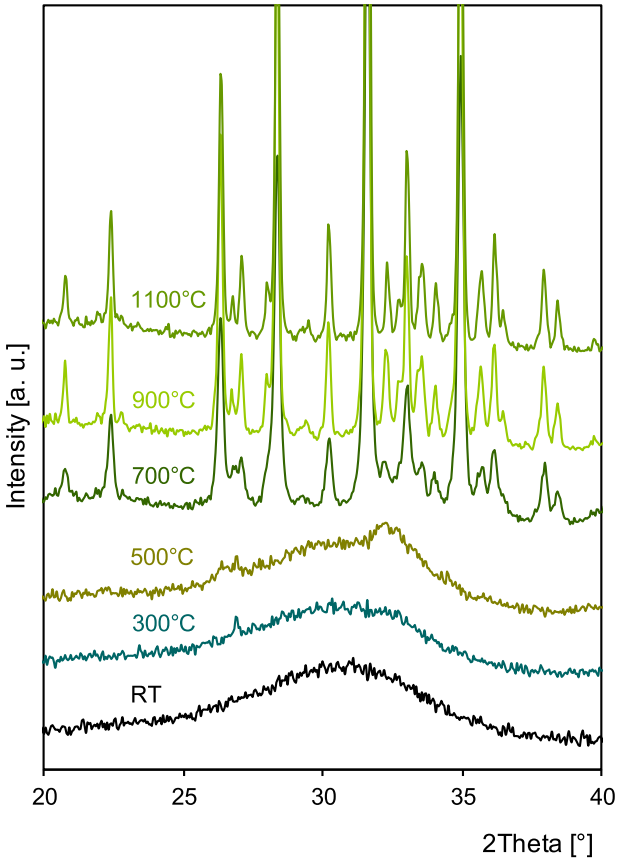

Fig. 6. X-Ray diffraction patterns: evolution of crystalline phases of calcium phosphate nanoparticles during heat treatments at different temperatures. Representative set of XRD patterns for sample obtained at pH 10 is shown, where the crystalline phase is hydroxyapatite.

These samples have wide and rounded absorption bands that are characteristic to amorphous and low crystalline materials [2], while sample prepared at pH 8 shows a little bit different behaviour. At pH 8 shoulder and sharp absorption band around 462 cm^{-1} (v_2 PO_4^{3-}) and 600 cm^{-1} (v_4 PO_4^{3-}) [22,23] were detected, these are the same as for the crystalline R-HAp at 469 cm^{-1} and 599 cm^{-1}. At pH 9 there is a slight similarity with sample obtained at pH 8 - a shoulder of bending mode v_4 PO_4^{3-} was identified at 597 cm^{-1} [23]. This complements the week diffraction peaks of sample prepared at pH 9. Both amorphous and low crystalline samples have intense and relatively wide band around 545–559 cm^{-1} (v_4 PO_4^{3-}) [22], however it is sharp in the case of sample prepared at pH 8. Sharp and split absorption bands are indicators of crystallinity [24,25]. While R-HAp has sharp absorption band (v_1 PO_4^{3-}) at 962 cm^{-1} because of its crystalline nature, the low crystalline CaP prepared at pH 8 has shoulder of the same band at 959 cm^{-1} [26]. All samples have a wide band around 999–1022 cm^{-1} that belongs to v_3 PO_4 [22]. Further the sample obtained at pH 8 have a shoulder of v_3 PO_4^{3-} band at 1089 cm^{-1} [23,26].

All amorphous and low crystalline samples have band at 866–869 cm^{-1}, that corresponds to v_2 CO_3^{2-} bending vibration and stretching of HPO_4^{2-} [23,27,28]. Carbonate ion absorption bands v_3 CO_3^{2-} were also present at 1412 cm^{-1} and 1479 cm^{-1} [29] implying some degree of carbonate ion substitution in the structure. Intensity of carbonate bands decreased with decreasing pH value of the synthesis. In our case this correlates with amount of added ammonia solution for pH regulation as ammonia solution can contain dissolved CO_2. Also carbonate uptake can increase with increasing pH [1]. Presence of carbonate ions into synthesis medium at low temperatures (e. g. room temperature) is inevitable due to good solubility of CO_2 at low temperatures. Carbonate ions stabilise ACP phase [2,10] and bring its composition closer to one of biological carbonated apatite [30]. Furthermore, incorporation of carbonate ions into structures of CaPs substantially improves biological behaviour towards them [31,32]. Presence of carbonate ions will have an effect on crystalline phase composition during heat treatment of synthesized CaPs as discussed later.

None of amorphous or low crystalline CaPs contain information about vibrations of structurally bound OH^- as R-HAp does at 3574 cm^{-1} [23,28]. Absence of OH^- groups is clear in the case of ACP, because it is composed only of Ca^{2+} and PO_4^{3-} ions and water molecules in interstices [1]. Lack of OH^- groups confirms purity of obtained ACP as it does not contain possible leftovers from incompletely dissolved HAp. Undetectable OH^- in CaP prepared at pH 8 might be due to its weak crystalline structure and small particle size [33]. Due to presence of adsorbed water molecules only a wide absorption band in range of 3680–2510 cm^{-1} can be seen on spectra of all samples, including R-HAp. Furthermore, bending vibration v_2 of water at 1637–1641 cm^{-1} is present on all spectra as well.

4.2. Specific surface area of CaP nanoparticles

SSA of precipitates is 40–62% larger than for starting material R-HAp (95 m^2/g). There is no distinct correlation between SSA values and synthesis end pH (Table 2). Taking into account the deviations for each sample series, it could be stated that pH practically has no influence on SSA of CaP nanoparticles prepared by the proposed reprecipitation process. To our knowledge the highest value of SSA reported elsewhere is 300 m^2/g [34] for nanocrystalline carbonated hydroxyapatite. In other cases values of 80 m^2/g [35] for ACP and values from 9 to 236 m^2/g [36,37] for nanocrystalline HAp have been reported depending on preparation technology. CaPs prepared by rapid reprecipitation method have achieved good results in terms of SSA. High SSA values of prepared CaPs indicate the small particle size, which is < 16 nm for all samples (see d_{BET} in Table 2). Particle sizes determined from TEM measurements cover the range of calculated particle sizes.

4.3. Crystallization behaviour of CaP nanoparticles at elevated temperatures

Heat treatment at different temperatures revealed what kind of crystalline phases form from CaPs reprecipitated at different pH. Corresponding XRD patterns for crystalized samples at 1100 °C are shown on Fig. 5a. At pH 8 and pH 9 *only* β-$Ca_3(PO_4)_3$ (β-TCP) phase was formed. While at pH 10 and pH 11 β-TCP was accompanied with HAp phase (see Fig. 5b). More HAp was formed at higher pH (Table 3). Formed phases corresponds to data Fellah et al. [38] have obtained for ACP during heat treatment at 1100 °C, where phase composition of heat treated samples was dependent on Ca/P molar ratio in synthesis medium. In our case different crystalline phases formed regardless the fact that initial Ca/P molar ratio in the synthesis medium was the same, therefore it could be assumed that pH has some impact on crystalline phase formation at high temperatures. Question arises – whether excess of Ca ions form soluble salts (e.g. $CaCl_2$) that are washed away or calcium ions stay in synthesis solution and is yet not used for further reorganization of ACP into more ordered structures. Formation of HAp phase can be explained by carbonate ion inclusion in structure of ACP as incorporation of carbonate ions increases Ca/P molar ratio [1]. Carbonate ions leave the structure during heat treatment of CaPs. Therefore Ca/P molar ratio increases and HAp phase forms. Comparing of FT-

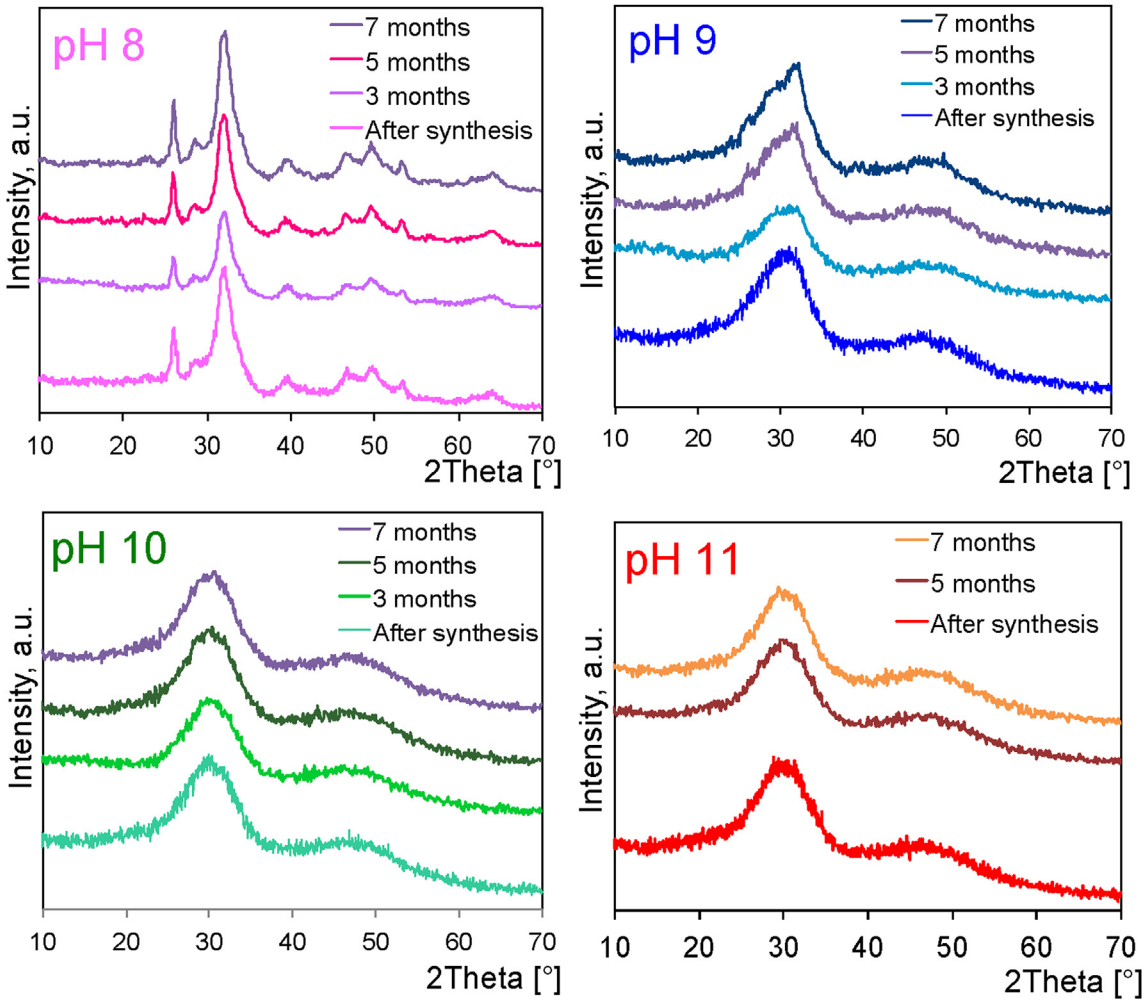

Fig. 7. X-Ray diffraction patterns of calcium phosphate nanoparticles obtained at different pH after selected periods of time: right after and 3, 5 and 7 months after synthesis.

IR spectra and XRD patterns confirms later statement – pronounced absorption bands corresponding to carbonate groups were visible for samples prepared at pH 10 and pH 11 and so was the HAp phase in corresponding XRD patterns.

Gradual thermal treatments (see example on Fig. 6) of prepared CaPs show pronounced short-range order until 500 °C. Small peaks begin to develop at 300 °C and 500 °C. This is where the ordering of material structure starts. More detailed thermal studies are needed for going into more detail about CaPs prepared by rapid reprecipitation route from dissolved CaP salts.

4.4. Structural stability of amorphous CaP nanoparticles in air

After spending 3 months in air the dried CaP samples showed negligible changes in XRD patterns (Fig. 7) – they still possessed XRD pattern characteristic to ACP (pH 10 and 11) and partially crystalline CaPs (pH 8 and 9). After 5 months sample obtained at pH 9 started to demonstrate diffraction peaks that correspond to HAp. While powders obtained at higher pH values stayed amorphous even after 7 months. Formation of new crystalline phases has been detected only for powder obtained at pH 9 by rapid reprecipitation method followed by drying in hot air. This might be the transitional pH value between obtaining crystalline or amorphous calcium phosphate. pH value 9 is the one where formation of crystalline phase happened, because XRD pattern contained slight deviations from pattern of truly amorphous calcium phosphate (like samples prepared at pH 10 and pH 11). Presence of initial structural ordering can provide sites for further transformation into crystalline sate. Ordering might have happened by internal hydrolysis as mentioned earlier. The incorporated carbonate ions could be responsible for the long term stability of ACP obtained at pH 10 and pH 11 as well, as it is reported by S. Dorozhkin [1].

5. Conclusions

Nanosized (11–30 nm) calcium phosphates with amorphous or partially crystalline structure were prepared by a novel rapid reprecipitation method based on fast pH change of calcium and phosphate ions containing solution. Amorphous calcium phosphate was formed at pH 10–11, while at pH 8 and 9 partially crystalline calcium phosphates were obtained. FT-IR spectra confirmed the formation of amorphous carbonated calcium phosphate. Crystallization of these phosphates begins at around 500 °C. First crystalline phase is hydroxyapatite. At higher temperatures only β-tricalcium phosphate phase (pH 8 and 9) or both – β-tricalcium phosphate and small amount of hydroxyapatite (pH 10 and 11) were formed. This could be a novel starting point for preparation of biphasic (HAp/β-TCP) calcium phosphate ceramics from amorphous calcium phosphate or low crystalline calcium phosphate powders obtained from solutions with different pH. Obtained calcium phosphates

possess high specific surface area (133–154 m^2/g) and they are structurally stable in dried state up to 7 months.

Acknowledgment

This work has been supported by the National Research Programme No. 2014.10–4/VPP-3/21 "MultIfunctional Materials and composItes, photonicS and nanotechnology ($IMIS^2$)" Project No. 4 "Nanomaterials and nanotechnologies for medical applications".

References

[1] S.V. Dorozhkin, Amorphous calcium (ortho)phosphates, Acta Biomater. 6 (no. 12) (Dec. 2010) 4457–4475.
[2] C. Combes, C. Rey, Amorphous calcium phosphates: synthesis, properties and uses in biomaterials, Acta Biomater. 6 (no. 9) (Sep. 2010) 3362–3378.
[3] W.J.E.M. Habraken, J. Tao, L.J. Brylka, H. Friedrich, L. Bertinetti, A.S. Schenk, A. Verch, V. Dmitrovic, P.H.H. Bomans, P.M. Frederik, J. Laven, P. van der Schoot, B. Aichmayer, G. de With, J.J. DeYoreo, N.A.J.M. Sommerdijk, Ion-association complexes unite classical and non-classical theories for the biomimetic nucleation of calcium phosphate, Nat. Commun. 4 (2013) 1507.
[4] S. Lala, S. Brahmachari, P.K. Das, D. Das, T. Kar, S.K. Pradhan, Biocompatible nanocrystalline natural bone like carbonated hydroxyapatite synthesized by mechanical alloying in a record minimum time, Mater. Sci. Eng. C. Mater. Biol. Appl. 42 (Sep. 2014) 647–656.
[5] J. Tao, H. Pan, J. Wang, J. Wu, B. Wang, X. Xu, R. Tang, Evolution of amorphous calcium phosphate to hydroxyapatite probed by gold nanoparticles, J. Phys. Chem. C 112 (no. 38) (Sep. 2008) 14929–14933.
[6] F. Abbona, A. Baronnet, A XRD and TEM study on the transformation of amorphous calcium phosphate in the presence of magnesium, J. Cryst. Growth 165 (1996) 98–105.
[7] E. Lam, Q. Gu, P.J. Swedlund, S. Marchesseau, Y. Hemar, X-ray diffraction investigation of amorphous calcium phosphate and hydroxyapatite under ultra-high hydrostatic pressure, Int. J. Min. Metall. Mater. 22 (no. 11) (2015) 1225–1231.
[8] S. Kim, H.S. Ryu, H. Shin, H.S. Jung, K.S. Hong, In situ observation of hydroxyapatite nanocrystal formation from amorphous calcium phosphate in calcium-rich solutions, Mater. Chem. Phys. 91 (2005) 500–506.
[9] Z.Z. Zyman, D.V. Rokhmistrov, V.I. Glushko, Structural and compositional features of amorphous calcium phosphate at the early stage of precipitation, J. Mater. Sci. Mater. Med. 21 (no. 1) (2010) 123–130.
[10] E.D. Eanes, Amorphous calcium phosphate: thermodynamic and kinetic considerations, in: Calcium Phosphates in Biological and Industrial Systems, 1998, pp. 21–39.
[11] E.D. Eanes, J.L. Meyer, The maturation of crystalline calcium phosphates in aqueous suspensions at physiologic pH, Calcif. Tissue Res. 23 (no. 1) (1977) 259–269.
[12] M. Sokolova, A. Putnins, I. Kreicbergs, J. Locs, Scale-up of wet precipitation calcium phosphate synthesis, Key Eng. Mater. 604 (2014) 216–219.
[13] N. Doebelin, R. Kleeberg, Profex: a graphical user interface for the Rietveld refinement program BGMN, J. Appl. Crystallogr. 48 (no. 5) (Oct. 2015) 1573–1580.
[14] R.E. Dinnebier, S.J.L. Billinge, Powder Diffraction: Theory and Practice, RSC Publishing, 2008.
[15] K. Smits, L. Grigorjeva, D. Millers, K. Kundzins, R. Ignatans, J. Grabis, C. Monty, Luminescence properties of zirconia nanocrystals prepared by solar physical vapor deposition, Opt. Mater. (Amst). 37 (no. C) (2014) 251–256.
[16] N.C. Blumenthal, A.S. Posner, J.M. Holmes, Effect of preparation conditions on the properties and transformation of amorphous calcium phosphate, Mater. Res. Bull. 7 (1972) 1181–1189.
[17] J.L. Meyer, E.D. Eanes, A thermodynamic analysis of the amorphous to crystalline calcium phosphate transformation, Calcif. Tissue Res. 25 (1978) 59–68.
[18] A. Lebugle, E. Zahidi, G. Bonel, Effect of structure and composition on the thermal decomposition of calcium phosphates (Ca/P = 1.33), React. Solids 2 (no. 1–2) (1986) 151–161.
[19] A. Rodrigues, A. Lebugle, Behavior in wet atmosphere of an amorphous calcium phosphate with an atomic Ca/P ratio of 1.33, J. Solid State Chem. 148 (1999) 308–315.
[20] J. Zhao, Y. Liu, W.-B. Sun, H. Zhang, Amorphous calcium phosphate and its application in dentistry, Chem. Cent. J. 5 (no. 1) (2011) 40.
[21] I. Lopez-Valero, C. Gomez-Lorente, R. Boistelle, Effects of sodium and ammonium ions on occurrence, evolution and crystallinity of calcium phosphates, J. Cryst. Growth 121 (1992) 297–304.
[22] A. Antonakos, E. Liarokapis, T. Leventouri, Micro-Raman and FTIR studies of synthetic and natural apatites, Biomaterials 28 (2007) 3043–3054.
[23] S. Koutsopoulos, Synthesis and characterization of hydroxyapatite crystals: a review study on the analytical methods, J. Biomed. Mater. Res. 62 (no. 4) (Dec. 2002) 600–612.
[24] D. Rabadjieva, R. Gergulova, R. Titorenkova, S. Tepavitcharova, E. Dyulgerova, C. Balarew, O. Petrov, Biomimetic transformations of amorphous calcium phosphate: kinetic and thermodynamic studies, J. Mater. Sci. Mater. Med. 21 (no. 9) (2010) 2501–2509.
[25] X.J. Zhang, D.Y. Lin, X.H. Yan, X.X. Wang, Evolution of the magnesium incorporated amorphous calcium phosphate to nano-crystallized hydroxyapatite in alkaline solution, J. Cryst. Growth 336 (no. 1) (2011) 60–66.
[26] D. Eichert, C. Drouet, H. Sfihia, C. Rey, C. Combes, Nanocrystalline Apatite-based Biomaterials, Nova Science Publishers, Inc., New York, 2009.
[27] A. Kaflak, A. Ślósarczyk, W. Kolodziejski, A comparative study of carbonate bands from nanocrystalline carbonated hydroxyapatites using FT-IR spectroscopy in the transmission and photoacoustic modes, J. Mol. Struct. 997 (no. 1–3) (Jun. 2011) 7–14.
[28] M.E. Fleet, Infrared spectra of carbonate apatites: ν_2-Region bands, Biomaterials 30 (no. 8) (2009) 1473–1481.
[29] Y. Li, F. Kong, W. Weng, Preparation and characterization of novel biphasic calcium phosphate powders (alpha-TCP/HA) derived from carbonated amorphous calcium phosphates, J. Biomed. Mater. Res. B. Appl. Biomater. 89B (no. 2) (2009) 508–517.
[30] J. Elliot, Studies in Inorganic Chemistry, Structure and Chemistry of the Apatites and Other Calcium Orthophosphates, vol. 18, Elsevier, Amsterdam, 1994.
[31] M. Nakamura, R. Hiratai, T. Hentunen, J. Salonen, K. Yamashita, Hydroxyapatite with high carbonate substitutions promotes osteoclast resorption through osteocyte-like cells, ACS Biomater. Sci. Eng. 2 (no. 2) (2016) 259–267.
[32] J.T.B. Ratnayake, M. Mucalo, G.J. Dias, Substituted hydroxyapatites for bone regeneration: a review of current trends, J. Biomed. Mater. Res. - Part B Appl. Biomater. (2016) 1–15.
[33] J.D. Pasteris, B. Wopenka, J.J. Freeman, K. Rogers, E. Valsami-Jones, J.A.M. van der Houwen, M.J. Silva, Lack of OH in nanocrystalline apatite as a function of degree of atomic order: implications for bone and biomaterials, Biomaterials 25 (no. 2) (Jan. 2004) 229–238.
[34] S. Padilla, I. Izquierdo-Barba, M. Vallet-Regí, High specific surface area in nanometric carbonated hydroxyapatite, Chem. Mater. 20 (no. 19) (Oct. 2008) 5942–5944.
[35] S. Somrani, C. Rey, M. Jemal, Thermal evolution of amorphous tricalcium phosphate, J. Mater. Chem. 13 (2003) 888–892.
[36] S.K. Ghosh, A. Prakash, S. Datta, S.K. Roy, D. Basu, Effect of fuel characteristics on synthesis of calcium hydroxyapatite by solution combustion route, Bull. Mater. Sci. 33 (no. 1) (Apr. 2010) 7–16.
[37] S. Ng, J. Guo, J. Ma, S.C.J. Loo, Synthesis of high surface area mesostructured calcium phosphate particles, Acta Biomater. 6 (no. 9) (2010) 3772–3781.
[38] B.H. Fellah, P. Layrolle, Sol-gel synthesis and characterization of macroporous calcium phosphate bioceramics containing microporosity, Acta Biomater. 5 (no. 2) (2009) 735–742.

3. PIELIKUMS / APPENDIX 3

3. PUBLIKĀCIJA / PUBLICATION 3

Vecstaudza, J., Gasik, M., Locs, J. Amorphous calcium phosphate materials: formation, structure and thermal behaviour, *Journal of the European Ceramic Society*, Vol. 39, **2019**, pp.1642-1649.

doi: 10.1016/j.jeurceramsoc.2018.11.003

Journal of the European Ceramic Society 39 (2019) 1642–1649

Contents lists available at ScienceDirect

Journal of the European Ceramic Society

journal homepage: www.elsevier.com/locate/jeurceramsoc

Original Article

Amorphous calcium phosphate materials: Formation, structure and thermal behaviour☆

Jana Vecstaudza[a,*], Michael Gasik[b], Janis Locs[a]

[a] Rudolfs Cimdins Riga Biomaterials Innovations and Development Centre of RTU, Institute of General Chemical Engineering, Faculty of Materials Science and Applied Chemistry, Riga Technical University, Pulka 3, Riga, LV-1007, Latvia
[b] Aalto University Foundation, School of Chemical Engineering, Espoo, Finland

ARTICLE INFO

Keywords:
Amorphous calcium phosphate
Crystallization
Degree of crystallinity
Thermal analysis
Nanoparticles

ABSTRACT

Amorphous calcium phosphate (ACP) is essential in formation of mineralized bone and using as a bone substitute. This study presents new aspects of carbonated ACP crystallization during heat treatment. Initially synthesis end pH and drying method (80 °C or freeze-drying) of ACP were varied. Thermal behaviour and structure of differently obtained ACP were evaluated using DSC-TGA, heating microscopy, XRD, FT-IR. In addition, degree of crystallinity (DOC), phase composition and chemical group information were compared for as-synthesized and heat-treated (crystallization end T and 1200 °C) ACP. For the first time DSC-TGA and heating microscopy methods were correlated. DOC of samples dried at 80 °C was synthesis end pH dependent. Heat treatment without temperature hold at crystallization end T produced materials with DOC of 82–91%, thus proving efficiency of low temperature processing. Variations in drying method and synthesis end pH affect structure of the samples heat treated at crystallization end T, but not at 1200 °C.

1. Introduction

Calcium phosphates (CaPs) are of high interest in biomaterial field because of their outstanding response to living tissues and body environment [1]. Human bone is composed of inorganic and organic (collagen and proteins) components [2]. The inorganic part is calcium-deficient, low- crystalline, usually non-stoichiometric and carbonated CaP that highly resembles chemical structure of hydroxyapatite (HAp) [3,4]. However, high crystallinity and stoichiometry of HAp lead to rather slow rates of dissolution [5] and therefore when used as an implant the process of bone remodelling is slow as well. Amorphous calcium phosphate (ACP) has high solubility, facilitated by its amorphous structure, the hydrated layer and defects. In particular, the lack of periodic long-range order in ACP allows formation of structural defects thus increasing both rates of solubility and resorption leading to improved bioactivity [6]. Use of ACP instead of widely used HAp or biphasic HAp/β-TCP could enhance the bone repair. However, at certain conditions (moisture, different pH and ion environment, elevated temperatures etc.) the metastable ACP transforms into other crystalline CaPs, usually HAp [7], α- or β- tricalcium phosphates [8] or mixtures of these [9]. Despite previous efforts in ACP studies, crystallization of ACP is still not properly understood. Actually presence of ACP in evolving bone was confirmed quite recently in 2008 [10].

Way to understand any amorphous material is to observe heat-induced crystallization of it (formed crystalline phases, associated thermal events etc.) by controlled heat treatments. Such knowledge on heat treated ACP is beneficent in preparation of CaP ceramics, specifically with certain degree of crystallinity (DOC). These CaP materials could mimic not only the chemical composition and chemical properties of bone minerals, but also provide a different starting point for bone repair process in comparison with conventional highly crystalline CaP materials. In fact, DOC is slightly overlooked property, however it influences protein adsorption, cell adhesion and differentiation especially for bone substitutes [11]. There is limited availability on exact DOC of human bone mineral as it is dependent on many factors (human age, bone type, disease history etc.). Newly formed bone usually has smaller DOC than older bone, because the transformation of amorphous phase into the crystalline phase is slow [12]. Grynpas [13] has determined DOC of bone mineral to be 51–58%.

Synthetic CaP with specific DOC can be obtained in several ways: 1) synthesis of CaP by fine tuning of process parameters (T, pH, additives etc.); 2) by aging of CaP suspensions after synthesis (T, time, pressure

☆ For the first time freeze dried and air dried carbonated amorphous calcium phosphates are compared and studied in conjunction with crystalline phase development of calcium phosphate ceramic materials.

* Corresponding author.
E-mail address: jana.vecstaudza@rtu.lv (J. Vecstaudza).

https://doi.org/10.1016/j.jeurceramsoc.2018.11.003
Received 16 May 2018; Received in revised form 15 October 2018; Accepted 2 November 2018
Available online 03 November 2018

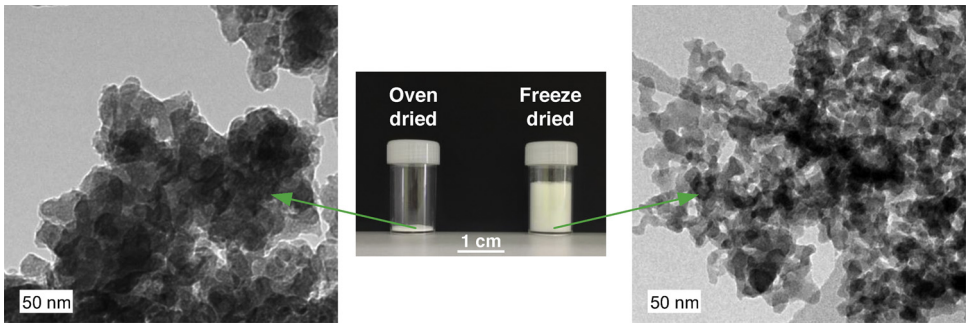

Fig. 1. Oven dried and freeze-dried samples of the same weight of ACP. Photographs and transmission electron microscopy (TEM) images.

etc. need to be considered); 3) crystallization of amorphous precursor by controlled heat treatment [14] or pressure [15]; 4) reduction of DOC of crystalline precursor (e.g. via extensive milling [16]) and 5) mechanochemical synthesis [17].

ACP is usually prepared by wet synthesis methods, therefore choice of drying method of such metastable phase is of crucial importance. Mostly ACP is dried by freeze-drying [18] and use of it is strongly emphasized, however in few reports stabilized ACP is dried in air [19,20]. Recently new synthesis has been developed where the product was dried in air at 80 °C and carbonated ACP was obtained [21]. The method proves to be time- and cost-saving, but in this work thorough analysis was done to test whether differently dried carbonated ACPs will crystallize identically, as they have different residual moisture content, powder appearance (free flowing voluminous powder for freeze-dried and agglomerated powder for oven-dried samples (see Fig. 1.)) and contact time with water during drying. The overall aim of the study was to evaluate drying methods and synthesis pH impact on carbonated ACP, complemented by analysis of thermal properties and structural features of heat treated products. Further it will give an insight on how to heat treat carbonated ACP to obtain both carbonated and partially crystalline CaP bone graft substitutes.

2. Materials and methods

2.1. Synthesis of amorphous calcium phosphate

ACP was synthesized by re-precipitation from solution containing homogenous mix of calcium and phosphate ions [21]. In brief, from HAp (further designated as R-HAp) initial suspension in water was prepared. R-HAp was dissolved in HCl and later NaOH was added to induce rapid precipitation of ACP. Final pH (8, 9, 10 and 11) of the synthesis was adjusted with diluted NH_4OH. Precipitates of ACP were separated by centrifuge, washed with deionized H_2O (30–40 min) and dried either in freeze-dryer (72 h) or drying oven (80 °C for 1 h). Prior to freeze-drying samples were frozen in liquid N_2 right after the washing procedure. Samples were further abbreviated as FrD or Ov together with corresponding synthesis end pH value, e.g., Ov_pH11.

2.2. Characterization methodology

2.2.1. Specific surface area and particle size

Specific surface area (SSA) was determined after Brunauer–Emmett–Teller (BET) method using N_2 adsorption system Quadrasorb SI (Quantachrome Instruments, USA). Samples were degassed at room temperature for 24 h to remove any moisture and vapours. Particle size d_{BET} was calculated after equation 1 assuming spherical particle shape [22]:

$$d_{BET} = 6/(\rho \times SSA), \quad (1)$$

where ρ – density of HAp (2.81 g/cm^3), determined with Micromeritics AccuPyc 1330.

2.2.2. Fourier transform infrared spectrometry

Chemical groups of samples were characterized with Fourier transform infrared (FT-IR) spectrometer 800 Scimitar Series (Varian, USA) with ATR unit. Scans (n = 50) were acquired in range of 4000-400 cm^{-1} with resolution of 4 cm^{-1}.

2.2.3. Differential scanning calorimetry and thermal gravimetry analysis

TG-DTA/DSC apparatus STA449C Jupiter® (Netzsch, Germany) was used. Amount of 20 mg for Ov or 5 mg for FrD samples was heated in alumina crucibles with lid and a hole in it. Sample chamber was purged with argon before and during experiment to avoid sample-gas interaction. Gas flow was 10 mL/min and heating rate was 10 °C/min in the range from 30 to 1200 °C. As a DSC reference, identical empty alumina crucible with lid was used. A baseline measurement with empty reference and sample crucibles was run as well to subtract influence of the empty crucibles and the sample holder. From DSC runs, crystallization onset, peak and end temperatures and enthalpies were determined.

2.2.4. X-ray diffraction

Powder x-ray diffractometer X'pert Pro (PANalytical, the Netherlands) equipped with Cu tube (Cu $K\alpha_1$ = 1.540598 Å) was used for phase determination. Measurements were done in 2θ range of 5-70°, step size was 0.05°, counting time – 69.85 s. Crystalline phases were identified using ICDD PDF-2 database with reference cards 1-072-1243 for HAp, 9-0169 for β-TCP and 9-0348 for α-TCP. Quantitative amount of crystalline phases was determined using software Maud [23]. Patterns for refinement of HAp [24], β-TCP [25] and α-TCP [26] were taken from Crystallography Open Database.

2.2.5. Degree of crystallinity

Degree of crystallinity (DOC) was calculated after at $T_{cryst.end}$ + 10 °C and 1200 °C (after full DSC run) to test whether DOC increases by continuing the heat treatment after the detected crystallization event on DSC. The extra 10 °C for $T_{cryst.end}$ were added as safety interval to make sure that the end of the crystallization effect was reached. Heating rate was 10 °C/min and samples were left to cool freely. DOC was calculated by dividing integrated intensity of following XRD patterns: sample of interest and the same sample heat-treated at 1000 °C for 15 h [22]. Heat treatment for 15 h would give the most crystalline sample of the same composition.

2.2.6. Heating microscopy

Sintering behaviour of as-synthesized samples was observed *in situ* using high temperature microscope (Hesse Instruments, Germany) equipped with Sony B&W camera. Samples were prepared by manual uniaxial pressing into round die thus obtaining cylindrical test piece (d = 2.5 mm, h = 3.0 mm). Pressing load of stainless steel punch with integrated spring was approximately 1.5 N/mm^2. The test piece was placed on alumina plate for observation of its cross-section area change. Heat treatment was the same as in DSC runs. Characteristic temperatures were determined as intersection of tangents.

Table 1
Synthesis and drying parameters and characteristics of as-synthesized ACP and reference samples.

Sample abbreviation	Drying method	Specific surface area, m^2/g	Particle size d_{BET}, nm
Ov_pH8	Oven, 80 °C (Ov)	154 ± 9	14 ± 1
Ov_pH9	[21]	141 ± 8	15 ± 1
Ov_pH10		133 ± 25	16 ± 4
Ov_pH11		150 ± 28	14 ± 4
FrD_pH8	Freeze drying for	115 ± 10	19 ± 2
FrD_pH9	72 h (FrD)	116 ± 15	19 ± 2
FrD_pH10		125 ± 16	17 ± 2
FrD_pH11		120 ± 17	18 ± 2
R-HAp	Oven, 80 °C (Ov)	95 ± 3	22 ± 1
n-HAp	–	12	178

2.2.7. Reference samples

n-HAp nanopowder purchased from Sigma-Aldrich and unsintered R-HAp prepared in the RTU laboratory by wet precipitation method [27] were used as references. n-HAp was chosen as a reference as it represents thermodynamically stable and highly crystalline CaP phase contrary to ACP. R-HAp is also referenced as it was raw material for ACP synthesis and has a structure of partially crystalline CaP.

3. Results and discussion

3.1. Characteristics of starting powders

Specific surface area (SSA) and particle size d_{BET}, XRD patterns and FT-IR spectra of samples are summarized in Table 1, Figs. 2 and 3.

3.1.1. Phase analysis of as-synthesized ACP

In XRD patterns (see Fig. 2) of the as-synthesized ACP samples position and shape of broad maxima correspond to the structure of ACP published by Eanes [28]. Samples are well washed as there are no peaks of NaCl impurity. Depending on synthesis pH the as-synthesized Ov samples are low crystalline (pH 8) or x-ray amorphous (pH 9–11) [21] while pH has no effect on the crystallinity in the case of FrD samples. Later is related to freezing of the FrD samples in liquid N_2 right after the synthesis thus suppressing crystallization. Obviously, the ionic environment of Ov_pH8 is not suitable to preserve the ACP through the 80 °C drying process while higher concentrations of NH_4^+ and OH^- ions (pH 9–11) hinder the transformation to crystalline CaP. Pattern of n-HAp matches the one of HAp while R-HAp has some peak shifts as it is nanosized, unsintered and partially crystalline.

3.1.2. Fourier transform infrared spectra of as-synthesized ACP

FT-IR spectra show the as-synthesized ACP samples to be carbonate ions containing ones. In this case presence of carbonate ions come from low synthesis temperature and vigorous mixing. These conditions introduce more air and thus CO_2 into the synthesis medium. Rounded absorption bands of ν_3 PO_4^{3-} around 1000 cm^{-1} and ν_4 PO_4^{3-} around 550 cm^{-1} confirm the amorphous character of the samples. In contrast, the spectra of crystalline n-HAp and R-HAp have sharp bands of the same groups. pH has negligible impact on band shifts within measurement resolution of 4 cm^{-1}. The same chemical groups are present in ACP samples dried by both methods (see Fig. 3) except for Ov_pH8, where ν_4 PO_4^{3-} band around 550 cm^{-1} splits into two ν_4 PO_4^{3-} bands at 559 and 599 cm^{-1}. The splitting of band for Ov_pH8 complements the partially crystalline CaP structure detected in XRD pattern on Fig. 2a. Detailed chemical group identification for each sample can be found in Supplementary data on Table S1. Overall both FT-IR and XRD results prove that freeze-drying produces ACP phase regardless of synthesis end pH while production technology employing drying at 80 °C is sensitive to synthesis end pH.

3.1.3. Specific surface area and particle size of as-synthesized ACP

ACPs dried by both methods are nanosized (14–19 nm) and have high SSA (115-154 m^2/g), that is 21–62% higher than that of the starting material R-HAp and approximately 10 times higher than of n-HAp (see Table 1). It was expected that FrD samples would have higher SSA than Ov samples, because freeze-drying produced free flowing powder compared to dense particle agglomerates obtained at 80 °C, see Fig. 1. However, statistically (two-tailed *t*-test with $p < 0.05$) only values for Ov_pH8 and FrD_pH8 differed. The SSA was higher for the Ov_pH8, that relates to crystallization resulting in nanoparticles with smaller particle size and/or different shape with developed surface features. Loss of hydrated layers that cover ACP particles might bring microstructural changes to the surface as well. Further, there was no statistical difference for other samples with the same pH value dried by different methods and there was no difference between different pH values within the same drying method.

3.2. Thermal behaviour of differently dried ACP

3.2.1. Thermogravimetric analysis

Curves of thermogravimetric analysis (TGA) are shown on Fig. 4. Mass loss is gradual for both Ov and FrD samples. The adsorbed water is reversibly removed in range from 25 to 200 °C and the chemically bound water is irreversibly lost between 200 and 400 °C [29]. Ammonia releases at temperatures up to 400 °C [30]. Around 550 °C small mass loss step is observed for several samples: Ov_pH9, Ov_pH10 and Ov_pH11.

The mass loss up to 200 °C and the total mass loss at 1200 °C were more expressed for Ov samples. In the case of Ov samples the total mass losses were from 11 up to 20% with increasing value of synthesis end pH. For FrD samples the total mass loss was up to 14%. Mass loss up to 200 °C clearly shows the difference between drying in air and freeze-drying. Larger amounts of physically adsorbed substances remain in the former case. Ways of reducing mass losses when drying in air would be to increase drying time or temperature. However longer drying times [18] and higher drying temperatures [31] lead to crystallization of ACP.

Synthesis pH correlated with the observed mass loss: the higher the pH value, the greater mass losses were observed. This trend was evident both for Ov and FrD samples. The impact of pH on mass losses originates from amount of added ammonia for pH adjustment.

R-HAp and n-HAp have negligible total mass losses – 4.8% and 1.7% at 1200 °C, respectively. TGA analysis confirmed that reference samples are stoichiometric HAp, otherwise a sharp weight loss in 700–800 °C region and a smaller weight loss above 900 °C would be observed [32].

3.2.2. Differential scanning calorimetry

DSC curves present exothermic crystallization effects of ACP phase transforming into crystalline CaP (several phases possible, see Table 2) for each sample (see Fig. 5). Here crystallization is not associated with simultaneous mass loss when compared with TGA curves (see Fig. 4). The negligible mass loss around 550 °C for few samples is completed before start of the crystallization. Reference HAp samples show no thermal effects, as they are composed of the most thermodynamically stable CaP [33].

Characteristic temperatures ($T_{cryst.onset}$ and $T_{cryst.end}$) and enhalpies are depicted on Fig. 6. There is no direct correlation between DSC peak parameters and synthesis end pH, drying method or amount of lost mass in TGA. $T_{cryst.end}$ and enthalpy values are slightly higher for the FrD samples (Fig. 6). This is related to structural differences, we could, say, that FrD samples have more distorted structure than Ov samples, therefore FrD samples require more energy to crystallize. However, XRD shows the same pattern for all ACP samples and such intimate differences are not distinguishable.

Particulary, Ov_pH8 has rather big peak area and a wide crystallization temperature region from 623 to 887 °C. It might be a sum of several thermal effects – conversion from already partially crystalline

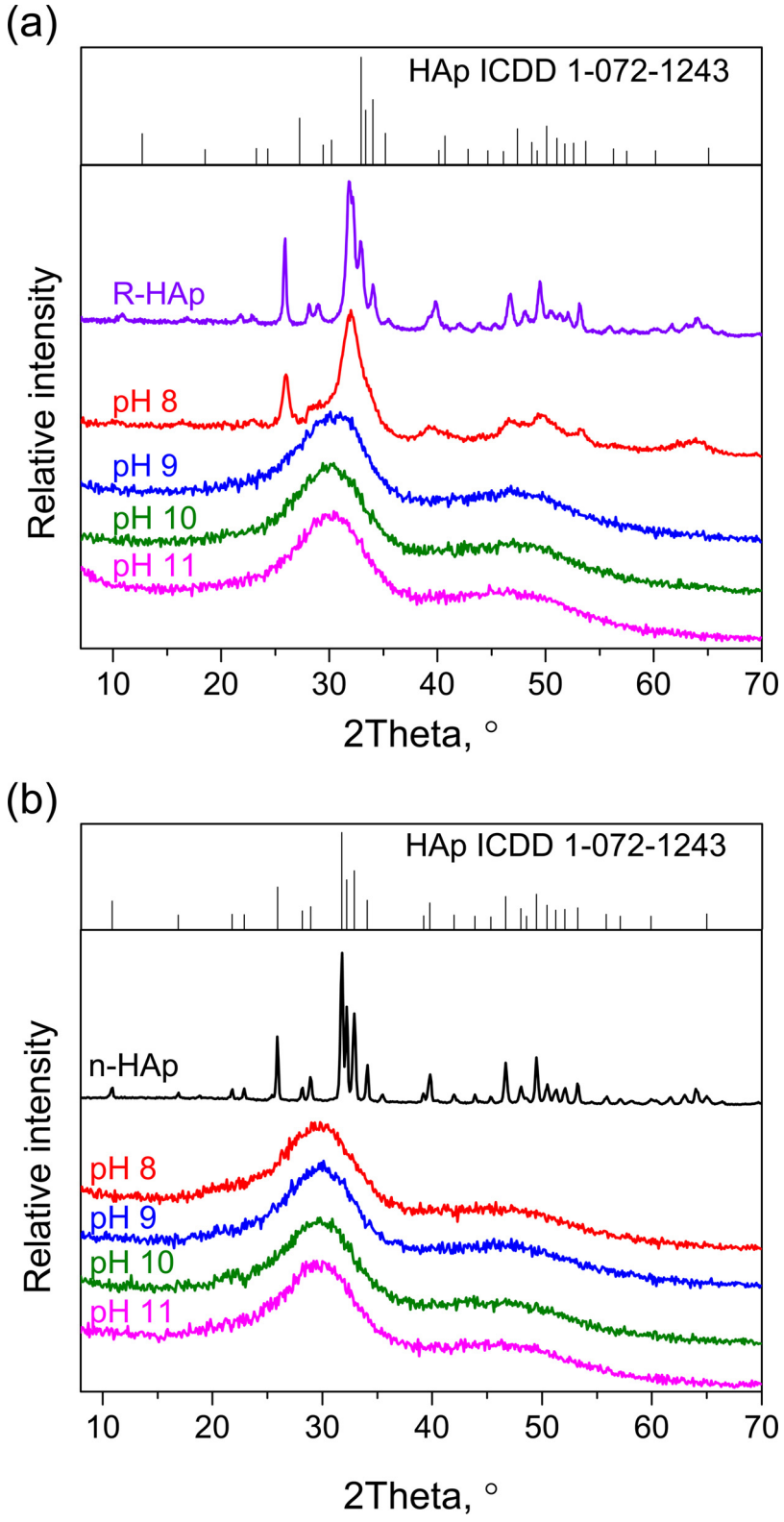

Fig. 2. X-Ray diffraction patterns of oven dried (a) and freeze dried (b) calcium phosphates; R-HAp and n-HAp are shown for reference purpose.

CaP with DOC of 50% to crystalline CaP with possible transformation from α-TCP (undetected) to β-TCP. However, for Ov_pH8 only β-TCP was found to be present at $T_{cryst.end}$ and 1200 °C (see Table 2).

The observed crystallization at 630–720 °C in Fig. 5 corresponds to formation of various CaP phases (see Table 2) from ACP. The dominant phase being β-TCP in most studied cases. Somrani et al [34] observed crystallization of ACP at 625 °C (peak temperature) into α-TCP and later to β-TCP. Feng and Khor [35] got exothermic peak with onset of 630 °C for plasma sprayed HAp containing amorphous phase. In their case ACP transformed into mixture of HAp, tetracalcium phosphate and CaO.

Crystallization observed in DSC starts at 150–200 °C higher temperature from the point in TGA where the greatest mass loss (up to

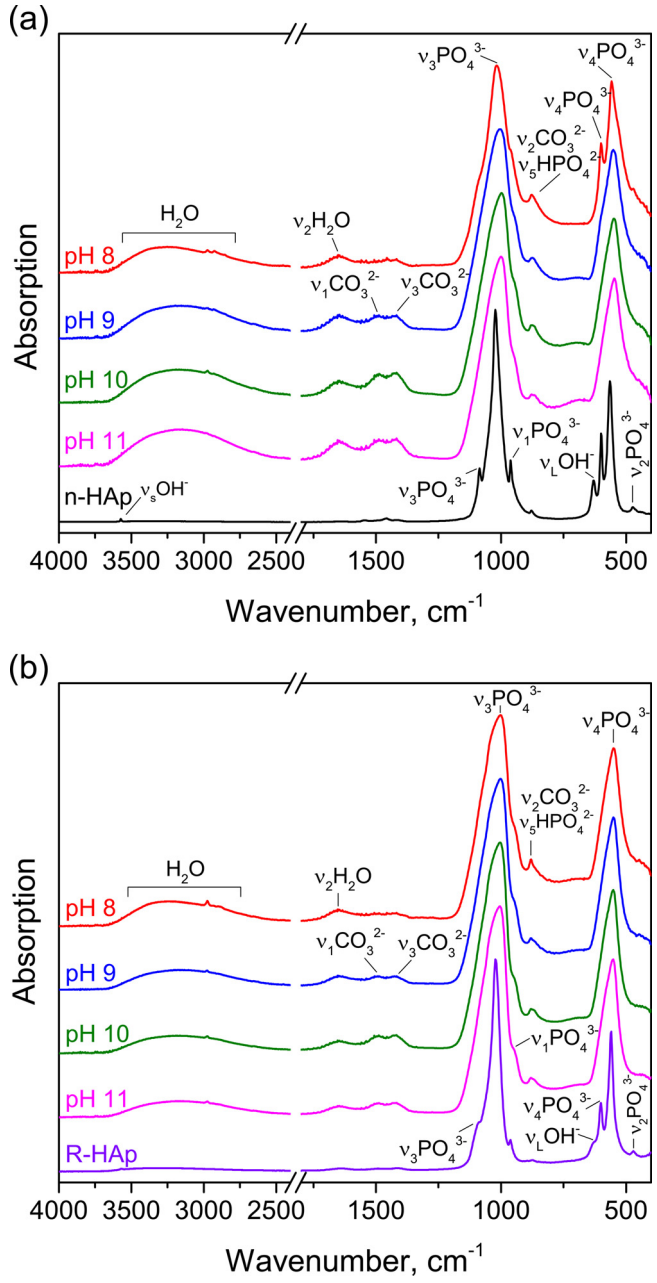

Fig. 3. FT-IR spectra of oven dried (a) and freeze dried (b) calcium phosphates; R-HAp and n-HAp are shown as reference to crystalline CaP.

Table 2
Phase composition and DOC of ACP samples at $T_{end.cryst}$ and 1200 °C.

Sample	Phase composition (amount in wt %), balance β-TCP		Degree of crystallinity (%)		
	$T_{end.cryst}$	1200 °C	$T_{end.cryst}$	1200 °C	Δ DOC
Ov_pH8*	β-TCP	β-TCP	100	95	5
Ov_pH9	26% HAp	β-TCP	91	95	4
Ov_pH10	21% HAp	23% HAp	85	98	13
Ov_pH11	14% HAp	13% HAp	86	99	13
FrD_pH8	49% HAp	β-TCP	87	98	15
FrD_pH9	80% α-TCP	β-TCP	84	100	16
FrD_pH10	α-TCP (8%), 25% HAp	21% HAp	83	96	13
FrD_pH11	26% α-TCP, 21% HAp	13% HAp	82	98	16

* Sample with initial DOC of 50%.

400 °C) was observed. Loss of chemically bound water does not trigger instant crystallization of ACP. Actually, Somrani et al [34] have observed that water molecules do not directly interact with phosphate groups and do not alter the structure when they leave the ACP on heating.

3.2.3. *Heating microscopy*

Heating microscopy (HM) was used to assess thermal behaviour of ACP *in situ* for the first time and to check whether standalone use of HM is possible for crystallization detection of ACP. HM curves are shown on Fig. 7 and their correlation with the DSC-TGA results (Fig. 8) will be discussed below.

Negligible differences in HM curves were observed for FrD samples at all synthesis end pH values, while Ov samples gave different curves. The observed cross-section area changes of sample during heat treatment partly correlated with crystallization events detected in DSC-TGA. Turns out that crystallization of ACP is accompanied by packing of particles thus decreasing cross-section area of the sample. The first cross-section area changes of the samples up to 400 °C is related to mass losses associated with loss of water as it is in TGA. Order of Ov sample HM curves as in TGA graphs (Fig. 4) – greatest cross-section area decrease in HM and mass loss in TGA is for Ov_pH 11 and the smallest for Ov_pH 8, while pH 9 and 10 have similar behaviour and lay in the middle. For FrD samples such HM graph order was not observed.

Further the next step of cross-section area decrease is related to crystallization. Here the data from both methods in the case of Ov samples were combined: 1) the $T_{cryst.onset}$ and $T_{cryst.end}$ from DSC were correlated with T *before* and *after* sample shrinkage in HM (Fig. 8a) and 2) the mass loss (TGA) at $T_{cryst.onset}$ and $T_{cryst.end}$ (DSC) and cross-section area change (HM) before and after sample shrinkage were correlated depending on synthesis end pH (Fig. 8b). In Fig. 8a close

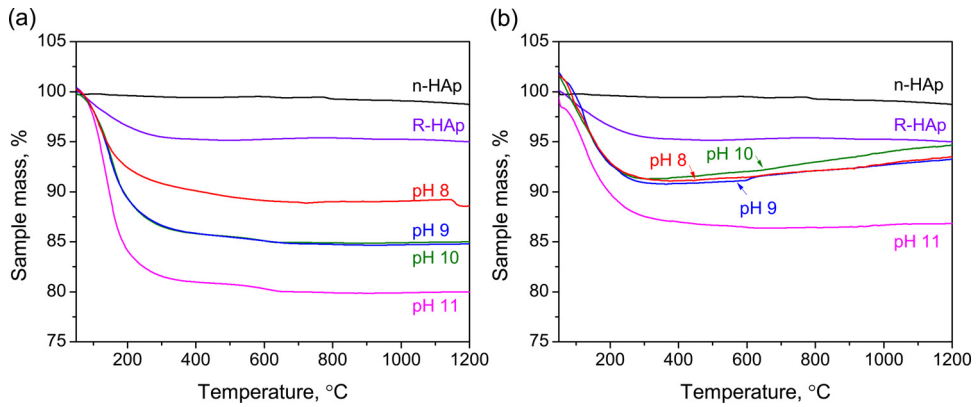

Fig. 4. TGA curves of oven dried (a) and freeze dried (b) calcium phosphates shown in the temperature range of.50–1200 °C.

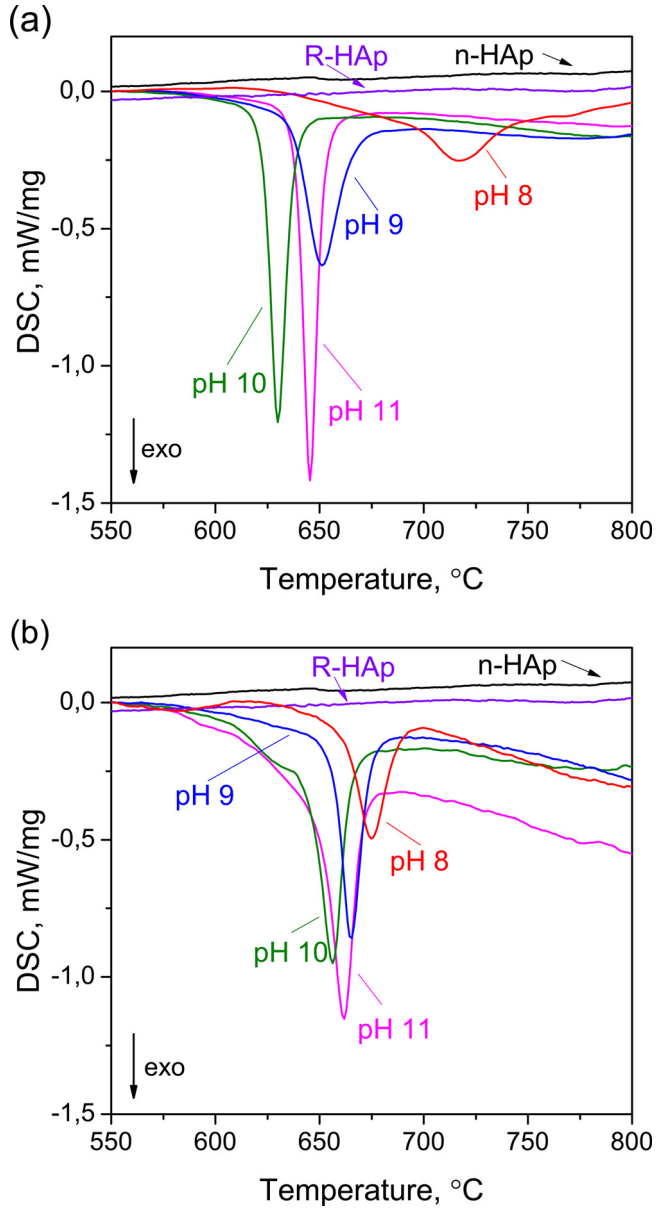

Fig. 5. DSC curves of oven dried (a) and freeze-dried (b) ACP shown in temperature range of.550–800 °C.

correlation for HM temperature *after* sample shrinkage with DSC $T_{cryst.end}$ for samples with synthesis end pH 9–11 is observed. HM temperature *before* sample shrinkage with DSC $T_{cryst.onset}$ has a similar trend, however here HM underestimates the $T_{cryst.onset}$ for 100–150 °C. Fig. 8b depicts close correlation for HM cross-section area before sample shrinkage with TGA mass loss at $T_{cryst.onset}$. Here HM cross-section area slightly overestimates the mass loss detected by TGA. Further the HM cross-section area after shrinkage of the sample with TGA mass loss at $T_{cryst.end}$ follows similar trend to previous one, but HM overestimates the TGA data by around 5%. Overall only few thermal characteristics acquirable by HM (HM T after sample shrinkage and cross-section area before sample shrinkage) are related to DSC-TGA parameters ($T_{cryst.end}$ and mass loss at $T_{cryst.onset}$).

Data for n-HAp and R-HAp between both methods were not correlated as crystallization related phenomena were absent in DSC-TGA.

3.3. Heat treated ACP samples

Phase composition and degree of crystallinity (DOC) of heat treated ACP samples are shown on Table 2.

3.3.1. Phase and chemical analysis of heat treated samples

XRD phase analysis revealed that n-HAp and R-HAp samples consisted of HAp phase only. Drying method and pH of the synthesis have an impact on phase composition for ACP samples heated up to $T_{end.cryst}$, however after 1200 °C such differences were not observed. After 1200 °C the same phase composition was obtained for each pH value regardless of chosen drying method. Still, there were differences present: it was only *β*-TCP for pH 8–9 and HAp/*β*-TCP for pH 10-11. Further, the phase composition for samples at $T_{end.cryst}$ was more diverse: only *β*-TCP; *β*-TCP and HAp; *β*-TCP and *α*-TCP; *α*-TCP, *β*-TCP and HAp. *α*-TCP was detected only for FrD samples precipitated at pH9, pH 10 and pH 11. All samples after both heat treatment temperatures, except FrD_pH9, contained *β*-TCP as the only or main crystalline phase. Main phase of FrD_pH9 was *α*-TCP. This demonstrates that differences in the drying process of ACP play an important role in structural development of CaPs during heat treatment, e.g., different times spent for samples in the wet state. In the case of FrD – sample was immediately frozen in liquid N_2 after washing while the Ov sample stayed wet with decreasing amount of moisture until it is dry. The conclusion is that heat treatment only at high temperatures (e.g. 1200 °C) does not tell the whole story about structural differences introduced in early stages of the CaP synthesis and post-processing. This is of interest for amorphous samples in particular as in this case XRD analysis for as-synthesized materials reveals little information.

FT-IR spectra of samples after $T_{cryst.end}$ and 1200 °C are shown on Fig. S1 and Fig. S2 with absorption band identification on Tables S2 and

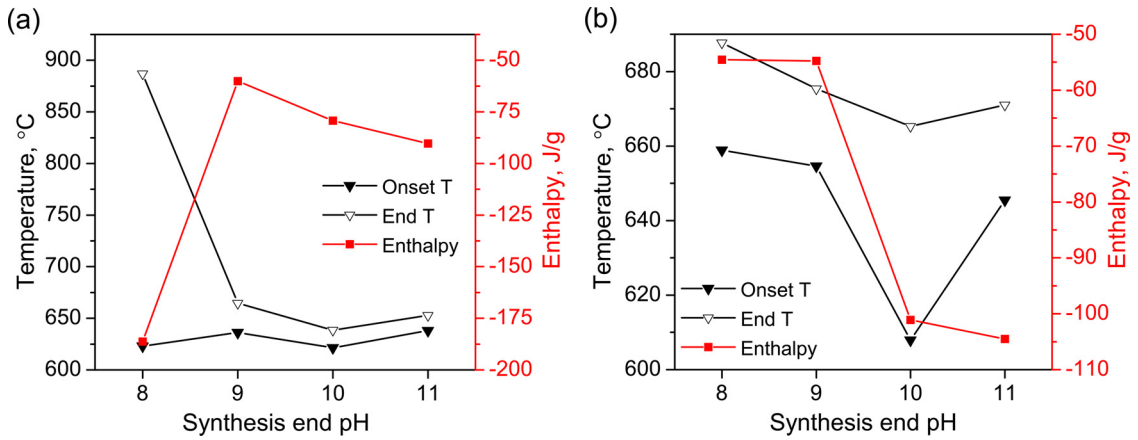

Fig. 6. Onset and endset temperatures and enthalpies of crystallization peaks for oven (a) and freeze dried (b) samples, determined from DSC curves.

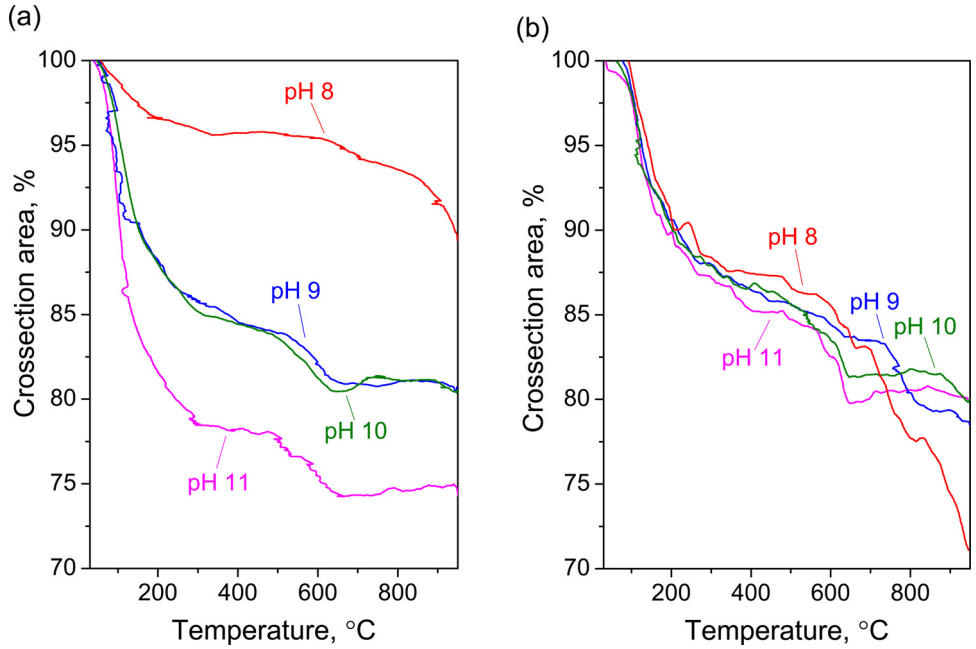

Fig. 7. Heating microscopy curves of oven (a) and freeze dried (b) CaP samples.

S3 in Supplementary data. Phosphate group absorption bands (ν_1, ν_2, ν_3 and ν_3 PO_4^{3-}) were identified belonging to phases identified with XRD. Interestingly, carbonate groups were detectable for samples prepared at pH 10 and pH 11 even at $T_{cryst.end}$. At 1200 °C carbonate groups were absent for all samples including n-HAp and R-HAp reference samples. Usually, loss of carbonate ions starts at 400–500 °C and is completed at 800–1200 °C [36] or between 630–1250 °C [37].

Formation of β-TCP from ACP is logical, because theoretical Ca/P molar ratio of both of them is 1.5 [38]. However, the synthesis system in this work have Ca/P of 1.67. Therefore, another phase or phases, e.g., non-stoichiometric calcium deficient HAp or biphasic mixture of HAp/β-TCP, can form. Formation of the biphasic mixture from ACP can be explained by presence of other ions (carbonate, excess of calcium and chlorine) in synthesis medium and later in the hydrated layer [39] of ACP particle.

As carbonate leaves the structure, the Ca/(P + C) ratio increases and the HAp could form as well. Further, excess of Ca^{2+} in synthesis medium facilitates CaP transformation to HAp. This was shown for brushite [33] and ACP [7]. It is known that higher Ca/P ratio in synthesis medium speeds up the transformation rate from ACP to HAp [40], therefore we assume that there will be differences in phase composition of such heat treated ACP. Further, obtaining of HAp/α-TCP was shown by thermally decomposing CaP product precipitated from solution with Ca/P = 1.60 [41]. And when there is chlorine in synthesis system it tends to transform calcium deficient apatite into mixture of HAp and β-TCP [42].

3.3.2. Degree of crystallinity

DOC was calculated after $T_{cryst.end}$ and 1200 °C treatment (see Table 2). For x-ray amorphous samples DOC was assumed to be zero. Samples after 1200 °C have reached DOC of 95–100%. Samples heat treated at $T_{cryst.end}$ reached DOC of 82–100%. For FrD samples difference in DOC after $T_{cryst.end}$ and 1200 °C is approximately the same for all samples (13–16%) (see Table 2). This clearly demonstrated that end pH of the synthesis medium does not eventually affect crystallinity of developing CaP phases from ACP, and further crystallization from $T_{cryst.end}$ up to 1200 °C follows the same route. For Ov samples difference between DOC at 1200 °C run and $T_{cryst.end}$ is 4–13%. Here pH of the synthesis has slight impact on DOC through the structural differences of the as synthesized samples. At pH 8 low-crystalline CaP is obtained right after synthesis [21], therefore heat treatment of such sample up to $T_{cryst.end}$ produces samples with higher DOC that is already comparable to samples obtained at 1200 °C. The initial crystallinity in ACP speeds up the crystallization process and allows to obtain higher DOC at lower temperatures. For fully amorphous samples drying method or synthesis end pH did not affect the amount of crystalline

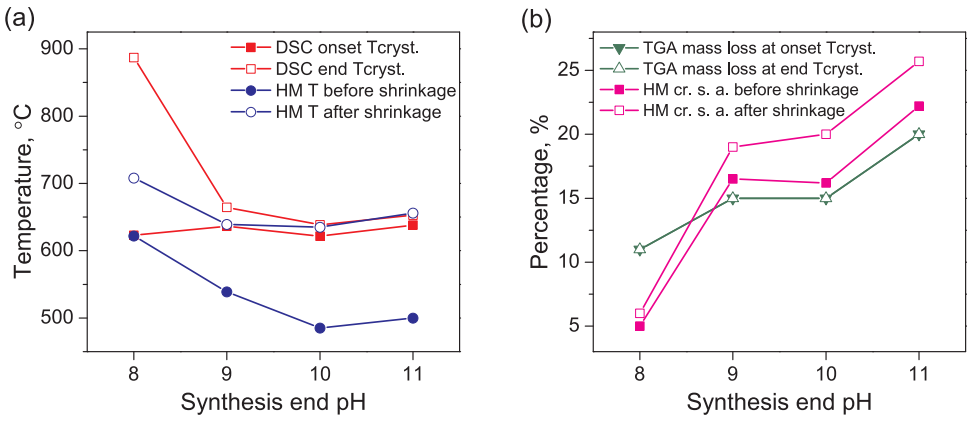

Fig. 8. (a) comparison of crystallization onset/end temperatures from DSC and temperatures corresponding to before/after shrinkage of sample from heating microscopy (HM); (b) comparison of mass losses from TGA at onset/end crystallization temperatures and cross-section area changes before/after sample shrinkage from HM.

fraction after heat treatment. Highly crystalline CaPs from ACP can be obtained roughly right after $T_{cryst.end}$ and further heat treatment up to 1000 °C or more is unnecessary if for example better mechanical properties are not of interest as well.

4. Conclusions

Study on crystallization of carbonated amorphous calcium phosphates obtained from solutions in pH range of 8–11 and air dried at 80 °C or freeze dried, increase the overall knowledge on crystallization of calcium phosphates. Synthesis pH affects the structure of as synthesized ACP and leads to differences in crystallization. Regardless of pH and drying method, all studied ACP transformed into crystalline phases upon heating, with onset of the process over 600–650 °C. For the first time it was shown that, heating of ACP at crystallization end temperature without temperature hold produces material with DOC = 82–90%; higher temperatures and/or hold times are needed to obtain fully crystalline calcium phosphate materials, thus reconsidering time and cost of production.

Acknowledgements

This work has received support from COST Action MP1301 "New generation biomimetic and customized implants for bone engineering (NewGen)" and project No. RTU/RSU-17 “Development of nanostructured bone substitute materials and study of immunological aspects in bone tissue regeneration”. J.V. has received grant from JECS Trust Fund to attend Winter Workshop 2018.

Appendix A. Supplementary data

Supplementary material related to this article can be found, in the online version, at doi:https://doi.org/10.1016/j.jeurceramsoc.2018.11.003.

References

[1] S. Bose, S. Tarafder, Calcium phosphate ceramic systems in growth factor and drug delivery for bone tissue engineering: a review, Acta Biomater. 8 (April (4)) (2012) 1401–1421.
[2] M.J. Olszta, X. Cheng, S.S. Jee, R. Kumar, Y.-Y. Kim, M.J. Kaufman, E.P. Douglas, L.B. Gower, Bone structure and formation: a new perspective, Mater. Sci. Eng. R Rep. 58 (November (3–5)) (2007) 77–116.
[3] S.V. Dorozhkin, Calcium Orthophosphates (CaPO4): Occurrence and Properties, (2015).
[4] L.S. Pryor, E. Gage, C.-J. Langevin, F. Herrera, A.D. Breithaupt, C.R. Gordon, A.M. Afifi, J.E. Zins, H. Meltzer, A. Gosman, S.R. Cohen, R. Holmes, Review of bone substitutes, Craniomaxillofac. Trauma Reconstr. 2 (3) (2009) 151–160.
[5] M.T. Fulmer, I.C. Ison, C.R. Hankermayer, B.R. Constantz, J. Ross, Measurements of the solubilities and dissolution rates of several hydroxyapatites, Biomaterials 23 (2002) 751–755.
[6] S.V. Dorozhkin, Amorphous calcium (ortho)phosphates, Acta Biomater. 6 (December (12)) (2010) 4457–4475.
[7] S. Kim, H.S. Ryu, H. Shin, H.S. Jung, K.S. Hong, In situ observation of hydroxyapatite nanocrystal formation from amorphous calcium phosphate in calcium-rich solutions, Mater. Chem. Phys. 91 (2005) 500–506.
[8] S. Liu, W. Weng, Z. Li, L. Pan, K. Cheng, C. Song, P. Du, G. Shen, G. Han, Effect of PEG amount in amorphous calcium phosphate on its crystallized products, J. Mater. Sci. Mater. Med. 20 (1) (2009) 359–363.
[9] M. Gasik, A. Keski-Honkola, Y. Bilotsky, M. Friman, Development and optimisation of hydroxyapatite-ß-TCP functionally gradated biomaterial, J. Mech. Behav. Biomed. Mater. 30 (2014) 266–273.
[10] J. Mahamid, A. Sharir, L. Addadi, S. Weiner, Amorphous calcium phosphate is a major component of the forming fin bones of zebrafish: indications for an amorphous precursor phase, Proc. Nat. Acad. Sci. U. S. A. 105 (35) (2008) 12748–12753.
[11] S. Samavedi, A.R. Whittington, A.S. Goldstein, Calcium phosphate ceramics in bone tissue engineering: a review of properties and their influence on cell behavior, Acta Biomater. 9 (9) (2013) 8037–8045.
[12] D. Farlay, G. Panczer, C. Rey, P.D. Delmas, G. Boivin, Mineral maturity and crystallinity index are distinct characteristics of bone mineral, J. Bone Miner. Metab. 28 (2010) 433–445.
[13] M. Grynpas, The crystallinity of bone mineral, J. Mater. Sci. 11 (September (9)) (1976) 1691–1696.
[14] N. D??belin, T.J. Brunner, W.J. Stark, M. Fisch, E. Conforto, M. Bohner, Thermal treatment of flame-synthesized amorphous tricalcium phosphate nanoparticles, J. Am. Ceram. Soc. 93 (10) (2010) 3455–3463.
[15] S.N. Vaidya, V. Sugandhi, Pressure induced amorphization in calcium phosphates, J. Mater. Sci. 34 (1999) 3769–3778.
[16] T. Nakano, Y. Umakoshi, A. Tokumura, Variation in crystallinity of hydroxyapatite and the related calcium phosphates by mechanical grinding and subsequent heat treatment, Metall. Mater. Trans. A 33 (3) (2002) 521–528.
[17] B. Nasiri-Tabrizi, A. Fahami, Mechanochemical synthesis and structural characterization of nano-sized amorphous tricalcium phosphate, Ceram. Int. 39 (8) (2013) 8657–8666.
[18] Z.Z. Zyman, D.V. Rokhmistrov, V.I. Glushko, Structural and compositional features of amorphous calcium phosphate at the early stage of precipitation, J. Mater. Sci. Mater. Med. 21 (1) (2010) 123–130.
[19] L. Medvecky, T. Sopcak, V. Girman, J. Briancin, Amorphous calcium phosphates synthesized by precipitation from calcium D-gluconate solutions, Colloids Surf. A Physicochem. Eng. Asp. 417 (January) (2013) 191–200.
[20] D. Lee, P.N. Kumta, Chemical synthesis and characterization of magnesium substituted amorphous calcium phosphate (MG-ACP), Mater. Sci. Eng. C 30 (October (8)) (2010) 1313–1317.
[21] J. Vecstaudza, J. Locs, Novel preparation route of stable amorphous calcium phosphate nanoparticles with high specific surface area, J. Alloys Compd. 700 (2017) 215–222.
[22] ISO 13779–3, Implants for Surgery – Hydroxyapatite – Part 3: Chemical Analysis and Characterization of Crystallinity and Phase Purity, (2008).
[23] L. Lutterotti, S. Matthies, H. Wenk, MAUD: a friendly java program for material analysis using diffraction, Newsl. CPD, (1999), pp. 14–16.
[24] K. Sudarsanan, R.A. Young, Significant precision in crystal structural details. Holly Springs hydroxyapatite, Acta Crystallogr. Sect. B Struct. Crystallogr. Cryst. Chem. 25 (August (8)) (1969) 1534–1543.
[25] M. Yashima, A. Sakai, T. Kamiyama, A. Hoshikawa, Crystal structure analysis of β-tricalcium phosphate Ca3(PO4)2 by neutron powder diffraction, J. Solid State Chem. 175 (November (2)) (2003) 272–277.
[26] M. Mathew, L.W. Schroeder, B. Dickens, W.E. Brown, The crystal structure of α-Ca3(PO4)2, Acta Crystallogr. Sect. B Struct. Crystallogr. Cryst. Chem. 33 (May (5)) (1977) 1325–1333.
[27] M. Sokolova, A. Putnins, I. Kreicbergs, J. Locs, Scale-up of wet precipitation calcium phosphate synthesis, Key Eng. Mater. 604 (2014) 216–219.
[28] E.D. Eanes, Amorphous calcium phosphate: thermodynamic and kinetic considerations, Calcium Phosphates in Biological and Industrial Systems, (1998), pp. 21–39.
[29] K. Tõnsuaadu, K.A. Gross, L. Pluduma, M. Veiderma, A review on the thermal stability of calcium apatites, J. Therm. Anal. Calorim. 110 (2) (2012) 647–659.
[30] K. Tônsuaadu, M. Peld, T. Leskelä, R. Mannonen, L. Niinistö, M. Veiderma, A thermoanalytical study of synthetic carbonate-containing apatites, Thermochim. Acta 256 (1) (1995) 55–65.
[31] A. Brangule, K. Gross, Effect on drying conditions on amorphous calcium phosphate, Key Eng. Mater. 631 (November) (2014) 99–103.
[32] Y. Fang, D.K. Agrawal, D.M. Roy, Thermal stability of synthetic hydroxyapatite, in: P.W. Brown, B. Constantz (Eds.), Hydroxyapatite and Related Materials, CRC Press, 1994, pp. 269–282.
[33] R. Štulajterová, Ľ. Medvecký, Effect of calcium ions on transformation brushite to hydroxyapatite in aqueous solutions, Colloids Surf. A Physicochem. Eng. Asp. 316 (1–3) (2008) 104–109.
[34] S. Somrani, C. Rey, M. Jemal, Thermal evolution of amorphous tricalcium phosphate, J. Mater. Chem. 13 (2003) 888–892.
[35] C.F. Feng, K. a Khor, S.W.K. Kweh, P. Cheang, Thermally induced crystallization of amorphous calcium phosphate in plasma-spheroidised hydroxyapatite powders, Mater. Lett. (November) (2000) 229–233.
[36] A. Krajewski, M. Mazzocchi, P.L. Buldini, A. Ravaglioli, A. Tinti, P. Taddei, C. Fagnano, Synthesis of carbonated hydroxyapatites: efficiency of the substitution and critical evaluation of analytical methods, J. Mol. Struct. 744–747 (2005) 221–228.
[37] D. Tadic, A thorough physicochemical characterisation of 14 calcium phosphate-based bone substitution materials in comparison to natural bone, Biomaterials 25 (6) (2004) 987–994.
[38] C. Combes, C. Rey, Amorphous calcium phosphates: synthesis, properties and uses in biomaterials, Acta Biomater. 6 (September (9)) (2010) 3362–3378.
[39] C. Rey, C. Combes, C. Drouet, S. Cazalbou, D. Grossin, F. Brouillet, S. Sarda, Surface properties of biomimetic nanocrystalline apatites; applications in biomaterials, Prog. Cryst. Growth Charact. Mater. 60 (3–4) (2014) 63–73.
[40] S. Kim, H.-S. Ryu, H.S. Jung, K.S. Hong, Influence of Ca/P ratios of starting solutions on the crystallization of amorphous calcium phosphate to hydroxyapatite, Met. Mater. Int. 10 (2) (2004) 171–175.
[41] Y. Li, F. Kong, W. Weng, Preparation and characterization of novel biphasic calcium phosphate powders (alpha-TCP/HA) derived from carbonated amorphous calcium phosphates, J. Biomed. Mater. Res. B. Appl. Biomater. 89B (2) (2009) 508–517.
[42] S. Kannan, A. Rebelo, A.F. Lemos, A. Barba, J.M.F. Ferreira, Synthesis and mechanical behaviour of chlorapatite and chlorapatite/β-TCP composites, J. Eur. Ceram. Soc. 27 (5) (2007) 2287–2294.

4. PIELIKUMS / APPENDIX 4

4. PUBLIKĀCIJA / PUBLICATION 4

Rubenis, K., Zemjane, S., Vecstaudza, J., Bitenieks, J., Locs, J. Densification of amorphous calcium phosphate using principles of the cold sintering process, *Journal of the European Ceramic Society*, Vol. 41, **2021**, pp. 912-919.

doi: 10.1016/j.jeurceramsoc.2020.08.074

Journal of the European Ceramic Society 41 (2021) 912–919

Contents lists available at ScienceDirect

Journal of the European Ceramic Society

journal homepage: www.elsevier.com/locate/jeurceramsoc

Original Article

Densification of amorphous calcium phosphate using principles of the cold sintering process

Kristaps Rubenis [a,*], Signe Zemjane [a], Jana Vecstaudza [a], Juris Bitenieks [b], Janis Locs [a,c]

[a] Rudolfs Cimdins Riga Biomaterials Innovations and Development Centre of RTU, Institute of General Chemical Engineering, Faculty of Materials Science and Applied Chemistry, Riga Technical University, Pulka St. 3/3, Riga, LV-1007, Latvia
[b] Institute of Polymer Materials, Faculty of Materials Science and Applied Chemistry, Riga Technical University, Paula Valdena 3/7, Riga, LV-1048, Latvia
[c] Baltic Biomaterials Centre of Excellence, Headquarters at Riga Technical University, Riga, Latvia

ARTICLE INFO

Keywords:
Cold sintering process
Amorphous calcium phosphate
Nanocrystalline hydroxyapatite
Relative density
Bioceramics

ABSTRACT

Despite considerable interest in amorphous calcium phosphate (ACP) bioceramics, it remains a challenge to sinter ACP to high relative density. Here, for sintering of ACP, we used principles of the so-called cold sintering process. We investigated the effect of sintering temperature (room temperature, 100, 120 and 150 °C) and presence or absence of transient liquid (20 wt. % water), while holding the pressure applied at 500 MPa, on densification and structure of ACP. Relative density of the samples that were produced from the dry starting powder at room temperature (the samples retained ACP structure) already reached 76.3 (±2.1) %. Neither increased sintering temperature nor the presence of transient liquid significantly affected bulk, true and the resulting relative density values of the samples that retained ACP structure. Our findings indicate that by applying moderate uniaxial pressure, ACP can be sintered to relatively high relative density already at room temperature.

1. Introduction

Bioceramics that contains or are made of amorphous calcium phosphate (ACP) are of considerable interest in the field of artificial bone substitute materials. This interest stems from the facts that low crystalline apatite is the main component of natural bone and that ceramics have a structure that mimics natural bone [1]. Nonetheless, it is still a great challenge to densify ACP without substantially affecting its structure and properties, especially if ceramic with high relative density is needed.

The main reason that makes densification of ACP difficult is its unique hydrated structure [2]. This structure is irreversibly altered when ACP is heated to temperatures above a few hundred degrees Celsius, that results in ACP crystallization and transformation to other less bioactive phases [3]. This eliminates the possibility to use conventional pressureless sintering technique for its sintering, because dense calcium phosphate ceramics by conventional sintering process can be obtained only at temperatures above 1000 °C [4]. In addition, so high sintering temperatures promote grain growth and remove carbonate groups from calcium phosphates that deteriorate their biological properties [5,6]. Therefore, alternative sintering techniques, such as hydrothermal hot-pressing and low-temperature spark plasma sintering, have been investigated for densification of ACP and low-crystalline apatites [7–12]. However, densification of ACP without induction of phase transformation is difficult even with these sintering techniques. To date, the most promising results have been obtained with a low-temperature spark plasma sintering technique - a recent study reported that carbonated, magnesium doped ACP retained its structure after spark plasma sintering at 150 °C. However, relative density of the obtained ACP ceramic reached only approximately 45 % of theoretical density [11].

Lately, great interest among the low-temperature sintering techniques has raised the so-called cold sintering process (CSP) [13]. This process uses transient liquid, an applied uniaxial force and heat to aid the densification of a powder compact. Many materials are already successfully sintered by CSP at ultra-low temperatures (≤300 °C) and few recent studies have reported that this process can also be used for sintering of low crystalline apatites [14–17]. These studies demonstrated that nanocrystalline hydroxyapatite can be sintered close to full density by CSP at temperatures 150–200 °C, even without the use of transient liquid. It was observed that presence of hydrated layer on the surface of nanocrystalline hydroxyapatite play an important role in the

* Corresponding author.
E-mail address: kristaps.rubenis@rtu.lv (K. Rubenis).

https://doi.org/10.1016/j.jeurceramsoc.2020.08.074
Received 15 April 2020; Received in revised form 24 August 2020; Accepted 30 August 2020
Available online 5 September 2020

densification process. Without it only slight densification of the samples was observed, even when transient liquid was used. These findings indicate that possibly ACP could also be sintered to high relative density by CSP because ACP contains more structural water than nanocrystalline apatites. However, ACP is relatively unstable and sensitive to external factors such as temperature, pressure and water vapor to which it would be subjected during the CSP [2]. Therefore, understanding how CSP affects densification and structure of ACP is needed to clarify whether this process is applicable for sintering of ACP.

In this study, we investigated the effect of CSP parameters such as sintering temperature and presence or absence of transient liquid (water) on densification and structure of ACP. After CSP, bulk, true and relative density of the samples were determined. In addition, the samples were characterized by X-ray diffraction (XRD), Attenuated total reflectance - Fourier transform infrared spectroscopy (ATR-FTIR), scanning electron microscopy (SEM), thermogravimetry-Fourier transform infrared spectroscopy (TG/FTIR) and BET method. Also, biaxial flexural strength of the samples that were produced from the dry ACP powder at room temperature was determined. We hypothesized that increased CSP temperature and use of transient liquid would enhance ACP densification.

2. Materials and methods

2.1. Amorphous calcium phosphate synthesis

For ACP synthesis, we used the dissolution-precipitation method [18]. First, 2 % (w/v) hydroxyapatite suspension in water was prepared by adding 10 g of commercial hydroxyapatite powder (#04238; Sigma-Aldrich, St. Louis, Missouri, USA) to 600 mL of deionized water that was stirred with a magnetic stirrer at 200 rpm. The resulting suspension was left stirring for 10 min before 64.46 ml of 3 M HCl solution (37 % HCl; Merck, Darmstadt, Germany) was added to it in order to dissolve the hydroxyapatite. When the obtained mixture was stirred for another 10 min, its stirring rate was increased to 600 rpm and 91.5 ml of 2 M NaOH aqueous solution (≥98 % NaOH; Merck, Darmstadt, Germany) was rapidly poured into it to induce precipitation of ACP. The addition of NaOH solution increased synthesis media pH to ~11.0, leading to the formation of a white slurry. The obtained slurry was left stirring for five more minutes before it was centrifuged. The collected white precipitates were washed with deionized water till the presence of NaCl in wash water could not be detected with 0.1 M $AgNO_3$ solution. Then, the precipitates were transferred into plastic containers that afterwards were submerged in liquid nitrogen. Finally, excess water from the frozen precipitates was removed by lyophilization technique. The synthesis, as described before, was repeated multiple times to produce enough ACP powder for the study.

2.2. Cold sintering process

Prior to the CSP, the synthesized ACP powder was kept in an oven at 80 °C for 24 h. Then 0.5 g of the powder was weighted and transferred to an easy-retrieve cylindrical pressing die (Across International, Berkeley Heights, New Jersey, USA) with an inner diameter of 13 mm. For investigating the effect of transient liquid on densification and structure of ACP, 0.5 g of the ACP powder was moistened with 0.1 mL (20 wt. %) of deionized water using a mortar and pestle before it was transferred to a pressing die. To prevent sample contamination during the CSP, surfaces of the cylinder-shape core dies that were in contact with the powder in the pressing die were covered with a 0.125 mm thick polyimide film (Kapton; DuPont, Wilmington, Delaware, USA). The pressing die with the ACP powder inside was placed in a two-column lab press (PW 40; P/O/WEBER, Remshalden, Germany) by which uniaxial pressure of 500 MPa was applied to the powder. If CSP was done at room temperature, the powder was held under this pressure for 30 min. If CSP was done at 100, 120 or 150 °C, the powder was held under the 500 MPa pressure through the heating stage (5 °C/min) and dwelling stage (30 min). Heating for the sample in the pressing die during the CSP was provided by an electrically controlled heater jacket that was wrapped around the die. A J-type thermocouple connected to a temperature controller was used to ensure controlled heating. The end of the thermocouple junction was pressed against the surface of the pressing die. After CSP, the pressing die was cooled to ambient temperature before the sample was removed from the die. Before any characterization, the CSP-sintered samples were held in an oven at 80 °C for 24 h. At least three samples were produced at each sintering condition.

2.3. BET method

Nitrogen adsorption/desorption isotherms of the synthesized ACP powder and the CSP sintered samples were generated at −196 °C using a Quadrasorb™ *SI* Surface Area and Pore Size Analyzer (Quantachrome Instruments, Boynton Beach, Florida, USA). Prior to the analysis, the samples were degassed under vacuum at room temperature for 24 h using an AUTOSORB Degasser (Quantachrome Instruments, Boynton Beach, Florida, USA). The Brunauer–Emmett–Teller (BET) model was applied to calculate specific surface area of the powder and the sintered samples based on the adsorption isotherm in the P/P_0 range from 0.05 to 0.3 [19]. By using the calculated value of specific surface area, the equivalent average primary particle diameter, D_{BET}, of the synthesized ACP was estimated using the following Eq. (1):

$$D_{BET} = 6000/(\rho_{true} \times SSA_{ACP}) \quad (1)$$

where ρ_{true} and SSA_{ACP} are true density (2.52 g/cm^3, determined by helium pycnometry) and the calculated specific surface area (109 (±11) m^2/g) of the synthesized ACP, respectively.

2.4. X-ray diffraction

XRD patterns of the synthesized ACP and the CSP-sintered samples were recorded on a PANalytical X-Pert PRO MPD (Panalytical, Almelo, Netherlands) X-ray diffractometer using a Cu K_α radiation (produced at 40 kV and 30 mA). Diffraction data were collected in a 10–70 °2θ range, with a step size of 0.05 °2θ and time per step of 2.5 s. Phases present in the recorded diffraction patterns were identified using a PANalytical X-Pert Highscore 2.2. software (Panalytical, Almelo, Netherlands) and the International Centre for Diffraction Data PDF-2 (ICDD, Newtown Square, Pennsylvania, USA) database. For recording of X-ray diffraction patterns, the CSP-sintered samples were ground into fine powder using a Mini-Mill PULVERISETTE 23 (FRITCH, Idar-Oberstein, Germany) ball mill.

2.5. Attenuated total reflectance - Fourier transform infrared spectroscopy

ATR-FTIR spectra of the synthesized ACP and the CSP-sintered samples were collected on a Varian FTS 800 FT-IR Scimitar Series spectrometer (Varian Inc., Palo Alto, California, USA) equipped with a GladiATR™ monolithic diamond ATR (PIKE Technologies, Madison, Wisconsin, USA). The spectra were collected in the mid-infrared range between 400 and 4000 cm^{-1} at a resolution of 4 cm^{-1} by co-adding 50 scans. Background spectrum with no sample in the infrared beam was acquired before collection of the sample spectrum. Then, background spectrum was subtracted from the sample spectrum. For spectra collection, the CSP-sintered samples were ground into fine powder using a Mini-Mill PULVERISETTE 23 (FRITCH, Idar-Oberstein, Germany) ball mill.

2.6. Scanning electron microscopy

Scanning electron microscope Tescan Mira\LMU (Tescan, Brno,

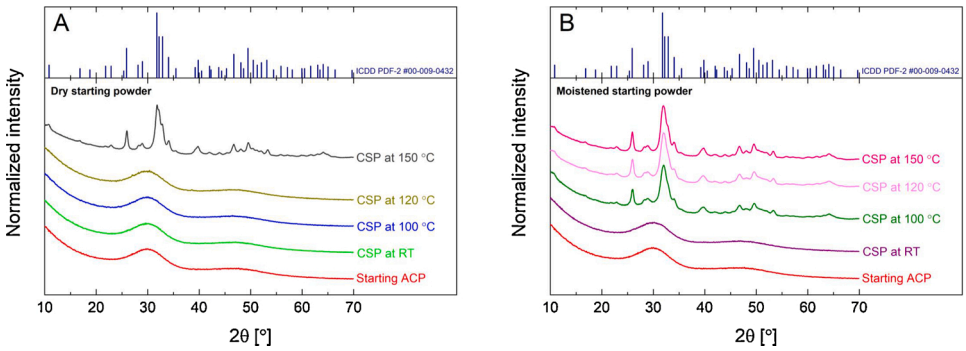

Fig. 1. XRD patterns of the starting ACP powder and the CSP-sintered samples produced from the dry (A) and from the moistened starting powder (B).

Czech Republic) was used to visualize surface morphology of the synthesized ACP powder and fracture surface morphology of the CSP-sintered samples. Secondary electrons created at an acceleration voltage of 30 kV was used for sample image generation. For microscopy, the samples were fixed on a standard aluminum pin stubs with an electrically conductive double-sided adhesive carbon tape. Before examination by SEM, the samples were sputter coated by a thin layer of gold using Emitech K550X (Quorum Technologies, Ashford, Kent, United Kingdom) sputter coater.

2.7. Helium pycnometry

True density of the synthesized ACP powder and the CSP-sintered samples was determined using a helium pycnometer Micro UltraPyc 1200e (Quantachrome Instruments, Boynton Beach, Florida, USA). To limit the influence of closed porosity on true density values, the CSP-sintered samples were ground into a fine powder using a Mini-Mill PULVERISETTE 23 (FRITCH, Idar-Oberstein, Germany) ball mill. Prior to the measurements, the instrument (added volume and cell volume) was calibrated using stainless-steel calibration spheres. After the calibration, the sample cell, filled with a powdered sample of known weight, was purged inside the sample cell holder with helium gas in a pulse mode (30 pulses). Then, volume of the powdered sample was measured by pressurizing the sample containing cell inside the sample cell holder with helium gas to a target pressure of 10 psig (reached in approximately 60 s). The measurements (runs) for each sample were repeated until the percent deviation requested for 5 consecutive runs was equal or less than 0.1 %. The sample weight was used in conjunction with the measured sample volume to determine true density of the sample.

2.8. Bulk density

Bulk density of the CSP-sintered samples was calculated by dividing the CSP-sintered sample mass with its bulk volume. Sample mass was determined by weighing the sample on an analytical balance. Bulk volume of the sample was calculated using the measured sample height and diameter values. For each sample, height and diameter was measured at 5 different positions around the sample using a digital caliper. The measured values were subsequently averaged. Bulk volume, V_{bulk}, of the sample was calculated using the following Eq. (2):

$$V_{bulk} = \pi d^2 h/4 \quad (2)$$

where d and h are sample diameter and sample height, respectively.

2.9. Relative density

Relative density values of the CSP-sintered samples were calculated by dividing the CSP-sintered sample bulk density by its true density and multiplying by 100 %. Afterwards, the mean and standard deviation of the relative density values for the samples produced at each sintering condition were calculated.

2.10. Thermogravimetry-Fourier transform infrared spectroscopy

TG/FTIR was used to estimate water and carbonate content in the synthesized ACP powder and in the CSP-sintered samples. TG/FTIR analysis was done by STA 6000 simultaneous thermal analyzer (PerkinElmer Inc., Waltham, Massachusetts, USA) coupled to the Spectrum 100 FTIR spectrometer (PerkinElmer Inc., Waltham, Massachusetts, USA) via TL 8000 transfer line (PerkinElmer Inc., Waltham, Massachusetts, USA). Prior to the analysis, the CSP-sintered samples were ground into fine powder using a Mini-Mill PULVERISETTE 23 (FRITCH, Idar-Oberstein, Germany) ball mill. Approximately 34 mg of the powdered material was used for the analysis. During the TG/FTIR analysis, the sample was heated at a constant rate of 100 °C/min to 800 °C and was held at this temperature for 10 min. The analysis was done under N_2 gas (flow rate of 20 ml/min). FTIR spectrum was collected every 9 s in the mid-infrared range between 650 and 4000 cm^{-1} at a resolution of 4 cm^{-1}. During the spectrum collection, the transfer line and gas cell were maintained at 230 °C temperature to limit condensation or adsorption of semi-volatile products. Volatile products were identified using Spectrum™ Timebase Software (PerkinElmer Inc., Waltham, Massachusetts, USA) and Spectrum Search Plus Software (PerkinElmer Inc., Waltham, Massachusetts, USA). The relative yield (wt. %) of CO_2 was assumed as an integrated intensity of absorbance-temperature curve and calculated according to the Eq. (3):

$$S = \sum_{n=30}^{n=final\ temperature} 0.5 \times (A_n + A_{n-1}) \times (T_n - T_{n-1}) \quad (3)$$

where S is relative yield, A is absorbance at specific wavenumber at temperatures T_n and T_{n-1}, T_n and T_{n-1} are experimental temperatures and n is point of measurement [20].

Calcium oxalate was used as a reference substance to determine CO_2 yield. TG/FTIR analysis of calcium oxalate was done at a constant heating rate of 100 °C/min to 1000 °C under N_2 gas (flow rate of 20 ml/min). CO_2 evolution profile as a function of temperature was obtained after FTIR data processing. A linear relationship between mass loss of calcium oxalate and relative yield of CO_2 was evaluated in the temperature range from 700 to 1000 °C (Supplementary Fig. 1) [21].

2.11. The ball on three balls test

The ball on three balls test was used to determine biaxial strength of the CSP-sintered samples [22,23]. The test was done in a 25 ST bench mounted universal testing machine (Tinius Olsen, Horsham, Pennsylvania, USA). A sample was symmetrically supported by three stainless steel balls on one side and loaded by a fourth ball in the center of the opposite side. All four balls had identical diameter of 7.93 mm. A pre-load of 7 N was applied to hold the sample between the four balls. Then, the load was increased with a rate of 1 mm/min until the sample

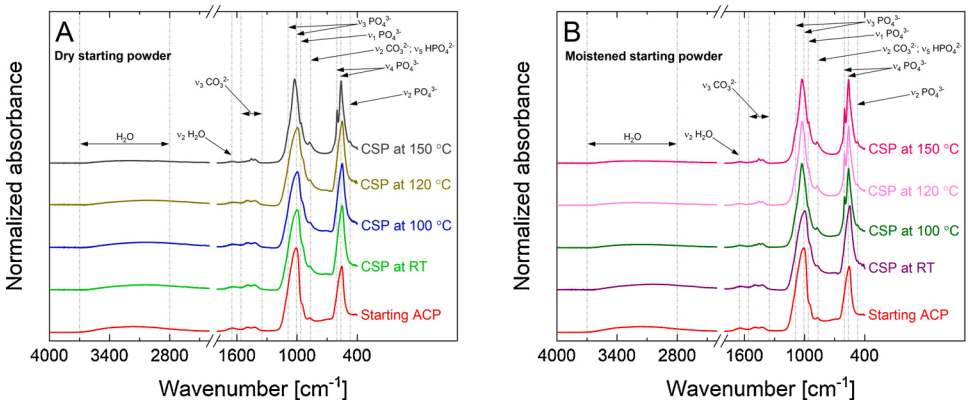

Fig. 2. ATR-FTIR spectra of the starting ACP powder and the CSP-sintered samples produced from the dry (A) and from the moistened starting powder (B).

fractured. The maximum tensile stress, σ_{max}, of the sample was calculated using the following equation (4):

$$\sigma_{max} = f \times \frac{F}{t^2}$$

where t is thickness of the sample, F is the fracture force and f is dimensionless factor which depends on the loading geometry, the sample geometry and the Poisson's ratio of the sample material. The Poisson's ratio was considered to be similar to that of the hydroxyapatite (0.27) [24].

Five samples were tested for a sintering condition.

3. Results and discussion

To evaluate how CSP affected ACP phase stability, XRD patterns of the CSP-sintered samples were recorded. XRD patterns of the samples that were produced from the dry ACP powder at room temperature, 100 or 120 °C were similar to that of the starting powder (Fig. 1A). Only two humps characteristic of ACP were present in these patterns. In contrast, broad, overlapping diffraction peaks were present in diffraction pattern of the sample sintered at 150 °C. All peaks in this pattern were indexed according to the known hydroxyapatite structure (ICDD PDF-2 #00−009-0432). From the samples that were made from the moistened ACP powder, only the sample sintered at room temperature produced diffraction pattern similar to that of the ACP powder (Fig. 1B). The samples sintered at higher temperatures produced diffraction patterns similar to that of the sample that was produced from the dry ACP powder at 150 °C (Fig. 1A). Diffraction peaks in these patterns become more distinguishable with increased sintering temperature of the samples.

Although ACP phase can be thermally stable up to 600 °C, in this study, the samples that were produced from the dry ACP powder at 150 °C were already transformed to nanocrystalline hydroxyapatite phase [25,26]. Furthermore, the samples that were produced from the moistened ACP powder were transformed to nanocrystalline hydroxyapatite phase at even lower temperatures. The phase transformation mechanism could be similar to the one that proposedly occurs when ACP is sintered by the low-temperature spark plasma sintering technique [12]. A combination of pressure and temperature could have activated surface diffusion processes and favored chemical reactions that lead to the phase transition. For example, internal hydrolysis of non-apatitic phosphates PO_4^{3-} may occurred in the ACP that lead to the formation of HPO_4^{2-} and OH^- ions. Phase transformation was induced when critical amount of PO_4^{3-} ions were transformed into HPO_4^{2-} [27]. Some of the formed HPO_4^{2-} ions might reacted with the carbonates that were present in the ACP, releasing CO_2 and forming H_2O and PO_4^{3-} [10,12]. In case of the samples produced from the moistened powder, the water added to the starting powder provided hydrothermal environment when the sintering was done at elevated temperatures [28]. Since the ion product of water increases with temperature, increased OH^- availability may led to ACP crystallization through hydroxylation process – through replenishment of OH^- groups [29,30].

ATR-FTIR spectra of the CSP-sintered samples were collected to evaluate how CSP affected local chemical environment of calcium phosphate. Broad, superimposed absorption bands that are characteristic to amorphous materials were observed in IR spectrum of the starting ACP powder and in the spectra of the CSP-sintered samples that were produced from the dry starting ACP powder at room temperature, 100 and 120 °C (Fig. 2A). Absorption bands around 550 and 1000 cm^{-1} were assigned to ν_3 and ν_1 PO_4^{3-} group vibrations, while the bands in the range of 1420–1490 and 871 cm^{-1} to carbonate vibrations. In addition, the bands at 1640 cm^{-1} and in the range of 2700 – 3500 cm^{-1} were attributed to H–O–H bending and O–H stretching modes, respectively. All these bands become sharper and some of them were shifted to higher wavenumbers in the IR spectra of the sample sintered at 150 °C. Furthermore, additional absorption bands around 470 and 600 cm^{-1} appeared in this sample spectrum. From the CSP-sintered samples that were produced from the moistened ACP powder, only the sample sintered at room temperature had similar IR spectra to the starting ACP powder (Fig. 2B). IR spectra of the samples that were sintered at higher temperatures resembled spectrum of the sample that was made from the dry ACP powder at 150 °C (Fig. 2A). Intensity of absorption bands around 470 and 600 cm^{-1} increased with increased sintering temperature of these samples.

Absorption bands (except the ones assigned to carbonate group vibrations) observed in IR spectrum of the starting ACP powder and in the spectra of the CSP-sintered samples that were produced from the dry ACP powder at room temperature, 100, 120 °C and from the moistened powder at room temperature were characteristic to ACP [10,31]. The fact that absorption bands become sharper, were shifted and additional absorption bands around 470 and 600 cm^{-1} appeared in IR spectra of the CSP sintered samples that were produced from the dry ACP powder at 150 °C and from the moistened powder at 100, 120 and 150 °C indicated that at least partially ACP was transformed to nanocrystalline apatite phase [10]. Observations in IR spectra of the CSP-sintered samples were consistent with observations in their XRD patterns. Although CO_3-containing chemicals were not used for ACP synthesis, presence of carbonate ions was detected both in the synthesized ACP as well as in the sintered samples. Most likely, the source of the carbonate ions was water that was used as a synthesis media. Since the synthesis was done under ambient conditions, the presence of carbonate ions in the synthesis media was unavoidable because CO_2 from air is rapidly absorbed in purified water. However, the presence of carbonate ions in calcium phosphates structure is desirable since carbonate ions are present in the biological apatites [1]. Furthermore, previous studies have shown that carbonate ions stabilize ACP structure and can inhibit its

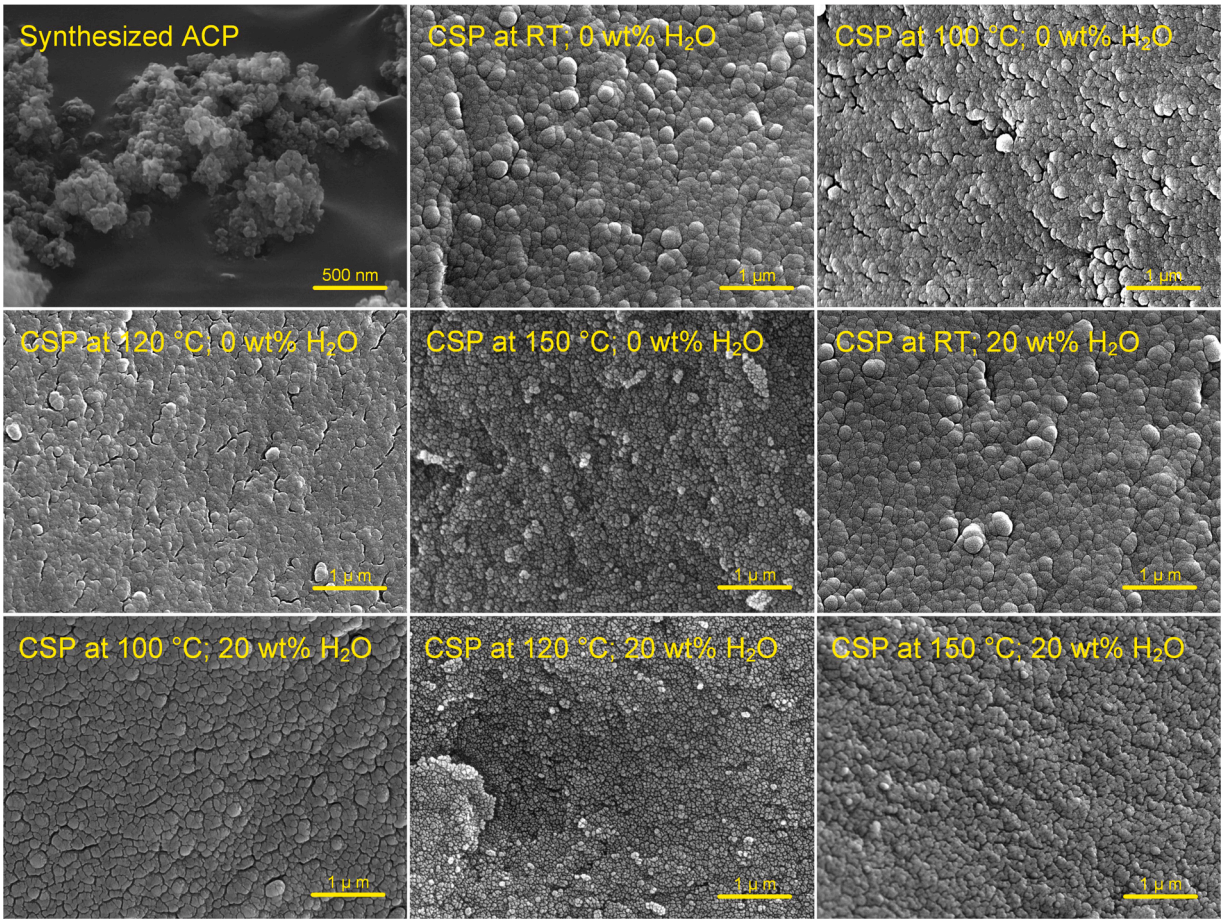

Fig. 3. SEM images of the synthesized ACP powder surface morphology and the CSP-sintered samples fracture surface morphology.

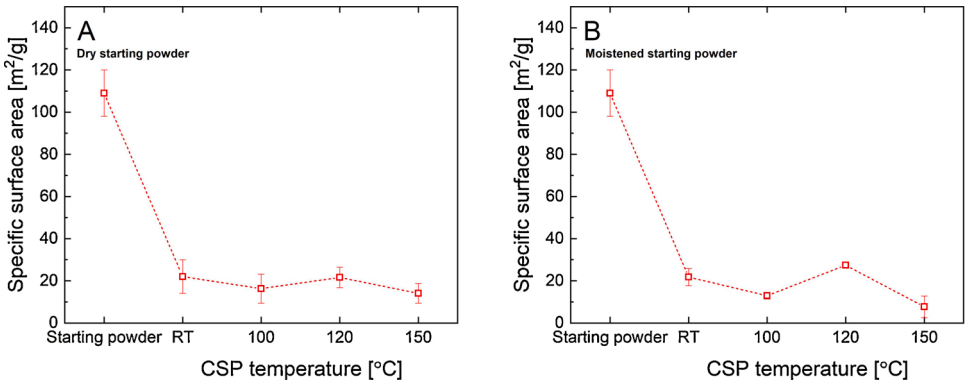

Fig. 4. Specific surface area of the starting ACP powder and the CSP-sintered samples produced from the dry (A) and from the moistened starting powder (B).

crystallization during the sintering process [2,11].

SEM was used to characterize surface morphology of the synthesized ACP powder and to evaluate microstructure of the CSP-sintered samples. The synthesized ACP powder consisted of agglomerated spheroidal particles with sizes below 100 nm (Fig. 3). The estimated equivalent average primary particle diameter of the synthesized powder was ~22 nm (as calculated by Eq. (1)). Similar values were obtained by manually measuring ACP particle diameters in the acquired SEM images (Supplementary Fig. 2). Spherical structures that consisted of smaller particles could be distinguished at fracture surfaces of the CSP-sintered samples that retained ACP structure. In contrast, the samples that consisted of nanocrystalline hydroxyapatite phase had comparably homogeneous fine-grained microstructure. The exception was the sample that was produced from the moistened starting powder at 100 °C whose microstructure was more similar to the samples that retained ACP structure. The cracks that can be observed at the fracture surfaces of the CSP-sintered samples formed during their examination by SEM (Supplementary Fig. 3).

BET method was used to determine specific surface area of the starting ACP powder and the CSP-sintered samples. Specific surface area of all CSP-sintered samples was several times lower compared to the starting powder (109 (±11) m^2/g) and varied in the range of 14–22 and 8–27 m^2/g for the samples that were produced from the dry and from the moistened starting powder, respectively (Fig. 4A and B).

Reduction in specific surface area of the starting powder indicates that during the sintering process necks have been formed between the

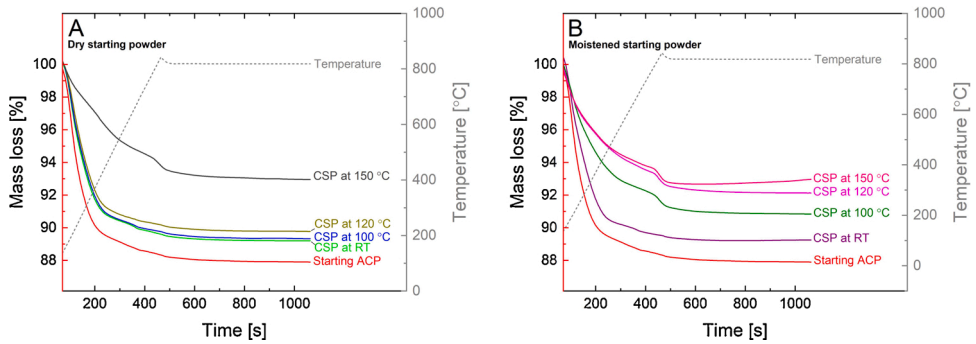

Fig. 5. Mass loss for the starting ACP powder and for the CSP-sintered samples produced from the dry (A) and from the moistened starting powder (B) as a function of temperature.

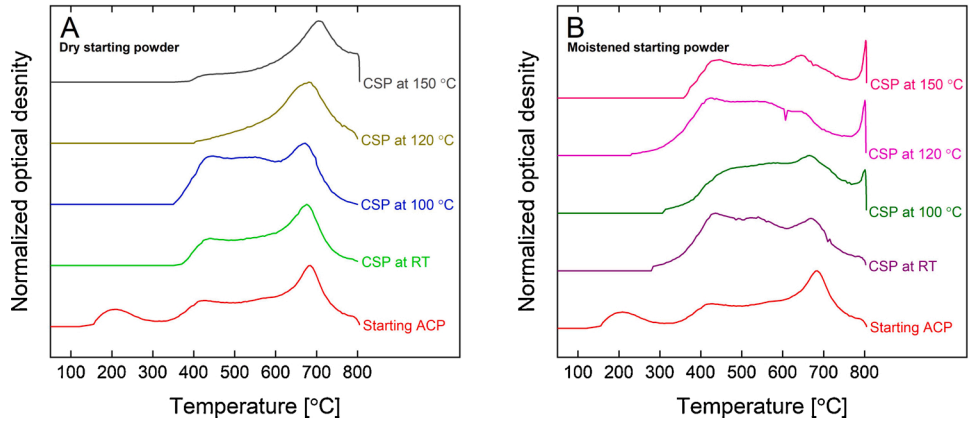

Fig. 6. CO_2 release profiles for the starting ACP powder and for the CSP-sintered samples produced from the dry (A) and from the moistened starting powder (B) as a function of temperature.

powder particles. When growing necks merge, initial particles coalesce and forms larger particles with comparably lower specific surface area. In addition, merging of necks produces interparticle porosity whose surface may be inaccessible to nitrogen used to measure the specific surface area [32]. Factors such as starting powder inhomogeneities and ACP crystallization might affected specific surface area of the samples sintered at different conditions.

To evaluate how CSP affected water and carbonate content that were present in the starting ACP powder, the CSP sintered samples were characterized by TG/FTIR. Before the analysis the samples were held in an oven at 80 °C for 24 h to limit the amount of water that was not related with calcium phosphate structure (remains of the water that was used for moistening of the ACP powder as well as the physically adsorbed water). TG analysis showed that mass loss for the starting ACP powder (used as a reference) reached 12.1 % when it was heated to 800 °C and was held at this temperature for 10 min (Fig. 5A). In comparison, mass loss for the CSP-sintered samples that were produced from the dry starting powder at room temperature, 100 and 120 °C reached 10.8 – 10.3 %, while for the sample produced at 150 °C only 7.1 %. Mass loss for the samples that were produced from the moistened ACP powder decreased with increased sintering temperature of the samples (Fig. 5B). The sample sintered at room temperature lost similar mass amount to the sample that was produced from the dry ACP powder at room temperature. The samples sintered at 100 and 120 °C lost significantly less mass compared to the samples that were produced from the dry ACP powder at the same temperatures. Mass loss for the sample sintered at 150 °C was comparable to that of the sample that was produced from the dry ACP powder at 150 °C.

FTIR analysis indicated that only water and CO_2 evolved from the starting ACP powder and the CSP-sintered samples when they were heated to 800 °C and were held at this temperature for 10 min. CO_2 from the starting ACP powder was released in two temperature regions: from 160 to 300 °C and from 320 to 800 °C (Fig. 6A). Most of the CO_2 was released in the temperature range from 320 to 800 °C, peaking at 680 °C. In comparison, CO_2 from all of the CSP-sintered samples that were produced from the dry starting powder was released only in one temperature range – from ~350 to 800 °C, peaking at ~700 °C similarly to the starting ACP powder. The estimated CO_2 yield from the starting ACP powder was 1.7 wt. %, while 0.71, 0.80, 0.60 and 1.0 wt. % from the CSP-sintered samples that were produced from the dry starting powder at room temperature, 100, 120 and 150 °C, respectively. CO_2 from all of the CSP-sintered samples that were produced from the moistened starting powder was also released in a single temperature range (Fig. 6B). For the samples that were sintered at 100, 120 and 150 °C, CO_2 release peaked at 800 °C. The estimated CO_2 yield from the CSP-sintered samples that were produced from the moistened starting powder at room temperature, 100, 120 and 150 °C was 1.2, 1.6, 1.3 and 0.6 wt. %, respectively.

TG analysis indicated that all samples that retained ACP structure (including the ones sintered at room temperature, Fig. 1) during the sintering process lost approximately 1.5 % of their initial mass. This loss can be attributed to both water and CO_2 loss, indicating that internal hydrolysis could play a role in ACP densification process [12,27]. Some water could also be lost from surface of the ACP particles (loosely bound water molecules adsorbed on surface of the particles) or/and from the inter-cluster space of ACP due to the influence of external pressure [2]. In addition, TG analysis indicated that the samples that were transformed to nanocrystalline hydroxyapatite lost less mass than the samples that retained ACP structure (Fig. 1). This difference can be attributed to ACP crystallization processes that led to further water loss

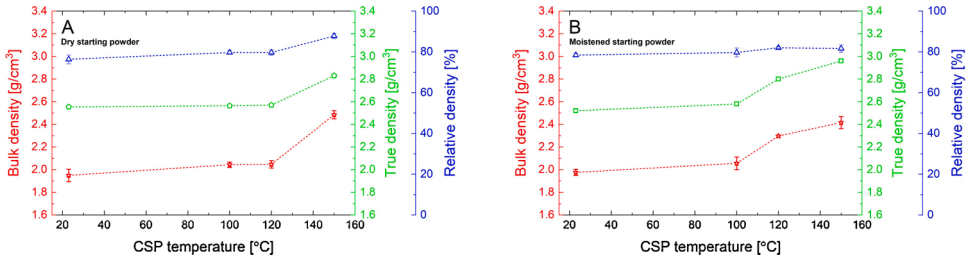

Fig. 7. Bulk, true and relative densities of the CSP-sintered samples produced from the dry (A) and from the moistened starting ACP powder (B).

from ACP structure [2,33,34].

To evaluate how CSP affected ACP densification, bulk and true density of the CSP-sintered samples were determined. Bulk and true density values of the CSP-sintered samples that were produced from the dry ACP powder remained relatively unchanged if sintering was done at room temperature, 100 or 120 °C (Fig. 7A). The sample sintered at 150 °C had significantly higher bulk, true and the resulting relative density values compared to the samples sintered at lower temperatures. Relative density of the samples sintered at room temperature, 100 and 120 °C was 76.3 (±2.1), 79.7 (±0.9) and 79.6 (±1.3) %, respectively, while 87.8 (±1.3) % for the sample sintered at 150 °C. Bulk and true density values for the samples that were produced from the moistened ACP powder at room temperature and 100 °C were similar and not significantly different from that of the samples that were produced from the dry ACP powder at the same temperatures (Fig. 7B). In comparison, bulk and true density of the samples sintered at 120 and 150 °C were higher and increased with increased sintering temperature. Still, relative density for all samples that were produced from the moistened ACP powder was similar (close to 80 %) because bulk and true density of the samples sintered at 120 and 150 °C increased almost proportionally.

Increased sintering temperature had little effect on bulk, true and the resulting relative density values of the samples that retained ACP structure after the CSP (Fig. 1). It seems likely that the pressure applied to the sample and dwelling time under the pressure were the main factors that affected bulk density of these samples. Such low sintering temperatures could not significantly increase diffusion processes to substantially improve their densification. Although the presence of liquid phase can be beneficial for powder particle rearrangement and compaction, bulk density of the samples that were produced from the moistened ACP powder and retained ACP structure after the CSP was comparable to the samples that were produced from the dry ACP powder at the same temperature [28]. Probably, the hydrated structure of ACP already performed similar function to transient liquid [10,11]. To our knowledge, the highest relative density value reported for ACP ceramic so far was ~45 % [11]. In this study, relative density values of the samples that after the sintering process retained ACP structure exceeded 75 %. Since nanocrystalline apatite structure is more compact and contains less water than ACP, true density values of the samples that were transformed to nanocrystalline apatite phase were higher compared to the samples that retained ACP structure (Fig. 1) [2]. Because ACP lost structural water during the phase transformation (Fig. 1 and Fig. 5), contact and interaction between the adjacent calcium phosphate particles increased that resulted in comparably higher bulk density values for the samples that transformed to nanocrystalline hydroxyapatite phase [35].

To gain insight about the mechanical properties of the samples that after the CSP retained ACP structure, biaxial flexural strength was determined for the samples that were produced from the dry starting ACP powder at room temperature. Biaxial flexural strength of the respective samples reached 32.3 (±4.6) MPa. This value exceeds the one (18.3 (±5) MPa) reported for the low-temperature spark plasma sintered low-crystalline apatite ceramics that had similar relative density (71 %) to the characterized samples (76.3 (±2.1) %) [10].

4. Conclusions

In summary, by applying moderate uniaxial pressure (500 MPa), ACP could be sintered to a relatively high relative density already at room temperature. Elevated sintering temperatures (in which ACP phase remained stable) did not significantly enhance ACP densification. Also, the presence of transient liquid had no significant effect on ACP densification. Furthermore, the use of transient liquid led to ACP crystallization at lower sintering temperatures. During the CSP, ACP lost part of its water and carbonate content, even when the sintering was done at room temperature. Possibly, ACP could be sintered to even higher relative density if sintering would be done under uniaxial pressure higher than 500 MPa.

Declaration of Competing Interest

The authors report no declarations of interest.

Acknowledgements

This work has been supported by the European Regional Development Fund within the Activity 1.1.1.2 "*Post-doctoral Research Aid*" of the Specific Aid Objective 1.1.1 "*To increase the research and innovative capacity of scientific institutions of Latvia and the ability to attract external financing, investing in human resources and infrastructure*" of the Operational Programme "*Growth and Employment*" (No.1.1.1.2/VIAA/2/18/318). The authors also acknowledge financial support for granting Open Access from the European Union's Horizon 2020 research and innovation programmeunder the grant agreement No. 857287.

Appendix A. Supplementary data

Supplementary material related to this article can be found, in the online version, at doi:https://doi.org/10.1016/j.jeurceramsoc.2020.08.074.

References

[1] M. Vallet-Regi, Calcium phosphates as substitution of bone tissues, Prog. Solid State Chem. 32 (2004) 1–31, https://doi.org/10.1016/j.progsolidstchem.2004.07.001.
[2] C. Combes, C. Rey, Amorphous calcium phosphates: synthesis, properties and uses in biomaterials, Acta Biomater. 6 (2010) 3362–3378, https://doi.org/10.1016/j.actbio.2010.02.017.
[3] S.V. Dorozhkin, Amorphous calcium (ortho)phosphates, Acta Biomater. 6 (2010) 4457–4475, https://doi.org/10.1016/J.ACTBIO.2010.06.031.
[4] P. Feng, M. Niu, C. Gao, S. Peng, C. Shuai, A novel two-step sintering for nano-hydroxyapatite scaffolds for bone tissue engineering, Sci. Rep. 4 (2014) 1–10, https://doi.org/10.1038/srep05599.
[5] E. Landi, G. Celotti, G. Logroscino, A. Tampieri, Carbonated hydroxyapatite as bone substitute, J. Eur. Ceram. Soc. 23 (2003) 2931–2937, https://doi.org/10.1016/S0955-2219(03)00304-2.
[6] E. Landi, A. Tampieri, G. Celotti, L. Vichi, M. Sandri, Influence of synthesis and sintering parameters on the characteristics of carbonate apatite, Biomaterials. 25 (2004) 1763–1770, https://doi.org/10.1016/j.biomaterials.2003.08.026.
[7] K. Ioku, K. Yamamoto, K. Yanagisawa, N. Yamasaki, Low temperature sintering of hydroxyapatite by hydrothermal Hot-pressing, Phosphorus Res. Bull. 4 (1994) 65–70, https://doi.org/10.3363/prb1992.4.0_65.

[8] J. Li, T. Hashida, Preparation of hydroxyapatite ceramics by hydrothermal hot-pressing method at 300 °C, J. Mater. Sci. 42 (2007) 5013–5019, https://doi.org/10.1007/s10853-006-0613-7.
[9] J.-G. Li, T. Hashida, In situ formation of hydroxyapatite-whisker ceramics by hydrothermal Hot-pressing method, J. Am. Ceram. Soc. 89 (2006) 3544–3546, https://doi.org/10.1111/j.1551-2916.2006.01149.x.
[10] C. Ortali, I. Julien, M. Vandenhende, C. Drouet, E. Champion, Consolidation of bone-like apatite bioceramics by spark plasma sintering of amorphous carbonated calcium phosphate at very low temperature, J. Eur. Ceram. Soc. 38 (2018) 2098–2109, https://doi.org/10.1016/j.jeurceramsoc.2017.11.051.
[11] M. Luginina, R. Orru, G. Cao, D. Grossin, F. Brouillet, G. Chevallier, C. Thouron, C. Drouet, First successful stabilization of consolidated amorphous calcium phosphate (ACP) by cold sintering: toward highly-resorbable reactive bioceramics, J. Mater. Chem. B. 8 (2020) 629–635, https://doi.org/10.1039/C9TB02121C.
[12] C. Ortali, I. Julien, C. Drouet, E. Champion, Influence of carbonation on the low-temperature consolidation by spark plasma sintering of carbonated calcium phosphate bioceramics, Ceram. Int. 46 (2020) 5799–5810, https://doi.org/10.1016/j.ceramint.2019.11.030.
[13] J. Guo, H. Guo, A.L. Baker, M.T. Lanagan, E.R. Kupp, G.L. Messing, C.A. Randall, Cold sintering: a paradigm shift for processing and integration of ceramics, Angew. Chemie - Int. Ed. 55 (2016) 11457–11461, https://doi.org/10.1002/anie.201605443.
[14] M. ul Hassan, H.J. Ryu, Cold sintering and durability of iodate-substituted calcium hydroxyapatite (IO-HAp) for the immobilization of radioiodine, J. Nucl. Mater. 514 (2019) 84–89, https://doi.org/10.1016/j.jnucmat.2018.11.024.
[15] S. Venkatesan, M. ul Hassan, H.J. Ryu, Adsorption and immobilization of radioactive ionic-corrosion-products using magnetic hydroxyapatite and cold-sintering for nuclear waste management applications, J. Nucl. Mater. 514 (2019) 40–49, https://doi.org/10.1016/j.jnucmat.2018.11.026.
[16] M. ul Hassan, S. Iqbal, J. Il Yun, H.J. Ryu, Immobilization of radioactive corrosion products by cold sintering of pure hydroxyapatite, J. Hazard. Mater. 374 (2019) 228–237, https://doi.org/10.1016/j.jhazmat.2019.04.038.
[17] H.Z. Shen, N. Guo, L. Zhao, P. Shen, Role of ion substitution and lattice water in the densification of cold-sintered hydroxyapatite, Scr. Mater. 177 (2020) 141–145, https://doi.org/10.1016/j.scriptamat.2019.10.024.
[18] J. Vecstaudza, J. Locs, Novel preparation route of stable amorphous calcium phosphate nanoparticles with high specific surface area, J. Alloys Compd. 700 (2017) 215–222, https://doi.org/10.1016/j.jallcom.2017.01.038.
[19] S. Brunauer, P.H. Emmett, E. Teller, Adsorption of gases in multimolecular layers, J. Am. Chem. Soc. 60 (1938) 309–319, https://doi.org/10.1021/ja01269a023.
[20] K. Lazdovica, V. Kampars, L. Liepina, M. Vilka, Comparative study on thermal pyrolysis of buckwheat and wheat straws by using TGA-FTIR and Py-GC/MS methods, J. Anal. Appl. Pyrolysis. 124 (2017) 1–15, https://doi.org/10.1016/j.jaap.2017.03.010.
[21] J. Lazdovica, K. Kampars, V. Grabis, Effect of zinc-containing nanopowders on the catalytic intermediate pyrolysis of buckwheat straw by using TGA-FTIR method, J. Anal. Appl. Pyrolysis (2020) (n.d.) In press.
[22] B3B web-App, (n.d.). http://webmath.unileoben.ac.at:8080/webMathematica/ISFK/B3B_strength_webApp.jsp (accessed August 16, 2020).
[23] A. Börger, P. Supancic, R. Danzer, The ball on three balls test for strength testing of brittle discs: stress distribution in the disc, J. Eur. Ceram. Soc. 22 (2002) 1425–1436, https://doi.org/10.1016/S0955-2219(01)00458-7.
[24] J. Park, R.S. Lakes, Biomaterials, Springer New York, New York, NY, 2007, https://doi.org/10.1007/978-0-387-37880-0.
[25] E.D. Eanes, Thermochemical studies on amorphous calcium phosphate, Calcif. Tissue Res. 5 (1970) 133–145, https://doi.org/10.1007/BF02017543.
[26] V. Uskoković, S. Marković, L. Veselinović, S. Škapin, N. Ignjatović, D.P. Uskoković, Insights into the kinetics of thermally induced crystallization of amorphous calcium phosphate, Phys. Chem. Chem. Phys. 20 (2018) 29221–29235, https://doi.org/10.1039/C8CP06460A.
[27] J.C. Heughebaert, G. Montel, Conversion of amorphous tricalcium phosphate into apatitic tricalcium phosphate, Calcif. Tissue Int. 34 (1982).
[28] H. Guo, A. Baker, J. Guo, C.A. Randall, D. Johnson, Cold sintering process: a novel technique for Low-temperature ceramic processing of ferroelectrics, J. Am. Ceram. Soc. 99 (2016) 3489–3507, https://doi.org/10.1111/jace.14554.
[29] W.L. Marshall, E.U. Franck, Ion product of water substance, 0-1000 °C, 1-10,000 bars New International formulation and its background, J. Phys. Chem. Ref. Data. 10 (1983) 295–304, https://doi.org/10.1063/1.555643.
[30] C.-W. Yang, T.-S. Lui, Kinetics of hydrothermal crystallization under saturated steam pressure and the self-healing effect by nanocrystallite for hydroxyapatite coatings, Acta Biomater. 5 (2009) 2728–2737, https://doi.org/10.1016/j.actbio.2009.03.014.
[31] C. Holt, M.J.J.M. Van Kemenade, L.S. Nelson, D.W.L. Hukins, R.T. Bailey, J. E. Harries, S.S. Hasnain, P.L. De Bruyn, Amorphous calcium phosphates prepared at pH 6.5 and 6.0, Mater. Res. Bull. 24 (1989) 55–62, https://doi.org/10.1016/0025-5408(89)90008-1.
[32] S. Bailliez, A. Nzihou, The kinetics of surface area reduction during isothermal sintering of hydroxyapatite adsorbent, Chem. Eng. J. 98 (2004) 141–152, https://doi.org/10.1016/j.cej.2003.07.001.
[33] D. Grossin, S. Rollin-Martinet, C. Estournès, F. Rossignol, E. Champion, C. Combes, C. Rey, C. Geoffroy, C. Drouet, Biomimetic apatite sintered at very low temperature by spark plasma sintering: physico-chemistry and microstructure aspects, Acta Biomater. 6 (2010) 577–585, https://doi.org/10.1016/j.actbio.2009.08.021.
[34] C. Rey, C. Combes, C. Drouet, H. Sfihi, A. Barroug, Physico-chemical properties of nanocrystalline apatites: implications for biominerals and biomaterials, Mater. Sci. Eng. C 27 (2007) 198–205, https://doi.org/10.1016/j.msec.2006.05.015.
[35] R. Valdes, A. Freulon, J.-B. Deschamps, M. Qian, J. Lacaze, Phase equilibria and solidification of Mg-rich Al-Mg-Si alloys, Mater. Sci. Forum. 508 (2006) 621–628, https://doi.org/10.4028/www.scientific.net/MSF.508.621.